applied sciences

MDPI

Review

Nitrogen Position Matters: Synthetic Strategies, Functional Behavior and Dual Roles in Medicine and Materials in the Imidazopyridine Family

Anita Cinco [1,2], Chiara Vola [1], G. Attilio Ardizzoia [1], Stefano Brenna [1] and Gioele Colombo [1,*]

[1] Department of Science and High Technology, University of Insubria, CIRCC, Via Valleggio, 9, 22100 Como, Italy; anita.cinco@iusspavia.it (A.C.); cvola@uninsubria.it (C.V.); attilio.ardizzoia@uninsubria.it (G.A.A.)
[2] Department of Science, Techonolgy and Society, University School for Advanced Studies IUSS Pavia, Palazzo del Broletto, Piazza della Vittoria, 15, 27100 Pavia, Italy
* Correspondence: gioele.colombo@uninsubria.it; Tel.: +39-(0)31-2386476

Abstract

Imidazopyridines are a versatile class of nitrogen-fused heterocycles bridging medicinal chemistry and materials science. Their π-conjugated framework allows broad structural tuning, yielding diverse biological and photophysical properties. The best-known isomers, imidazo[1,2-*a*]pyridine and imidazo[1,5-*a*]pyridine, have been widely studied as pharmacophores and luminescent materials, respectively. The less explored imidazo[4,5-*b*] and imidazo[4,5-*c*]pyridines are now emerging as alternative scaffolds with distinctive electronic and functional behavior. This review summarizes synthetic strategies, electronic features, and key applications—from kinase inhibition and antiviral activity to fluorescence imaging, down-conversion, Organic Light Emitting Diode (OLED)/Light-emitting Electrochemical Cell (LEC) and hybrid optoelectronic systems—outlining how imidazopyridines can evolve from molecular frameworks into multifunctional platforms for bioimaging and advanced optoelectronic technologies.

Keywords: imidazopyridines; luminescence; coordination compounds; optoelectronic devices

1. Introduction

Imidazopyridines represent a prominent class of fused nitrogen-containing heterocycles that have attracted high and steadily increasing attention across several areas of chemistry and chemical biology. Since their first reports in the 20th century (1925 for imidazo[1,2-*a*]pyridine [1], 1938 for imidazo[4,5-*c*]pyridine [2], 1948 for imidazo[4,5-*b*]pyridine [3] and 1955 for imidazo[1,5-*a*]pyridine [4]), these compounds have transitioned from relatively simple heteroaromatic frameworks of academic interest to highly versatile scaffolds exploited in medicinal chemistry, coordination chemistry, photophysics and materials science [5,6]. This evolution reflects both their intrinsic structural features, namely rigidity, electronic tunability and multiple heteroatom donors and the continuous development of synthetic methodologies that enable fine control over substitution patterns and molecular architecture [7–10].

The growing relevance of imidazopyridines is clearly mirrored by scientific literature. From the earliest isolated reports describing their synthesis and basic reactivity, the number of publications has increased steadily over the decades, with a particularly pronounced acceleration observed in the last decades. A bibliographic survey on CAS SciFinder® reveals that more than 2800 peer-reviewed articles and 1650 patents on imidazopyridine

Academic Editor: Andrey Miroshnichenko

Received: 12 January 2026
Revised: 6 February 2026
Accepted: 11 February 2026
Published: 14 February 2026

derivatives have been published to date, with approximately 1700 of these appearing in the last five years alone, highlighting the rapidly expanding interest in this class of compounds. This trend reflects not only methodological advances in heterocyclic synthesis, such as multicomponent reactions and C–H functionalization, but also the diversification of application-driven research spanning drug discovery, sensing, photophysics and optoelectronic devices.

In medicinal chemistry, imidazopyridines are also widely recognized as privileged scaffolds [11–13]. Their ability to engage in multiple noncovalent interactions, combined with favorable physicochemical properties, has led to their incorporation into a variety of bioactive molecules, including marketed drugs and advanced clinical candidates. Extensive structure–activity relationship studies [14] have demonstrated how subtle changes in substitution and heteroatom positioning can profoundly influence target selectivity, potency and pharmacokinetic profiles. As a result, imidazopyridines continue to serve as valuable platforms for the development of therapeutic agents targeting the central nervous system [15,16], infectious diseases [12,17] and cancer-related pathways [18,19].

Beyond their biological relevance, imidazopyridines have increasingly emerged as functional building blocks in coordination chemistry and materials science. Their fused heteroaromatic cores provide rigid, π-conjugated systems capable of coordinating metal centers through one or more nitrogen atoms, or of acting as precursors to N-heterocyclic carbenes [20,21]. These features have enabled the design of metal complexes with tailored electronic structures and excited-state properties, as well as purely organic luminophores exhibiting fluorescence [5,22], aggregation-induced emission [23,24] or excited-state intramolecular proton transfer [25,26]. In parallel, the integration of imidazopyridine-based systems into optoelectronic devices, such as OLEDs [22,27] and LECs [22], has further fueled interest in this class of compounds.

Despite the abundance of studies devoted to imidazopyridines, much of the existing literature treats these compounds as a relatively homogeneous family, with limited emphasis on how regioisomerism within the fused framework governs their properties. In particular, the relative positioning of the nitrogen atoms gives rise to distinct regioisomers (imidazo[1,2-*a*], imidazo[1,5-*a*], and imidazo[4,5-*b*/*c*] pyridines) (Figure 1) that differ not only in synthetic accessibility but also in electronic distribution, coordination behavior, photophysical response and suitability for specific applications. For example, while imidazo[1,2-*a*]pyridines have been extensively explored across all fields, the other regioisomers have historically received less attention, although recent years have witnessed a marked increase in studies dedicated to imidazo[1,5-*a*] and imidazo[4,5-*b*/*c*] frameworks.

This review aims to provide a unified and comparative perspective on the imidazopyridine family by explicitly focusing on the role of nitrogen positioning as a key structure–property determinant. By correlating synthetic strategies, coordination modes, photophysical behavior, biological activity and functional applications across the major regioisomers, we seek to move beyond a compound-centric view and establish general design principles that can guide future developments. Through this approach, imidazopyridines are presented not merely as isolated heterocycles, but as a coherent platform in which regioisomerism enables rational tuning of function at the interface of chemistry, biology, and materials science.

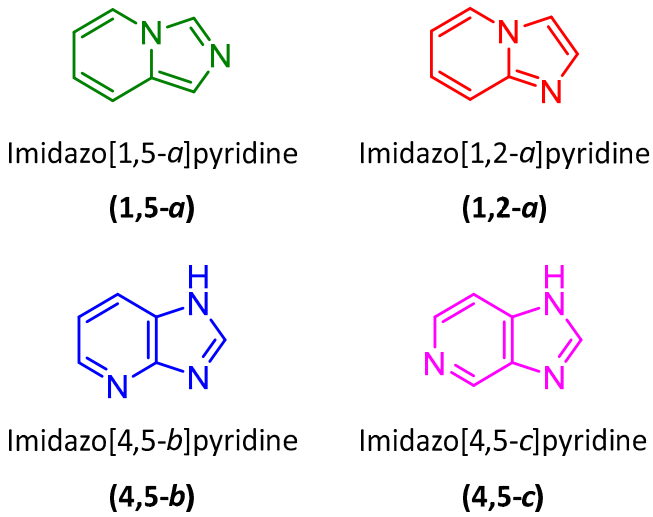

Figure 1. Structure of the four imidazopyridine regioisomers. These colors will be used throughout the review to highlight the different regioisomers (green: imidazo[1,5-*a*]pyridine; red: imidazo[1,2-*a*]pyridine; blue: imidazo[4,5-*b*]pyridine; pink: imidazo[4,5-*c*]pyridine).

2. Synthetic Methodologies to Obtain Imidazopyridines

2.1. Imidazo[1,5-a]pyridines

The synthesis of imidazo[1,5-*a*]pyridines (1,5-*a*) has been an area of great interest for decades, due to the remarkable chemical versatility and broad biological significance of this nitrogen heterocycle. Although the earliest methodologies were relatively simple condensations, recent advances have led to a varied set of strategies that are efficient, selective, and environmentally advantageous (Figure 2). Classical acid-catalyzed cyclocondensation remains the cornerstone of imidazopyridine chemistry, typically involving the reaction of 2-pyridyl derivatives with aldehydes or ketones in the presence of ammonium acetate as a source of nitrogen. For example, reacting 2,2′-pyridil with substituted benzaldehydes in acetic acid yielded 1-(2-pyridoyl)-3-phenylimidazo[1,5-*a*]pyridines in excellent yields, with the amount of ammonium acetate employed determining the main product obtained [28]. Notably, when substitution at the imidazole nitrogen is required, the use of primary amines as nitrogen sources provides a viable alternative to ammonium acetate. This modification allows for the direct installation of diverse *N*-substituents, further expanding the structural tunability of the 1,5-*a* framework [29]. When aliphatic aldehydes were used instead, 3-alkyl-substituted derivatives could be obtained under either conventional heating or microwave irradiation, the latter significantly accelerating the reaction and improving efficiency [30]. This conversion could be further enhanced by adding LiCl as a co-catalyst capable of activating the 2-pyridyl ketone, achieving up to 94% yield for the corresponding 3-aryl derivatives [31]. Similar condensations have been extended to various substrates: coupling of 2-pyridyl ketones with aldehydes in the presence of magnesium nitride (Mg_3N_2) under ethanol/water conditions affords 1,3-disubstituted imidazopyridines in high yields [32], while a greener protocol in PEG-400 could be developed, reacting 2-cyanopyridine with brominated benzaldehydes to obtain bis-bromo-substituted derivatives [33]. These examples show how the traditional condensation approach remains highly exploitable and compatible with both aromatic and aliphatic substrates, especially when optimization through modern methods are used.

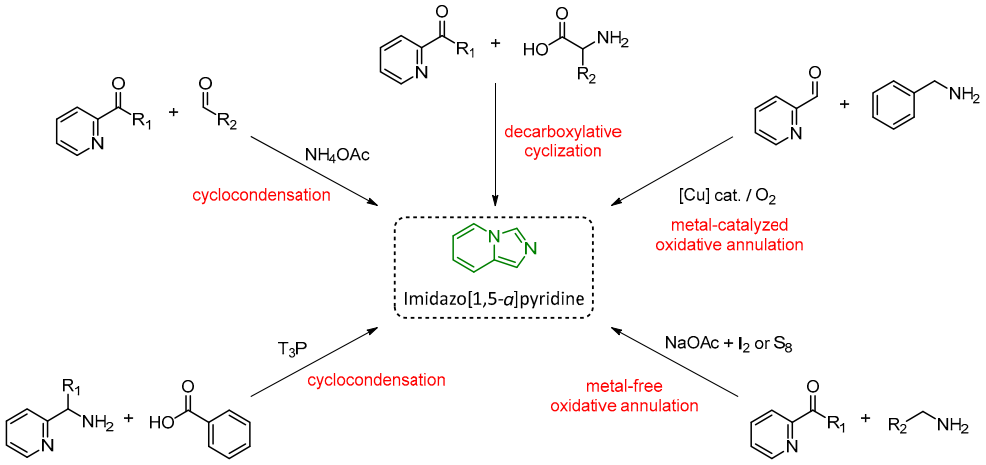

Figure 2. Selected examples of synthetic strategies towards imidazo[1,5-*a*]pyridines.

Another approach requires the use of oxidative and metal-catalyzed annulation strategies, which have become particularly valuable for constructing complex substitution patterns. As an example, copper-catalyzed oxidative cyclization of 2-formylpyridines with benzylamines using CuBr and molecular oxygen as the sole oxidant could be achieved, obtaining 1-substituted imidazopyridines in yields up to 88% [34]. Subsequently, $Cu(OAc)_2$ under aerobic conditions could also BE employed to promote the condensation of 2-pyridyl ketones and benzylamines, producing 1,3-diarylated derivatives with broad functional group tolerance [35]. On the other hand, homogeneous copper systems could be also substituted by heterogeneous catalysis: Cu-MOF-74 could be used to catalyze the oxidative annulation with comparable efficiency and easier catalyst recovery [36], while a related Cu-FMOF catalyst was capable of maintaining performance over up to four cycles [37]. In these cases, the mechanism typically involves initial imine formation, single-electron oxidation, and intramolecular C(sp^3)–H amination, followed by dehydrogenative aromatization to yield the fused heterocycle. Other metals, such as Ru(II) for acceptorless dehydrogenative coupling of primary alcohols with 2-benzoylpyridine [38] and Bi(III) for Ritter-type reactions [39], could be used.

Similarly, iodine-mediated oxidative annulation of 2-pyridyl ketones with alkylamines in the presence of sodium acetate could be performed also in metal-free conditions, providing 1,3-diaryl imidazopyridines in high yield under mild conditions [40], with many of the obtained compounds prepared on a gram scale. Alternatively, iodide could also be used as a co-catalyst with flavin in the reaction between benzylamine and ethyl-2-(pyridin-2-yl)acetate [41].

Elemental sulfur could also be used as a stoichiometric oxidant in the coupling of aryl-2-pyridylmethylamines with aldehydes to obtain 1,3-diarylated imidazopyridines [42].

Parallel to these developments, a large number of metal-free cyclization protocols have emerged, offering operational simplicity and wide substrate compatibility, such as a one-pot transformation of 2-methylaminopyridines and benzoic acids using propylphosphonic anhydride (T_3P) as both a coupling and dehydrating agent, giving 3-phenylimidazopyridines in good yields [43]. This strategy was refined through a T_3P–DMSO system that enabled the condensation of 2-methylaminopyridines with dithioesters to produce a broad library of substituted imidazopyridines under mild conditions [44]. Remarkably, an iodine-mediated C–H functionalization of 2-methylaminopyridines with sulfonyl hydrazides, furnishing 3-sulfenyl derivatives without the need for transition metals, was also reported [45]. Mechanistic studies indicate that these reactions proceed via initial thioamide formation, followed by iodination and intramolecular cyclization to deliver the aromatic product. The iodine-based approach was further extended to the oxidative desulfurization of *N*-

2-pyridylmethylthioamides, generating 3-substituted imidazopyridines [46]. Later, the same principle was also applied to the synthesis of bis(1-imidazopyridyl)arylmethanes by I_2-mediated cyclization of *N*-thioacyl aminoalcohols [47]. Collectively, these examples highlight how halogen-mediated pathways provide both synthetic versatility and access to functional materials with interesting optical behavior.

Another powerful set of strategies relies on multicomponent and decarboxylative annulations, which merge condensation and cyclization steps in a single operation. As an example, the acetic acid-mediated one-pot reaction of pyridine-2-carbaldehydes with ammonium acetate was reported to give imidazopyridines in moderate to good yields (32–77%) [48], while more recently, an iodine-promoted decarboxylative cyclization between α-amino acids and 2-benzoylpyridines or 2-benzoylquinolines was reported, forming 1,3-disubstituted imidazopyridines via a cascade of imine formation, *N*-iodination, decarboxylation, and oxidative aromatization [49]. This approach efficiently transforms renewable amino acid feedstocks into high-value heterocycles, demonstrating the potential of biogenic precursors in modern heterocyclic synthesis. Related transformations using the copper/I_2 dual catalysis and tert-butyl peroxide as an oxidant gave similar products with excellent yields, expanding the scope to various linear and branched amino acids [50]. Overall, these decarboxylative methodologies elegantly bridge bio-derived substrates and advanced heterocyclic frameworks through atom-economic processes.

Beyond these examples, other innovative techniques have also contributed to the diversification of synthetic access to 1,5-*a*. Microwave-assisted routes from picolinic esters and amides provide 3-substituted products in two steps via intermediate imidoyl chlorides and nitrile ylides [51], while iodine-promoted reactions of 2-pyridylmethylamines with aryl methyl ketones afford 1-iodoimidazopyridine ketones through sequential oxidative coupling and electrophilic substitution [52]. Furthermore, a solvent-free, microwave-assisted protocol was also developed for the synthesis of 1,3-disubstituted 1,5-*a* derivatives through a condensation–oxidative cyclization sequence using MnO_2 as an oxidant and *p*-toluenesulfonic acid as a source of catalytic H^+, delivering the target heterocycles in moderate yields [53].

The introduction of heterogeneous catalysts, solvent-free microwave activation, and even flow-compatible oxidative systems illustrates how imidazopyridine synthesis has evolved into a platform for testing new enabling technologies in organic synthesis. Altogether, the breadth of methodologies now available underscores the extraordinary synthetic flexibility of the 1,5-*a* scaffold. From classic acid-driven condensations to oxidative and metal-free annulations, these approaches collectively provide modular, scalable, and sustainable access to a wide range of substitution patterns.

2.2. Imidazo[1,2-a]pyridines

1,5-*a* have historically required more specialized precursors and tactics and therefore have been less explored compared to the other regioisomers, also in light of their more recent discovery, although recent methodological work has significantly improved routes to the 1,5-isomer (*vide supra*). By contrast, Imidazo[1,2-*a*]pyridines (1,2-*a*) are generally more synthetically accessible than the corresponding 1,5-*a* isomers. The classical route comprises the synthesis from 2-aminopyridines by the versatile Groebke–Blackburn–Bienaymé (GBB) three-component reaction, with many one-pot, metal-free, microwave- or supported-catalyst variants, making rapid library generation straightforward.

Historically, GBB reactions have been the most used methods to afford 1,2-*a*: Groebke [54], Blackburn [55], and Bienaymé's [56] early reports demonstrated that a substituted 2-aminopyridine, an aldehyde, and an isocyanide combine in one pot to give 3-substituted

1,2-*a* via imine formation, with yields ranging from 40 to 80% and an exceptional library of aldehydes and isocyanides to be used (Figure 3) [57].

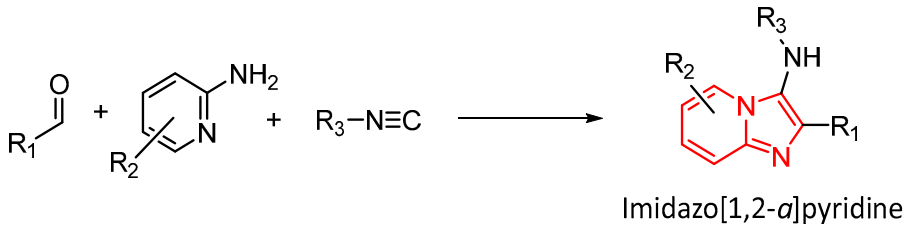

Figure 3. Groebke-Blackburn-Bienaymé reaction to give imidazo[1,2-*a*]pyridines.

Building on that mechanistic and tactical foundation, it has been shown that simple operational modifications (e.g., microwave irradiation on montmorillonite clay under solvent-free conditions) [58] could shorten reaction time to minutes while maintaining good yields. Complementary to multi-component reactions, classical condensation/cyclization strategies such as condensation of 2-aminopyridines with α-halo ketones [59–61], phenacyl derivatives [62,63] or β-ketoesters [64,65], remain indispensable to access defined 2- or 3-substitution and reliable scalability (Figure 4). These routes are often the highest-yielding (commonly 60–90% in optimized examples), use well-known reagents and straightforward work-ups, and thus underpin many early industrial syntheses; their main drawback is the need to prepare or handle pre-functionalized electrophiles, which pushed the research to develop numerous one-pot, supported-catalyst and Lewis-acid-promoted variants (e.g., $InBr_3$ protocols, $ZnCl_2 \cdot SiO_2$ and other recoverable heterogeneous catalysts) that ease handling and allow greater operational convenience at scale [66].

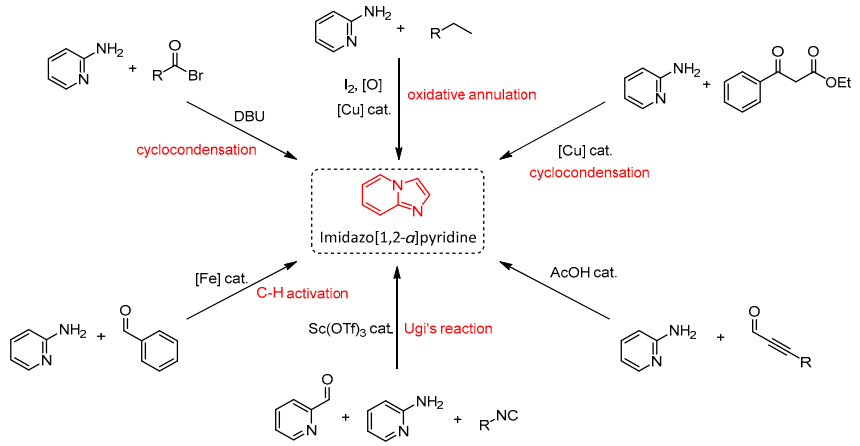

Figure 4. Selected examples of synthetic strategies towards imidazo[1,2-*a*]pyridines.

Where classical condensation and GBB approaches are not enough (i.e., when sterically congested positions, fused polycyclic architectures or complex π-extended substituents are required), oxidative domino/tandem annulations [67] and transition-metal-catalyzed C–H activation/annulation strategies could be useful alternatives [68]. In this context, a Fe(III)-catalyzed three-component domino sequence reaction was developed, involving a nitroolefin, an aldehyde and 2-aminopyridine, that yields highly substituted 1,2-*a* in moderate-to-good yields [69]. Other synthetic methodologies rely on the use of other transition metals (i.e., Pd [70], Cu [71–75]) with the use of metal-carbene intermediates (or directed C–H activation) to effect annulations or late-stage functionalization [66]. On the other hand, a regiospecific metal-free three-component route starting from acetylenes and 2-aminopyridines was also possible, capable of forming multiple heteroatomic bonds with

synthetically useful isolated yields across a range of examples [76]. Methodological creativity also yielded a number of catalysts and promoters: microwave/clay protocol [35,77], $ZnCl_2/SiO_2$ [78] or $InBr_3$ [79] promoted one-pot condensations, graphene-oxide carbocatalysis [80] for recyclable, metal-free routes to 3-sulfenyl substituted 1,2-*a*, as well as photocatalyzed reaction, exploiting eosine as a catalyst [81].

Post-GBB complexity escalation has also become a routine tactic: as an example, simple GBB adducts can be obtained by retro-aza-ene/A^3-like cascades into fused isoquinoline–imidazo[1,2-*a*]pyridine systems or tetracyclic frameworks, thus positioning the multicomponent reaction product as an effective strategy towards much higher architectural complexity [82,83]. Also, a sonochemical GBB variation, catalyzed by *p*-toluenesulfonic acid, has been developed, providing yields up to 90% [84].

Also, alternative three-component reactions could be used in the synthesis of 1,2-*a*, like Ugi's reaction using 2-pyridinecarboxaldehyde, 2-aminopyridine and an isonitrile, in the presence of scandium triflate as a catalyst [85].

Post-synthetic functionalization has also been proved viable, especially arylation. In this context, the use of a palladium catalyst afforded substitution both on the main 1,2-*a* core [86] and on sp^2 pendants [87].

2.3. Imidazo[4,5-b]pyridines and Imidazo[4,5-c]pyridines

The synthetic accessibility of imidazo[4,5-*b*]pyridines (4,5-*b*) and imidazo[4,5-*c*]pyridines (4,5-*c*) has evolved considerably over the past two decades, although these systems remain somewhat less straightforward to access than their 1,2- and 1,5-fused counterparts. The difference arises from the less reactive positions on the pyridine ring and the absence of a general multicomponent strategy like the Groebke–Blackburn–Bienaymé reaction exploited for the 1,2-regioisomer. As a result, most successful approaches rely on stepwise annulation or reductive condensation between appropriately functionalized pyridines and simple one-carbon donors [88] (Figure 5). Reductive tandem cyclization of 2-chloro-3-nitropyridine also proved effective as a synthetic route for such systems, with the use of a green solvent mixture (water and isopropyl alcohol) resulting in an additional value [89]. The classical condensation of diaminopyridines with carboxylic acids or their derivatives remains the cornerstone of synthetic methodology for both the 4,5-*b* and 4,5-*c* series [90]. As an example, heating 2,3-diaminopyridine in neat formic acid for several hours afforded 1*H*-4,5-*b* in yields exceeding 70%, while the analogous 3,4-diaminopyridine gave the corresponding 1*H*-4,5-*c* under identical conditions [91]. The use of polyphosphoric acid (PPA) as the condensing agent typically improves both rate and conversion, frequently providing isolated yields up to 85%, as well as inhibiting the formation of side products [92]. Using microwave-assisted methodologies also positively affects reaction yields, even using silica gel as a solid support and carboxylic acids or esters as carbonyl partners, exhibiting excellent chemoselectivity toward mono-condensed products [93,94].

Subsequently, several catalytic or solvent-free improvements have been reported. As an example, a solvent-free condensation between 2,3-diaminopyridines and esters has been developed, using lithium bromide as a catalyst, affording 2-substituted 4,5-*b* in up to 90% yield with simple work-up and minimal waste [95]. The same condensation principle could also be applied for the synthesis of fluoroalkyl-substituted 4,5-*b*, demonstrating exceptional tolerance for strongly electron-withdrawing substituents [96].

Alternative dehydrating or oxidative systems have also proven effective when using a picolinothioamide intermediate derived from nitriles and methyl carbimidate, cyclizing it with ammonium polysulfide in ethylene glycol to give both 4,5-*b* and 4,5-*c* derivatives [97]. A mild air-oxidative, water-mediated condensation could also be used, reacting 2,3-diaminopyridines with aldehydes without any added oxidant [98].

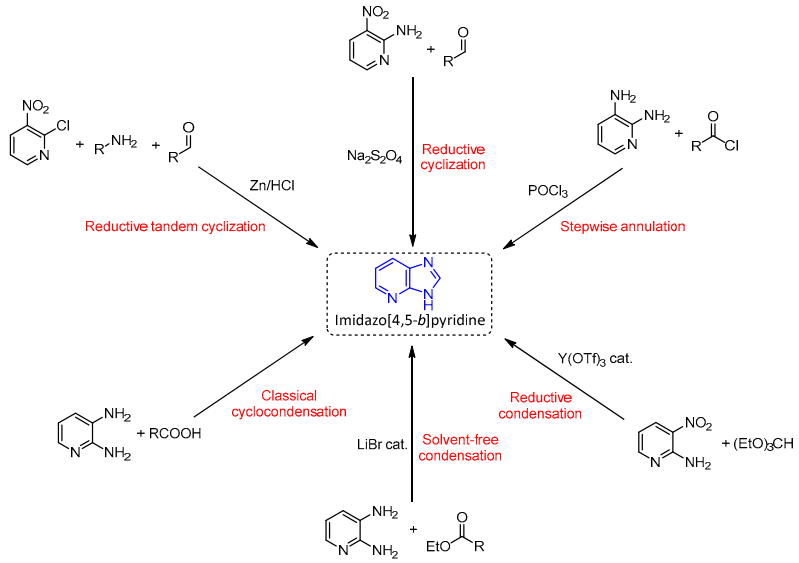

Figure 5. Selected examples of synthetic strategies towards imidazo[4,5-*b*]pyridines. Changing regioisomer of the starting pyridine derivative gives imidazo[4,5-*c*]pyridines.

Metal-assisted and reductive annulation routes further expanded the scope of these frameworks. Ytterbium(III) triflate can efficiently catalyze the condensation of 3,4-diaminopyridines with triethyl orthoformate to produce 4,5-*c*, offering high functional-group tolerance under relatively mild conditions [99]. In a complementary reductive variant, 3*H*-4,5-*b* could be prepared by reacting aldehydes with 2-nitro-3-aminopyridines, using sodium dithionite ($Na_2S_2O_4$) as a dual reductant and cyclizing agent, and employing ketones and $SnCl_2/HCO_2H$ to give comparable or higher yields (typically 70–85%) [100].

Finally, solid-state synthesis was effective as well, generating both the 4,5-*b* and 4,5-*c* isomers from common precursors (e.g., starting from 2,4-dichloro-3-nitropyridine and diverging in the functionalization sequence to afford both isomers), thereby enabling head-to-head screening of both scaffolds from the same synthetic route [101].

Across this wide methodological spectrum, the yields achieved by modern protocols typically range from 70% to 95%, and product selectivity strongly favors the desired *N*-fused framework. Collectively, the available data show that 4,5-*b* and 4,5-*c*, once challenging to obtain, can now be accessed reproducibly and efficiently by choosing among several complementary routes. This diversity of options has effectively removed synthetic accessibility as a limiting factor for the exploration of these pharmacologically important fused systems.

3. Imidazopyridines as Ligands in Coordination Chemistry

3.1. Imidazo[1,5-a]pyridines

1,5-*a* are good, versatile ligands for coordination chemistry because they combine a rigid fused heterocycle with a nitrogen donor site and a scaffold that tolerates many substituents (i.e., additional donor atoms) without losing planarity or donor ability. In many complexes the ligand behaves as a bidentate N^N chelator, giving well-defined five- or six-membered chelate rings that stabilize mono- and polynuclear coordination compounds. Chelation is often observed through the imidazole-type nitrogen together with a pendant pyridinic nitrogen when a 2-pyridyl substituent is introduced in positions 1 or 3 [102–104].

Because 1,5-*a* are structurally compact but electronically tunable, they have been used to control metal coordination geometry: they form tetrahedral (e.g., Zn(II) mono/bi/tris-chelates) [105], square-planar (Pd(II) [106], Pt(II) [107]) and octahedral coordination en-

vironments depending on metal ancillary ligands and substitution pattern on the heterocycle [108,109], as well as macrostructures such as molecular cylinders [110]. X-ray crystallography documents these geometries and shows that small changes in ligand substitution (e.g., 1-aryl vs. 1-pyridyl, or substitution on the imidazo ring) change bite angles and overall complex topology [111].

Where the imidazole ring is functionalized at C3 to give an ylidene (N-heterocyclic carbene, NHC [20,29,112–114]), or when sulfur/oxygen substituents are used, mixed-donor C/S [115] or C/O [116–119] coordination modes are observed, producing stable coordination complexes. These alternative donor modes broaden the ligand's utility for building well-defined coordination architectures.

A commonly exploited design motif is to attach a 2-pyridyl arm at C1 so that the internal imidazole N and the pendant pyridyl N atoms form a robust chelate, while additional functional groups (e.g., bridging methylene [120,121] or phenyl [122,123] group) can make the ligand ditopic or even polytopic [124]. Following this, recent structural studies on Zn(II) coordination polymers and 1D/2D frameworks explicitly show how linear ditopic 1,5-*a* derivatives act as nodes or propagation units in extended architectures [125].

In light of the above, the coordination motifs in 1,5-*a* can be defined as very variable and strongly dependent on the substitution on the core moiety (Figure 6).

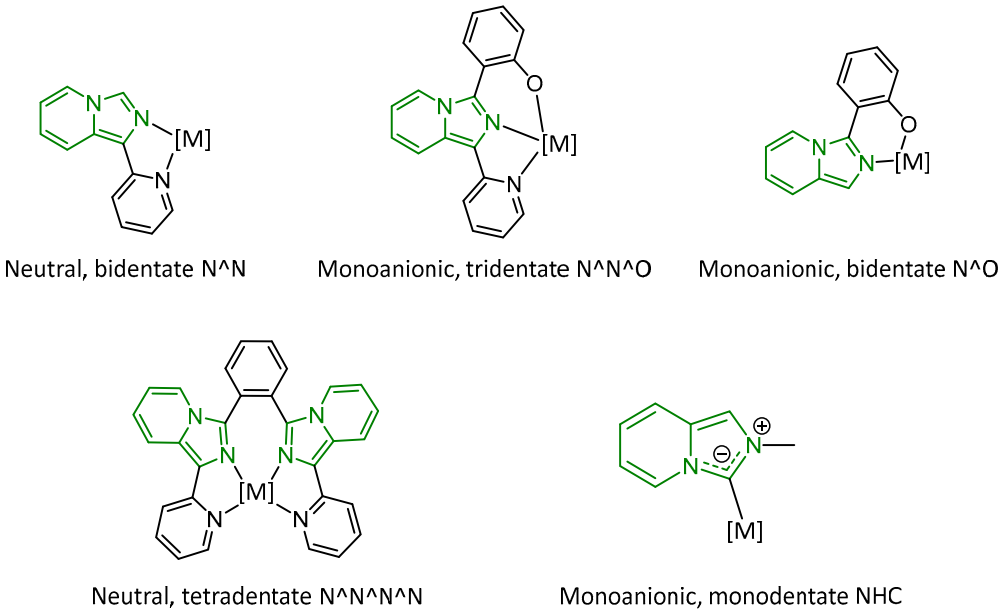

Figure 6. Possible coordination modes in substituted imidazo[1,5-*a*]pyridines.

3.2. Imidazo[1,2-a]pyridines

1,2-*a* make convenient and flexible ligands for coordination chemistry (Figure 7) because the fused imidazole–pyridine core offers clear donor atoms and a compact, rigid framework that tolerates many substituents, just like the 1,5 counterpart. In many compounds the heterocycle behaves as an N-donor, and where two 1,2-*a* units are linked (bis- or tris-ligands), they can act as bidentate or tridentate chelators that form well-defined five- or six-membered chelate rings with metals [126,127].

Different metals and ligand substitution patterns give predictable geometries: homoleptic Zn(II) complexes with bis-1,2-*a* ligands are often pseudo-octahedral highly symmetric cationic species [127] or tetrahedral coordination compounds [128], while first-row transition metals coordinated by 2,6-bis(imidazo[1,2-*a*]pyridin-2-yl)pyridine-type ligands commonly adopt distorted octahedral coordination at an Fe(II) center [126]. Discrete

Cu(II) species are also reported when the ligands and ancillary anions favor octahedral geometries [129].

Several papers report Zn(II) and Cd(II) coordination polymers built from ditopic 1,2-*a* ligands and simple carboxylate co-linkers, with crystallographic descriptions of the resulting 1D/2D networks and their packing motifs [130].

Modified 1,2-*a* also supports alternative donor behavior: examples in the literature show imidazole cores converted into N-heterocyclic-carbene (NHC) precursors (imidazo[1,2-*a*]pyridin-3-ylidenes) [131–133].

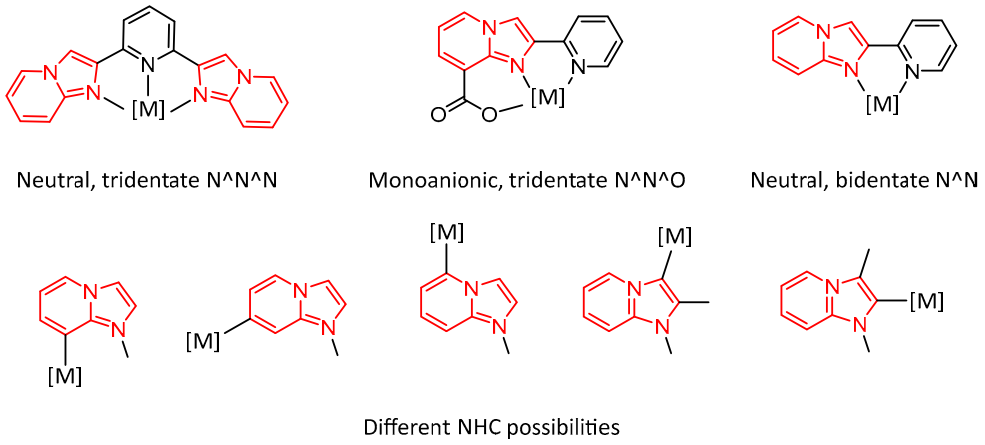

Figure 7. Possible coordination modes in substituted imidazo[1,2-*a*]pyridines.

3.3. Imidazo[4,5-b]pyridines and Imidazo[4,5-c]pyridines

4,5-*b* and 4,5-*c* are compact fused heterocycles whose ring topology gives clear donor sites and predictable coordination behavior. Nevertheless, structural work on coordination compounds with these systems is somewhat limited [134], as they are usually studied for their relevant biological properties, rather than as ligands in coordination chemistry. Still, this class has been proven to also be able to act as an NHC ligand [135] (Figure 8).

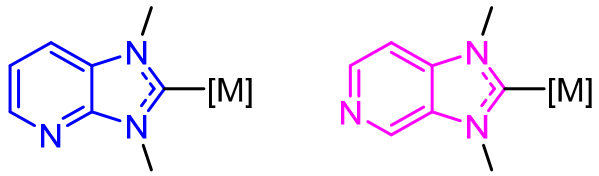

Figure 8. NHC derived from imidazo[4,5-*b*]pyridines and imidazo[4,5-*c*]pyridines.

4. Luminescence Properties of Imidazopyridines Compounds

4.1. Imidazo[1,5-a]pyridines

1,5-*a* present a compact, rigid fused-ring π-system whose lowest excited states are generally involved in locally excited π→π* transitions [136] with varying degrees of intramolecular charge-transfer character when donor/acceptor substituents are present [137]. Substitution patterns and electronic properties give predictable and reproducible shifts in these basic parameters. Introducing π-extending aryl groups [138,139] (Figure 9a) or electron-donating substituents [140] at positions conjugated to the fused core (Figure 9b) produces bathochromic shifts in both absorption and emission (λ_{abs} commonly moves toward 350–390 nm and λ_{em} toward 430–500 nm) and, when planarity is preserved, substantially increases the fluorescence quantum yield. Conversely, strongly electron-withdrawing substituents tend to slightly shifted towards blue bands and to lower fluorescence quantum yield (Φ_F) because of enhanced non-radiative decay pathways (intersystem crossing or in-

ternal conversion) [141]. Furthermore, contrary to what might be expected, hydrogenation of the pyridinic ring also results in an increase in the fluorescence quantum yield [119,142].

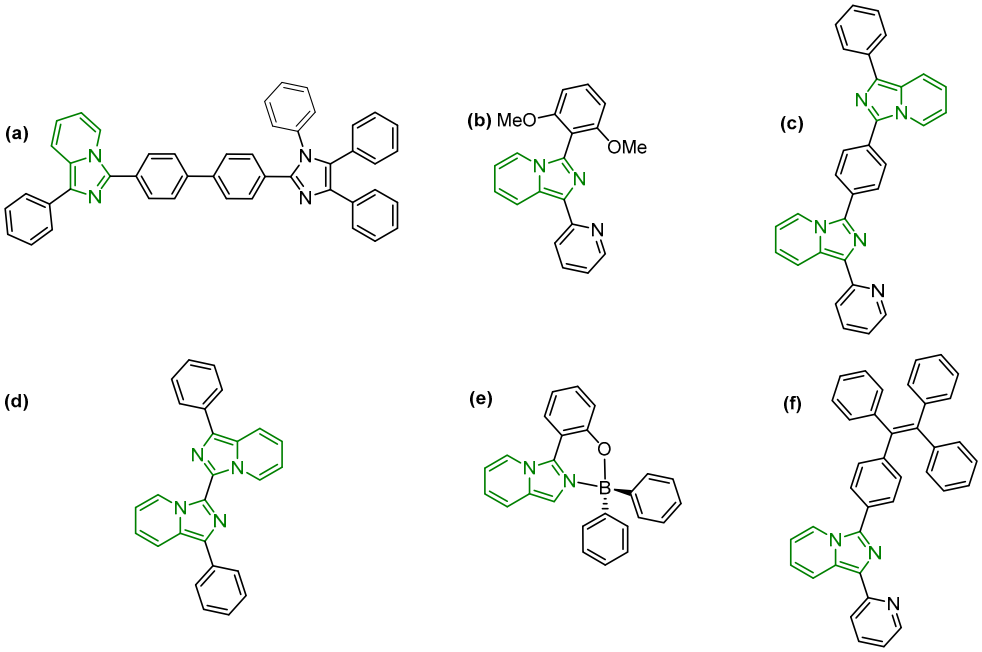

Figure 9. Selected examples of luminescent imidazo[1,5-*a*]pyridine compounds reported in this section. See text for the reported subfigures.

Solvent polarity and local environment can modulate emission through modest intramolecular charge-transfer (ICT) character present in many substituted 1,5-*a* derivatives. Solvatochromic studies on 1,5-*a*-derived dyes (Figure 9a) confirm that increasing solvent polarity frequently produces a red-shift in the emission maximum, consistent with stabilization of a more polar excited state (ICT/charge-transfer character). For example, in a donor–π–acceptor (D–π–A) series based on 1,5-*a* as the donor core, a clear positive solvatochromism was documented: switching from a low-polarity (hexane) to a high-polarity (acetonitrile) solvent caused a red-shift of ~85–90 nm in the photoluminescence spectra [138]. In the same series, this shift was accompanied by broadening of the emission band and disappearance of vibrational fine structure in polar media, which is typical for excited states with charge-transfer character. Moreover, 1,5-*a*-based probes (Figure 9c) in various organic solvents displayed an appreciable CT character, with the emission maxima shifting systematically with solvent polarity, revealing a linear correlation typical of Lippert–Mataga type behavior [143]. Also, reversible acido-chromic emission could be observed in dimeric 1,5-*a*, with a red shift of the emission spectra in an acidic environment reverting back upon addition of a base [144] (Figure 9d). Furthermore, it has been proven that the nature and the position of the linker for the dimerization influence the photophysical properties of the whole system [145]. Interestingly, also in monomeric 1,5-*a* species (Figure 9e), positions are important in determining the luminescence properties: in boron complexes, the presence of a phenolic substituent can either increase or quench fluorescence emission due to the activation of intersystem crossing depending on the position of the substitution (1 or 3, respectively) [146].

Aggregation and solid-state packing can also have a pronounced effect for many 1,5-*a* derivatives. Several independent experimental reports show weak or quenched fluorescence in dilute solution (PLQY < 0.05) but strong, often greenish emission in the aggregated or crystalline state, a behavior assigned to restriction of intramolecular rotation (RIR) and aggregation-induced emission (AIE) [147] (Figure 9f). In some other cases instead,

1,5-*a* boron complexes displayed intense fluorescence emission both in solution and in solid state, without experiencing any dramatic quenching [148] (Figure 9e).

Conversely, other boron coordination compounds based on the 1,5-*a* framework have exhibited the opposite behavior, showing a decrease in luminescence intensity upon going from solution to the solid state [116,117]. Moreover, in the solid state, the presence of π–π stacking interactions completely quenches fluorescence, whereas the absence of such interactions allows fluorescence to persist, albeit with low quantum yields (Figure 10).

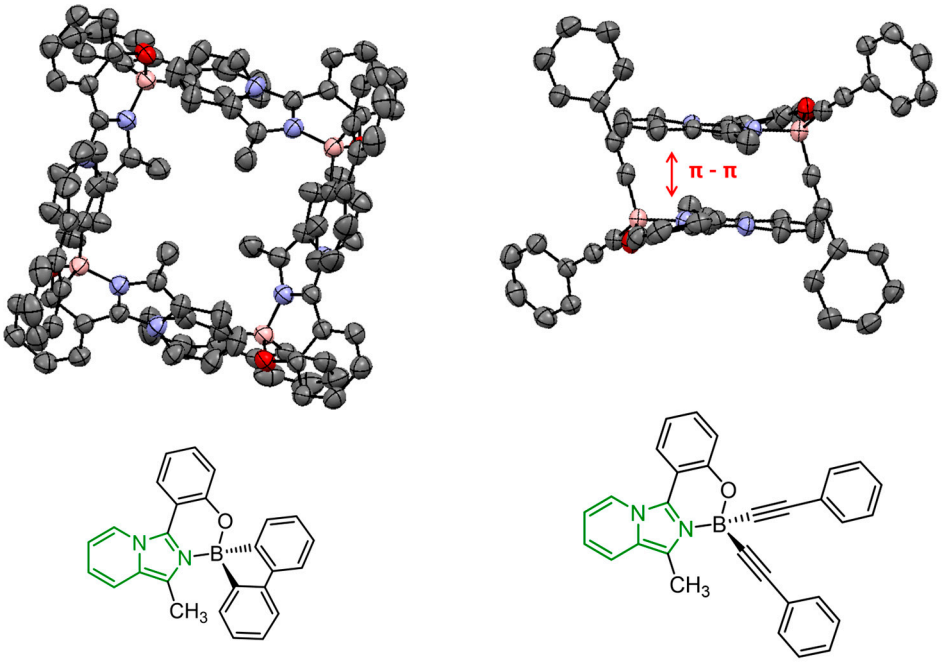

Figure 10. Example of how the π–π stacking can be present and interfering with the emission properties in the solid state of boron complexes of imidazo[1,5-*a*]derivatives (grey, carbon; light blue, nitrogen; red, oxygen; pink, boron). Hydrogens have been omitted for clarity.

Coordination to closed-shell metal centers typically increases rigidity, shifts absorption/emission energies and commonly enhances PLQY relative to the free ligand. Careful photophysical studies of mono-, bis- and homoleptic Zn(II) 1,5-*a* complexes show systematic hypsochromic or bathochromic shifts depending on coordination geometry and ligand substitution, and improved quantum yields (examples in the literature report ligand-centered emission peaks in the 410–490 nm window for Zn adducts with PLQY values that can reach the mid-tens of percent) [105,149,150]. Time-resolved experiments in those same papers show that the improved brightness is mainly due to increases in the radiative rate constant (k_r) upon coordination and concurrent suppression of low-energy non-radiative channels. Coordination to Zn(II) centers typically increases rigidity, causes blue-shifts in emission (e.g., ligand vs. complex shifts from 460 nm ca. to 440 ca. range across a family) and can raise quantum yields substantially (examples cited report quantum yields up to the low-30% range) [151] (Figure 11).

Notably, a series of homoleptic Zn(II) complexes also displayed unusual symmetry-broken charge-transfer excited states, underlining that metal coordination can do more than simply rigidify the ligand, like also changing excited-state character [152] (Figure 12a).

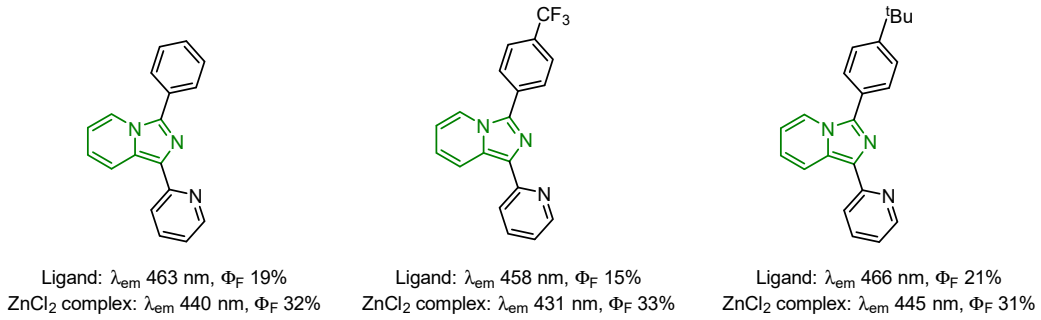

Figure 11. Example of how zinc coordination can affect the fluorescence properties in imidazo[1,5-*a*]pyridine.

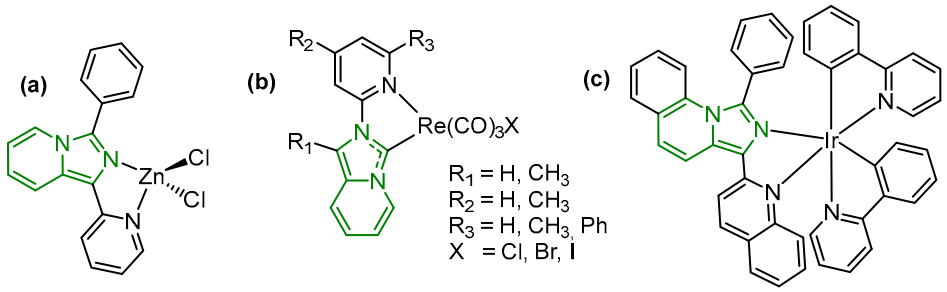

Figure 12. Selected examples of luminescent imidazo[1,5-*a*]pyridine metal coordination compounds reported in this section. See text for the reported subfigures.

Heavier-atom incorporation and coordination to heavy d^6/d^8 metals (for example, Ir(III) [153,154], Pt(II) [155], Re(I) [156–158]) predictably open efficient intersystem-crossing pathways and produce phosphorescent emission with long lifetimes (microseconds to milliseconds) and structured spectra in the 500–700 nm region. Furthermore, Re(I) NHC complexes based on the 1,5-*a* isomer have been reported to exhibit significant chiroptical properties, specifically as circularly polarized luminescent emitters [159] (Figure 12b).

Thermal Activated Delayed Fluorescence (TADF, delayed fluorescence via reverse intersystem crossing from T_1 to S_1) is not commonly reported for simple 1,5-*a* derivatives. To obtain TADF, a small singlet-triplet gap (ΔE_{ST}) and appropriate donor-acceptor separation are needed [160]. While some recently engineered D–π–A 1,5-*a* systems and fused heterocycles have been tested for delayed fluorescence behavior or used in OLED-oriented studies [152], the mainstream photophysical response of the family remains prompt fluorescence or, in heavy-atom/metalated systems, phosphorescence [155], with a single example of TADF displaying Ir(III) complex [153] (Figure 12c). Moreover, unlike the other regioisomers, 1,5-*a* derivatives are not known to exhibit excited-state intramolecular proton transfer (ESIPT) [161].

4.2. Imidazo[1,2-a]pyridines

The 1,2-*a* core exhibits a markedly different electronic distribution from its 1,5-*a* counterpart: fusion at the N(1)–C(2) bond positions of the imidazole nitrogen adjacent to the pyridine ring leads to a stronger π–π conjugation and a higher-lying HOMO delocalized over both rings. This connectivity produces characteristic photophysical fingerprints as π→π* transitions at higher energy ($\lambda_{abs} \approx$ 280–340 nm) and blue-shifted fluorescence ($\lambda_{em} \approx$ 360–460 nm) compared to the 1,5-*a* isomers [162–164]. Experimental absorption spectra consistently show two intense π→π* bands, one centered near 310 nm and a secondary CT-enhanced band near 340 nm, both sensitive to electronic substitution.

Substitution at position 2 or 3 profoundly tunes emissive behavior [164–166]. Electron-donating aryl or alkoxy groups extend conjugation, pushing emission toward the green

region while increasing fluorescence quantum yields in rigid derivatives. Conversely, strong electron-withdrawing substituents stabilize the LUMO and favor non-radiative decay, decreasing PLQY. These trends are quantitatively confirmed by time-resolved studies: rigid donor–acceptor systems display single-exponential decays with lifetimes of 3–8 ns, while flexible or twisted analogues show biexponential kinetics with a fast (<1 ns) non-radiative component. Increasing the dimension of the π system is also a way to improve the photoluminescence performances in 1,2-*a* derivatives, with examples reporting naphthalene-fused 1,2-*a* with large Stokes shifts and quantum yields up to 77% [167] (Figure 13a).

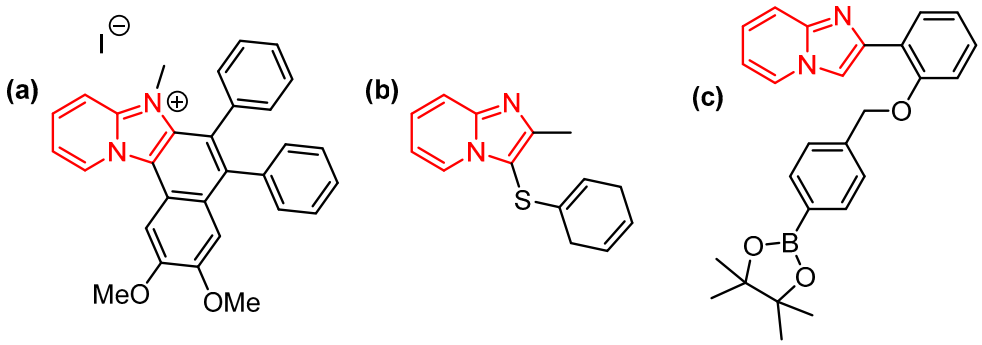

Figure 13. Selected examples of luminescent imidazo[1,2-*a*]pyridine compounds reported in this section. See text for the reported subfigures.

Solvent and medium effects highlight the partial intramolecular charge-transfer (ICT) character of the S_1 state. Multiple solvatochromic studies report emission red-shifts of 20–50 nm and significant lifetime shortening when moving from toluene to acetonitrile or DMSO [168]. The observed positive solvatochromism can correlate with increased excited-state dipole moments ($\Delta\mu \approx 4$–8 D from Lippert–Mataga analyses), confirming ICT contributions typical of 1,2-*a* fusion but less pronounced than in classical donor–acceptor dyes, with the possibility for these same compounds to also display two-photon absorption behavior [169] (Figure 13b). Aggregation and crystal packing also play a critical role in modulating emissive output with substituted derivatives displaying aggregation-induced emission (AIE) exploitable in sensing experiments [170,171] (Figure 13c).

Metal coordination introduces additional, well-characterized perturbations. In some cases, coordination of 1,2-*a* to d^{10} metal via the imidazole nitrogen induces planarization/rigidification and activates or enhances fluorescence, with emission in the near-blue region (≈380–450 nm) and quantum yields up to ~0.50. In particular, Zn(II) complexes [127,172,173] often exhibit increased radiative constants (k_r up to 2–3 × 10^7 s^{-1}) and reduced non-radiative rates due to ligand rigidification. In contrast, coordination to d^6 heavy metals (particularly Ir(III) [174–176]) opens efficient intersystem crossing channels, yielding phosphorescent states that stem from mixed metal-to-ligand charge-transfer (MLCT) processes.

Particularly distinctive in the 1,2-*a* family is the occurrence of excited-state intramolecular proton transfer (ESIPT) in solution when a proximal phenolic donor (e.g., 2′-hydroxyphenyl) is introduced at position 2 (Figure 14) [37,177,178]. For instance, several derivatives exhibit ESIPT-active behavior: in a rigid (solid-state [179] or matrix [180]) environment, they show emission with large Stokes shifts, good quantum yields and emission colors tunable from blue-green to orange/red depending on substitution and crystalline packing. The polymorph-dependent luminescence, consistent with computational studies [181], indicates that suppression of non-radiative decay and stabilization of the keto tautomer in the excited state play a key role in enabling efficient ESIPT.

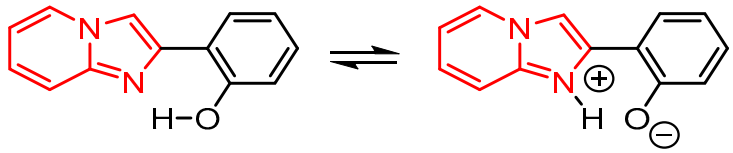

Figure 14. ESIPT process in imidazo[1,2-*a*]pyridines.

No clear evidence of TADF has been firmly established for simple 1,2-*a* systems, but a few donor–acceptor architectures with spatially separated frontier orbitals and small ΔE_{ST} down to 0.01 eV were obtained, hinting at emerging TADF behavior [182] (Figure 15a). However, most emissions remain prompt fluorescence or heavy-atom-assisted phosphorescence depending on the coordination environment.

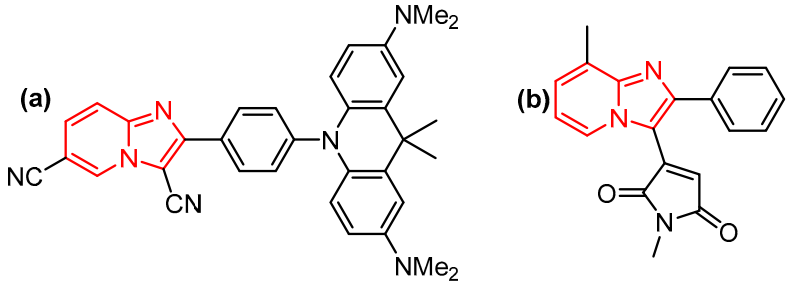

Figure 15. Other examples of luminescent imidazo[1,2-*a*]pyridine compounds reported in this section. See text for the reported subfigures.

Finally, donor–acceptor dyads based on 1,2-*a* frameworks could also be constructed and investigated from a photochemical perspective, showing the occurrence of intramolecular charge transfer and photoinduced electron transfer processes. In such systems, ground- and excited-state ICT character as well as dual fluorescence associated with excited-state conformational heterogeneity have been reported, indicating that these heterocyclic architectures can support rich and tunable photochemical behavior [183] (Figure 15b).

4.3. Imidazo[4,5-b]pyridines and Imidazo[4,5-c]pyridines

4,5-*b* and 4,5-*c* form two closely related but topologically distinct fused heterocycles whose photophysics and coordination chemistry have been increasingly documented in the literature. For the 4,5-*b* family, a clear example of protonation- and solvent-dependent photophysics comes from iminocoumarin-type derivatives [184] (Figure 16a): in these systems, comprehensive UV–Vis and fluorescence titrations, combined with TD-DFT computations, show that protonation equilibria (and solvent polarity) significantly shift both absorption and emission wavelengths. This demonstrates that 4,5-*b* scaffolds can exhibit marked sensitivity to environment and substitution pattern, making them viable candidates for pH- or solvato-responsive dyes.

The pyridinic nitrogen position in regioisomers of the same 4,5-*b* pyridine derivative also can play a role in determining the photophysical properties of these systems [185]: even subtle variations in nitrogen placement led to pronounced differences in UV/Vis absorption and fluorescence behavior (Figure 16b). Solvatochromic effects are evident in both absorption and emission spectra, with one regioisomer exhibiting hypsochromic shifts and the other bathochromic shifts. Their acid–base equilibria further modulate the photophysical response, as reflected in distinct pK_a values and differential spectral changes under acidic conditions.

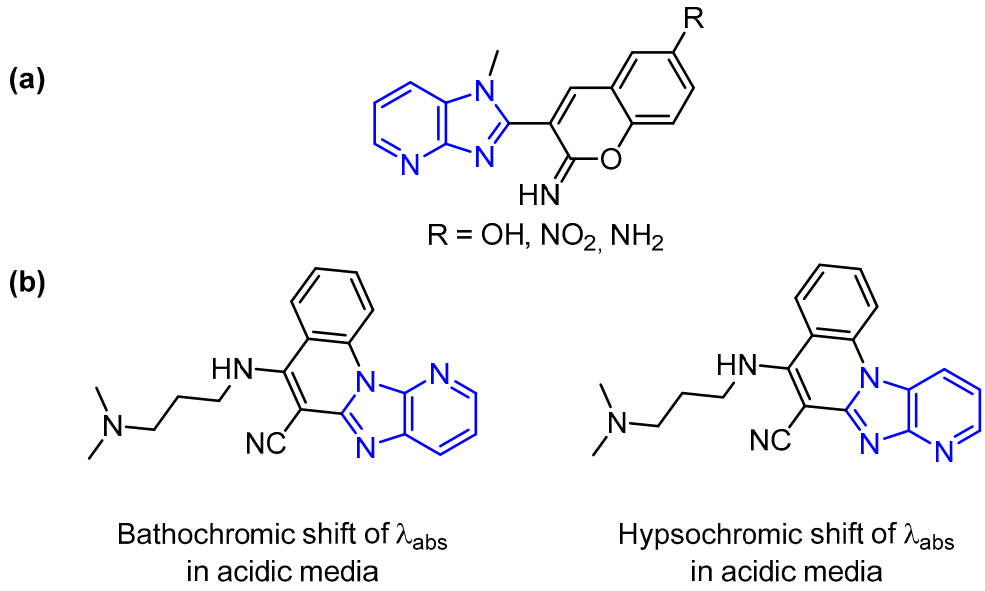

Figure 16. Selected examples of luminescent imidazo[4,5-*b*]pyridine compounds reported in this section. See text for the reported subfigures.

Coordination chemistry exerts a particularly strong influence on 4,5-*b*/4,5-*c* photophysics, both by rigidifying the ligand and by altering excited-state character. Ligands of the 4,5-*b* type have been used as cyclometallating chelates for heavy-metal complexes, and recent advanced-materials reports show that carefully functionalized 4,5-*b*-derived chelates give very high photoluminescence quantum yields and narrow blue emission when bound to Ir(III) [186] (Figure 17a). For example, blue-emissive Ir(III) complexes containing cyano-modified 4,5-*b*-based chelates have been reported with emission maxima in the 448–467 nm range and exceptionally high photoluminescence quantum yields (reported up to ~81–88%) in toluene solution [135]. Pt(II) complexes could be obtained as well, displaying aggregation-induced emission and aggregation shortening of phosphorescence lifetimes, giving excellent blue phosphorescent emitters with fluorescence quantum yields up to more than 90% [187] (Figure 17b).

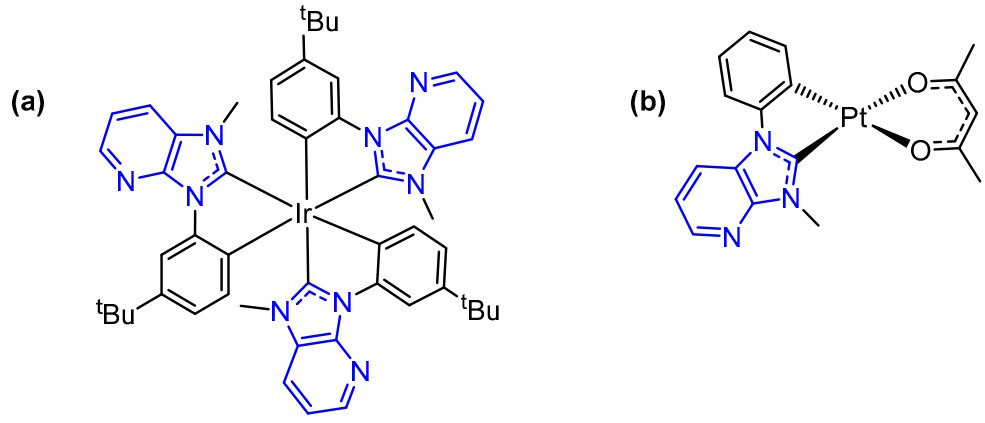

Figure 17. Selected examples of luminescent imidazo[4,5-*b*]pyridine coordination compounds reported in this section. See text for the reported subfigures.

These studies make it clear that the 4,5-*b* core can serve as a highly efficient cyclometallating fragment that, when combined with appropriate electron-withdrawing substituents (e.g., cyano or CF_3 groups), yields bright, narrowband blue phosphors.

Although coordination to closed-shell d^{10} centers (e.g., Zn(II), Ag(I)) is a common strategy to rigidify N-heterocyclic ligands and modulate their photophysics, no systematic studies have yet demonstrated that this leads in a reproducible way to enhanced fluorescence or predictable emission shifts for 4,5-*b*. The absence of well-characterized coordination complexes with full photophysical characterization suggests this remains an open area for research.

Among the 4,5-*c* isomers, there are very few studies about their photophysical properties. In particular, they have been proved to be ESIPT-active if adequately substituted (i.e., with a phenolic group) (Figure 18) [188,189]. These molecules commonly display dual fluorescence arising from normal and tautomeric excited states, with the two bands well separated and associated with distinct nanosecond lifetimes, reflecting clean parallel decay pathways rather than complex multicomponent kinetics. The ESIPT-generated tautomer emission is typically solvent-dependent, often exhibiting negative solvatochromism (with a blue shift in more polar media) consistent with an excited tautomeric form of lower polarity than its ground-state precursor. At the same time, the presence of an intramolecular O–H···N hydrogen bond tends to suppress competing ICT or twisted-ICT (TICT) relaxation channels, stabilizing the proton-transfer pathway even in highly polar or protic environments.

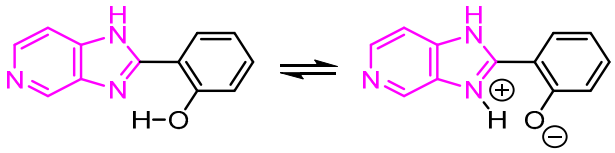

Figure 18. ESIPT process in imidazo[4,5-*c*]pyridines.

In related analogues lacking the hydrogen-bond donor, the photophysics shift toward charge-transfer emission with reduced intensity and broadened, red-shifted bands, underscoring how the 4,5-*c* topology places substituents in a geometry that strongly favors intramolecular H-bonding. When this interaction is present, the result is large Stokes shifts, robust dual emission, and pronounced sensitivity to solvent and proton-donating ability, making ESIPT-active 4,5-*c* derivatives one of the most responsive subclasses within the imidazo-fused heterocycles.

5. Optoelectronic Devices Incorporating Imidazopyridines

5.1. Imidazo[1,5-a]pyridines

The bicyclic 1,5-*a* structure has emerged as a particularly versatile and promising scaffold in the design of optoelectronic materials, thanks to its unique structural and electronic characteristics. Structural modifications such as donor–π–acceptor (D–π–A) conjugation, substitution with long alkyl chains to enhance solubility and film formation, or ionic quaternization to generate salts for LECs have been shown to manipulate key parameters including photoluminescence quantum yield (PLQY), emission wavelength, Stokes shift and solid-state behavior.

For instance, BF_2-chelated 1,5-*a* phenolates bearing long alkyl chains exhibit blue emission both in solution and in thin polymeric films, with large Stokes shifts and good fluorescence yields [190] (Figure 19a).

The presence of a long alkyl chain improves the film-forming properties and increases the solubility in organic media, necessary for solution-processed devices. Similarly, hybrid white LEDs have been fabricated by using D–π–A 1,5-*a*-based fluorophores as down-conversion layers, producing devices with a color rendering index (CRI) of ~90% and CIE *x*,*y* coordinates of ~(0.37,0.32), with solid-state quantum yields up to 93% [138]. Increasing

delocalization also positively affects the device performance: for example, expanding the ring from imidazopyridine to imidazoquinoline increased the fluorescence quantum yield and decreased the HOMO-LUMO gap, eventually leading to a first test of OLED fabrication [191] (Figure 19b). Solution-processed sky-blue OLEDs could also be fabricated, with a maximum EQE of 4.3% and a good current efficiency of 8.4 cd A^{-1} at 100 cd m^{-2} [192].

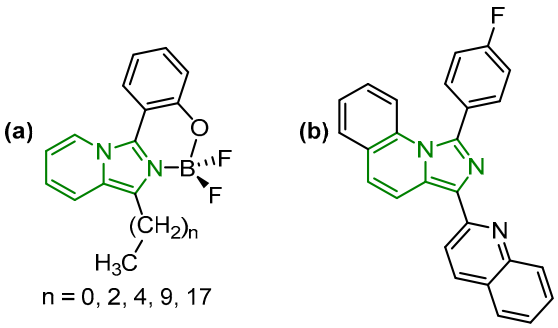

Figure 19. Selected example imidazo[1,5-*a*]pyridine compounds reported in this section. See text for the reported subfigures.

Ionic 1,5-*a* derivatives have also been used in LECs, where the quaternization of a pendant pyridinic nitrogen provides mobile counter-ions that facilitate in situ electrochemical doping under bias [122] (Figure 20a). 1,5-*a* derivatives could be used in LECs even without quaternization, using TMPE:LiOTf (TMPE: trimethylolpropane ethoxylate) for ion mobility. For example, 3-(2-methoxyphenyl)-5-methyl-1-(6-methylpyridin-2-yl)imidazo[1,5-*a*]pyridine emits blue light (~436 nm) in solution with a quantum yield of ~0.40, but aggregation in the solid state leads to yellow-shifted emission. When incorporated into LEC devices, electroluminescence shifts further, highlighting the importance of controlling film morphology to achieve optimal device performance [193].

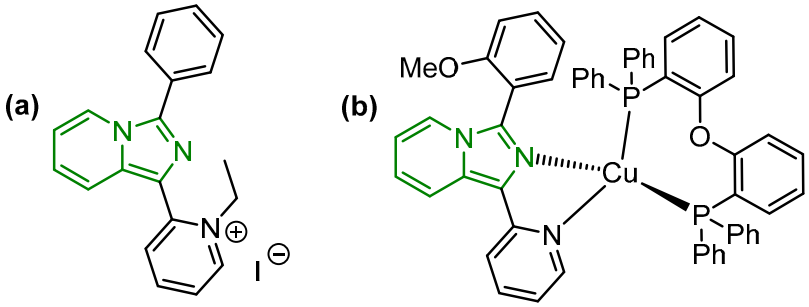

Figure 20. Selected examples imidazo[1,5-*a*]pyridine compounds used in LEC devices reported in this section. See text for the reported subfigures.

LECs based on heteroleptic copper(I) complexes, such as [Cu(1,5-*a*)(POP)][PF_6], (POP: bis{2-(diphenylphosphanyl)phenyl}ether) further illustrate that metal coordination can tune device emission: while photoluminescence is blue (~450 nm) in solution, electroluminescence in the device shifts to ~550 nm due to film and excited-state effects [194] (Figure 20b).

Despite these advances, challenges remain, including the scarcity of high-efficiency deep-blue 1,5-*a* emitters, limited operational lifetimes for full-color devices, and underexplored photovoltaic applications, with few studies exploring the optoelectronic and charge carrier properties of such compounds [195]. Moreover, thin-film morphology control remains crucial, as the difference between quantum yields in the solid state and device performance often reflects exciton quenching, film formation, and interface effects. For these reasons, the applications of 1,5-*a* derivatives in optoelectronic devices remain limited.

5.2. Imidazo[1,2-a]pyridines

The literature on 1,2-*a* derivatives exploited in optoelectronic applications is broader than that of the 1,5-*a* counterpart. Structural modification at multiple positions allows fine-tuning of absorption and emission wavelengths, frontier orbital levels, and solid-state behavior, making 1,2-*a* derivatives attractive for electroluminescent devices such as OLEDs and LECs, and as electron-transporting or acceptor units in organic photovoltaics. Early studies highlighted these derivatives as bright luminogens with quantum yields up to ~70%, depending on substitution, displaying strong solvatochromism and indicating their potential in electroluminescent applications [196] (Figure 21a).

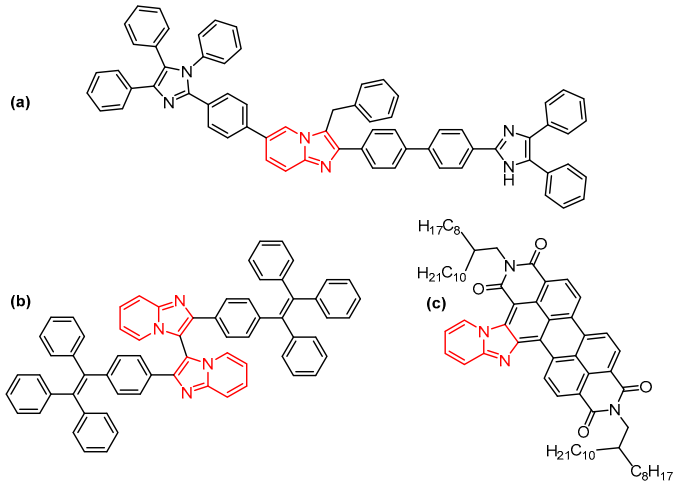

Figure 21. Selected examples of imidazo[1,2-*a*]pyridine compounds reported in this section. See text for the reported subfigures.

A major advance in OLED applications was achieved by pairing 1,2-*a* cores as electron acceptors with robust donor units such as phenanthroimidazole [197]. For example, two reported deep-blue emitters based on this motif exhibited non-doped OLED external quantum efficiencies (EQEs) of 4.85% and 4.74% at ~10,000 cd m^{-2}, respectively. When used in doped devices (20–40 wt%), the EQEs increased to 5.23% and 6.13%, with CIE *x*,*y* coordinates of (0.15, 0.08 for deep-blue emission. These devices exemplify the suitability of this class of compounds as an electron-accepting unit in efficient deep-blue OLEDs with low efficiency roll-off, highlighting the importance of donor-acceptor design and careful device and molecular engineering.

More recently, aggregation-induced emission luminogens (AIEgens) incorporating 1,2-*a* have demonstrated the versatility of this scaffold. These compounds combine 1,2-*a* cores with sterically hindered tetraphenyl ethylene units to suppress aggregation-caused quenching [198] (Figure 21b). In vacuum-deposited non-doped OLEDs, these compounds emitted cyan light at 496 nm (CIE*x*,*y* = 0.23, 0.42) with a luminance of 4420 cd m^{-2}, and an EQE of 15.6%, or orange emission at 623 nm (CIE*x*,*y* = 0.59, 0.38) with a maximum luminance of 2740 cd m^{-2} and an EQE of 10.9%. These results illustrate that judicious structural design can yield non-doped emissive layers with high efficiency and tunable emission colors while maintaining good morphological stability.

Coordination to heavy metals, such as Ir(III), enables efficient activation of the triplet excited state through enhanced spin–orbit coupling, thereby allowing phosphorescent emission [174,176]. As a result, 1,2-*a*-based ligands coordinated to Ir(III) can give rise to phosphorescent OLEDs, benefiting from efficient harvesting of both singlet and triplet excitons and leading to high electroluminescence efficiencies.

1,2-*a* derivatives have also been incorporated into extended π-systems for charge transport. For example, perylene diimide (PDI) molecules functionalized with 1,2-*a* act as n-type semiconductors in organic field-effect transistors (OFETs), with reported electron mobilities of ~0.116 cm^2 V^{-1} s^{-1} [199] (Figure 21c). While the latter study focuses on transport rather than emission, they underscore the versatility of this class of compounds in optoelectronic device architectures, including potential photovoltaic applications, even though full Dye-Sensitized Solar Cells (DSSCs) or Organic PhotoVoltaics (OPV) metrics remain absent.

Despite the encouraging progress, challenges remain. High-efficiency blue and deep-blue 1,2-*a* OLED emitters are still less developed than commercial phosphorescent or TADF emitters, and, therefore, devices such as LECs, solar cells or down-conversion layers, are underexplored.

In conclusion, 1,2-*a* derivatives represent a functionalizable, electronically tunable and increasingly device-relevant class of materials. Their combination of rigid fused-ring frameworks, donor-acceptor tunability and coordination versatility enables applications in deep-blue and multi-color OLEDs, AIE-based non-doped devices, and charge-transport architectures. With continued advances in thin-film processing, structural design, and device engineering, 1,2-*a* derivatives are poised to play an increasingly important role in next-generation optoelectronic devices.

5.3. Imidazo[4,5-b]pyridines and Imidazo[4,5-c]pyridines

Although well established in heterocyclic chemistry, the 4,5-*b* and 4,5-*c* ring systems have only recently been examined for their optoelectronic properties in device-oriented applications. In particular, Ir(III)-carbene complexes based on the 4,5-*b* skeleton produced a string of high-efficiency blue phosphors with reported narrow true-blue phosphorescence with high photoluminescence quantum yields and devices with EQEs up to almost 30% [186,200]. Building on that concept, peripheral engineering and cyano-substituted 4,5-*b*-derived carbenes produced Ir(III) phosphors whose photophysics ($\lambda_{em} \simeq$ 448–467 nm, PLQY = 81–88%) and radiative lifetimes in the microsecond range translated into PhOLEDs with external quantum efficiencies of up to ~34.7% in a hyper-OLED stack [135]. The iridium-carbene strategy using 4,5-*b* cyclometalates has been extended through several structural permutations (i.e., introduction of bulky ortho-substituents to suppress aggregation [201] and desymmetrization [202]), and working OLEDs (vacuum-deposited and solution-processed) have been reported, where the 4,5-*b* motif is the key emissive ligand.

Compared with the *b*-isomer, the 4,5-*c* regioisomer has been even less prominent in optoelectronic device work, with no reports to date.

6. Molecular Sensors Based on Imidazopyridines

6.1. Imidazo[1,5-a]pyridines

1,5-*a* derivatives have also become a recurring fluorescent scaffold in modern chemosensor design because the fused imidazole–pyridine core gives an easily tunable π-chromophore with large Stokes shifts and multiple points for attaching recognition motifs; this photophysical platform has been exploited both as free organic probes and as a ligand that forms emissive coordination compounds whose optical properties change on interaction with analytes.

A clear example of a 1,5-*a* chromophore used as a probe exploits the Fluorescence Resonance Energy Transfer (FRET) donor properties of such a compound, coupling it to a tricyanofuran acceptor. With this architecture, an energy-transfer efficiency of ~95% and a pseudo-Stokes shift of ≈259 nm (10,402 cm^{-1}) were reported, with a linear ratiometric response to SO_3^{2-}/HSO_3^- in two concentration ranges (1.5–7.5 μM and 9–20 μM) and

a calculated limit of detection (LOD) of about 55 nM [203] (Figure 22a). The same FRET mechanism can also be exploited in the sensing of Hg^{2+}, with even lower LOD in the μM range [204].

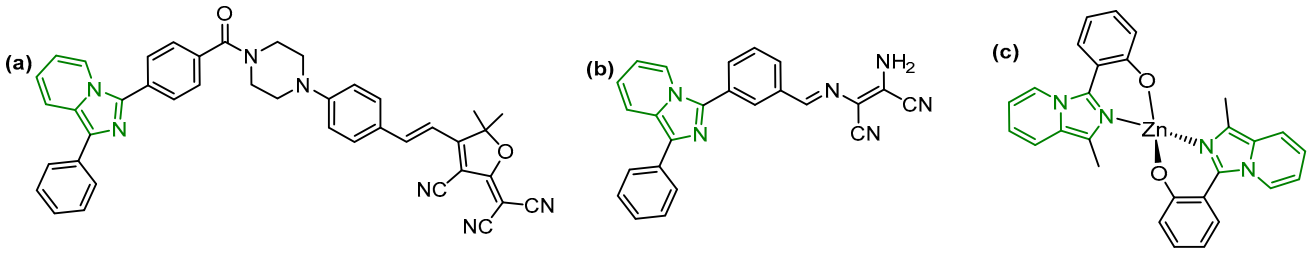

Figure 22. Selected examples of molecular probes based on imidazo[1,5-*a*]pyridine reported in this section. See text for the reported subfigures.

Additionally, the 1,5-*a* nucleus can be designed with chemo-dosimeter architectures that undergo irreversible (or quasi-irreversible) chemical transformations on reaction with the analyte. For sulfite detection, for example, a 1,5-*a*-based probe responding within one minute has been developed, showing a very large Stokes shift (~130 nm, 7933 cm^{-1}), operating across pH 5–11 and with an LOD of ~50 nM [205]. Similarly, 1,5-*a* chemo-dosimeters have been tailored to detect oxidants (e.g., hypochlorite [206] (Figure 22b)) with a mechanism comprising covalent transformation (cleavage) that abolishes/creates conjugation and produces the turn-on/turn-off optical signal. Analogously, thiophenols could be detected with an LOD of 5.6 nM upon luminescence enhancement due to an ether bond cleavage [207].

Aggregation-induced emission mechanism can also be useful for the development of 1,5-*a* probes for metal ions: conjugating the core motifs to classical AIE units (e.g., tetraphenyl ethylene, TPE) yields probes that are weakly emissive in dilute solution but become strongly fluorescent upon aggregation triggered or modulated by metal binding. On this topic, TPE-tethered 1-(2-pyridyl)imidazo[1,5-*a*]pyridine probes displaying aggregation-induced emission and selective Cu^{2+} detection with an LOD of 83 nM have been reported. These AIE designs exploit metal-induced aggregation or metal-coordination-promoted restriction of intramolecular motion as the sensing mechanism. Such a system proved to be sensitive and robust enough for the development of latent fingerprint analysis, thus revealing a possible application even in forensic sciences [147].

The coordination capability of 1,5-*a* derivatives can be exploited beyond the AIE phenomenon for sensor applications. For example, a second, important approach is to pre-coordinate 1,5-*a* ligands to d^{10} metal centers (most commonly Zn(II)) to obtain complexes whose emission is strongly ligand-centered but tunable by coordination geometry and substituents [151]. Such Zn(II) complexes therefore form a ready platform for analyte sensing either by displacement (analyte binds to Zn and perturbs emission) or by direct reaction at an ancillary site. In these regards, Zn(II) complexes have been developed for hydrogen-sulfide (H_2S/HS^-) sensing. Through spectroscopic titrations, time-resolved fluorescence and competition experiments, it has been determined that HS^- interacts with the Zn center (either through direct binding or ligand substitution), giving clear spectral changes consistent with analytical sensing of sulfide [208] (Figure 22c).

6.2. Imidazo[1,2-a]pyridines

Over the last few years, 1,2-*a* derivatives have been developed into a rich set of optical sensing motifs, both as purely organic fluorophores and as metal-coordinated luminophores. A recurring approach uses 1,2-*a* units in aggregation-induced emission (AIE) constructs, with species essentially non-emissive in solution but turning strongly

fluorescent on aggregation in the presence of Cd^{2+}, Hg^{2+} and Al^{3+}, demonstrating that metal-induced aggregation or metal-triggered restriction of intramolecular motion is a practical sensing mechanism also in this family of compounds [170] (Figure 23a).

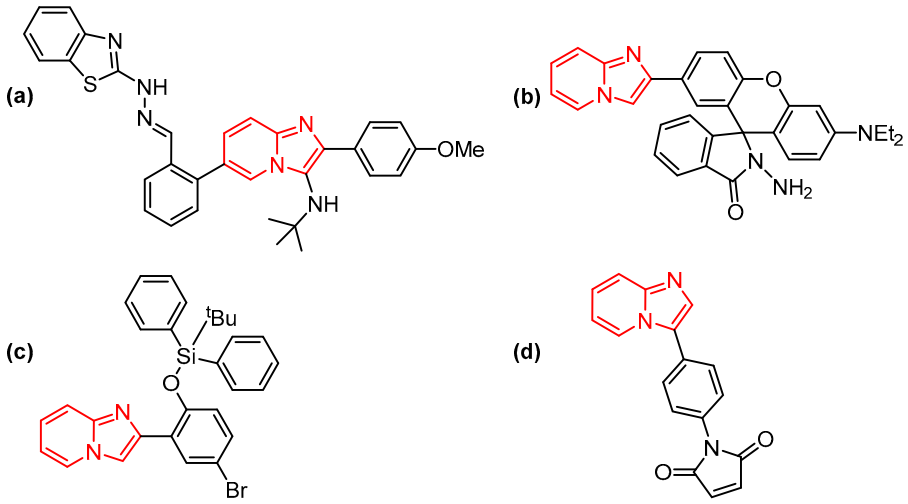

Figure 23. Selected examples of molecular probes based on imidazo[1,2-*a*]pyridine reported in this section. See text for the reported subfigures.

Closely related AIE designs have been adapted to other reactive analyte sensing: a 1,2-*a*-bearing boronate ester AIE probe has been proven effective in reacting selectively with H_2O_2, resulting in a pronounced fluorescence enhancement around 500 nm, leading to imaging applications for both exogenous and endogenous hydrogen peroxide in live cells, showing that a 1,2-*a* chromophore can be combined with a reactive handle to give a selective, cell-compatible AIE chemo-dosimeter [171].

Analogously to 1,5-*a* derivatives, a second, widely used strategy is to pre-coordinate 1,2-*a* ligands to d^{10} metal centers to make luminescent complexes whose emission is sensitive to analyte binding or displacement. Also, in this case coordination to Zn(II) resulted as the prominent strategy, as homoleptic bis-1,2-*a* Zn(II) complexes usually display robust ligand-centered luminescence, rigidification upon coordination, altering intraligand charge distribution [127], and producing photophysical behavior that can be exploited for sensing. Building on these premises, 1,2-*a* derivatives have been reported as sensors showing measurable spectral shifts and fluorescence modulation on addition of Zn^{2+}, even in the presence of competing species [172].

1,2-*a* cores have also been embedded into classic fluorophore scaffolds to provide ratiometric or "switchable" probes with defined recognition chemistry, fusing a 1,2-*a* unit to a xanthene moiety and exploiting the spirolactam ring-opening reaction to detect Hg^{2+}. As the closed spirolactam form is non-fluorescent and the addition of Hg^{2+} induces ring opening, the probe turns into a large Stokes shift (≈75 nm, 2609 cm^{-1}), strong fluorescent emitter, with good pH tolerance and low cytotoxicity. This approach has also been pushed further by using the same sensor for fluorescence imaging in HeLa cells and by paper-strip tests in water samples [209] (Figure 23b).

Complementary chemo-dosimeter designs exploit excited-state intramolecular proton transfer (ESIPT) or protective groups that are removed by specific analytes. For example, a protected a 2-(2′-hydroxyphenyl)-1,2-*a* derivative as a *tert*-butyldiphenylsilyl ether afforded a fluoride-selective ESIPT-based probe that turns on after fluoride-induced deprotection and subsequent ESIPT [178] (Figure 23c). Cyanide could be sensed as well through a nucleophilic addition mechanism that turns on fluorescence, giving LOD below the World Health Organization guidelines [85].

Several 1,2-*a*-based hydrazine and nitro-organophosphate simulant probes (multicomponent D–π–A 1,2-*a* designs) have also been reported with rapid response kinetics and low-micromolar detection limits, illustrating the scaffold's versatility for nucleophile- or electrophile-triggered sensing [210,211] (Figure 23d).

The 1,2-*a* scaffold could also afford polarity- and viscosity-sensitive sensors [212], also capable of detecting pesticides in the ppb concentration range [168].

6.3. Imidazo[4,5-b]pyridines and Imidazo[4,5-c]pyridines

Over the last years, 4,5-*b* and 4,5-*c* derivatives have been established as a compact, electron-rich class of chromophores that can be turned into effective optical sensors either as purely organic probes or after simple coordination to metals, although fewer in number than the 1,5-*a* and 1,2-*a* families. For example, attaching the 4,5-*b* core to conventional fluorophore motifs (i.e., by fusing it into iminocoumarin frameworks) produces pH-responsive chromophores whose protonation equilibria and spectral responses are readily tunable by substitution and solvent polarity: careful UV–Vis/fluorescence titrations and TD-DFT calculations demonstrated that representative iminocoumarin-4,5-*b* compounds exist predominantly as monoprotonated cations at neutral pH, undergoing double protonation between pH ≈ 3.4–4.4 and reverting to neutral species only at very high pH (≈10.4–13.7), showing solvent- and substituent-dependent absorption/emission shifts and quantum-yields up to 0.414, demonstrating that the 4,5-*b* scaffold can be used to build reliable small-molecule pH indicators [184].

Other work emphasizes metal-ion sensing through the introduction of a redox core bound to the 4,5-*b* core so that the molecule itself becomes a chemo-sensor: in these regards, ferrocenyl-4,5-*b* act as multiresponsive chemo-sensors for Hg^{2+} and Pb^{2+}, with solvent-dependent selectivity (Pb^{2+} in acetonitrile, Hg^{2+} in methanol/water mixture), after displaying clear fluorescence quenching or enhancement on metal binding [213] (Figure 24a). The same approach could be further developed, constructing self-assembling monolayers through thiol-containing derivatives and anchoring them to a gold surface. This application revealed ion-sensing electrodes whose electrochemical properties depend on the presence of Pb^{2+} ions [214] (Figure 24b). On the other hand, simple sulfur containing 4,5-*b* ferrocenyl derivatives are still effective as Hg^{2+} sensors, with LOD as low as 10^{-7}–10^{-8} mol/L [215] (Figure 24c).

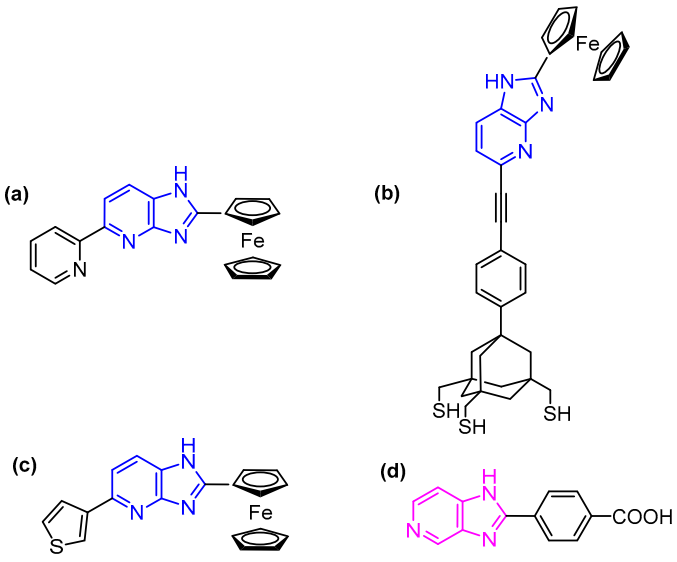

Figure 24. Selected examples of molecular probes based on imidazo[4,5-*b*]pyridine and imidazo[4,5-*c*]pyridine reported in this section. See text for the reported subfigures.

Compared to its 4,5-*b* counterpart, the 4,5-*c* isomer has not yet been the subject of sufficiently extensive experimental or theoretical investigation in this field, and key structure–property relationships remain unestablished. As a sole example, the lanthanide complexes of this regioisomer are known to form coordination polymers capable of Fe(III) sensing and Congo red adsorption through hydrogen bonding and π–π interactions [216] (Figure 24d).

7. Imidazopyridine Derivatives as Sensitizers for Confocal Microscopy and Fluorescent Luminogens for Cell Sensing

7.1. Imidazo[1,5-a]pyridines

1,5-*a* derivatives have increasingly gained prominence not only as molecular sensors but also as fluorescent probes for confocal microscopy and live-cell imaging. Initial demonstrations of 1,5-*a* fluorophores in biological imaging showed that even minimally substituted derivatives possess bright emission, large Stokes shifts, and resistance to photobleaching, enabling the acquisition of high-contrast confocal micrographs in *Arabidopsis thaliana* seedlings, with good permeability to the plant cell wall and plasma membrane [217] (Figure 25a).

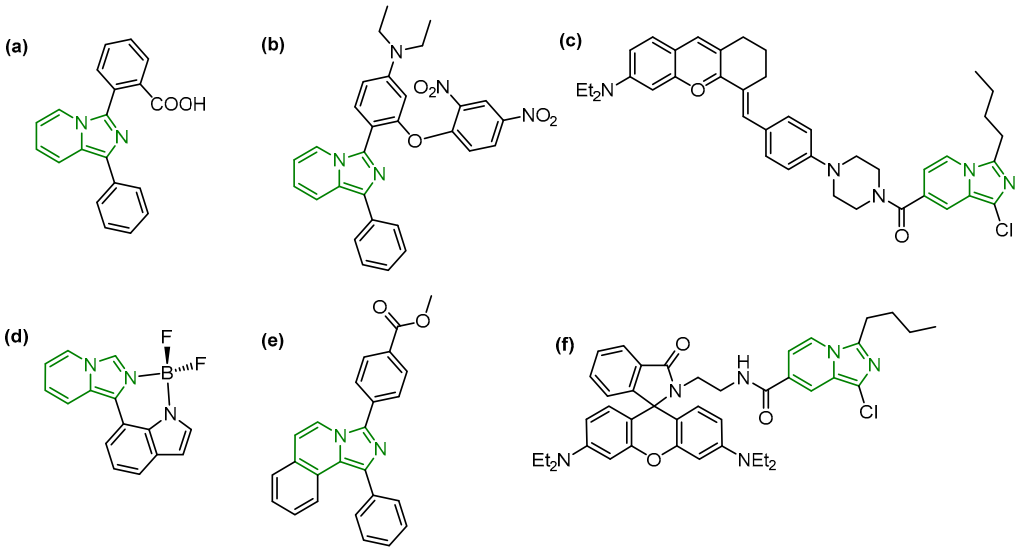

Figure 25. Selected examples of imidazo[1,5-*a*]pyridine derivatives used as luminogens reported in this section. See text for the reported subfigures.

Building on this foundation, 1,5-*a* scaffold could be refined through substitution at positions 1 and 3 to modulate electronic structure and environmental sensitivity. These modifications introduce intramolecular charge-transfer character and pronounced solvatochromism, leading to fluorescence enhancement in less polar or membrane-like environments. Such behavior has been validated through detailed spectroscopic studies and confocal fluorescence imaging in lipid vesicles and related model systems, highlighting the potential of 1,5-*a* derivatives as environment-responsive probes [143].

Furthermore, the responsiveness of the 1,5-*a* core to specific analytes has been exploited in a broad family of intracellular chemical sensors, where the heterocycle functions as a turn-on or ratiometric fluorophore. For example, 1,5-*a*-based probes for H_2S demonstrated rapid reaction kinetics and strong signal amplification in confocal imaging, providing real-time visualization of reactive sulfur species with sub-cellular spatial precision [218] (Figure 25b). Enzymes could also be tracked, such as carboxylesterase in macrophages during bone homeostasis [219].

Further advances include FRET- and ICT-modulated 1,5-*a* sensors, which permit ratiometric imaging of SO_3^{2-} or thiols [205] with confocal acquisition for intracellular

mapping [203]. Additionally, by fusing the 1,5-*a* core with benzopyrylium, a NIR-emitting 1,5-*a* dye was obtained, enabling clear imaging of cellular compartments in mitochondria [220] (Figure 25c). Boron coordination compounds also proved effective for mitochondria fluorescence imaging [221] (Figure 25d). In parallel, the incorporation of the 1,5-*a* core into stimuli-responsive architectures has enabled highly selective imaging of biological processes: methylated derivatives show enzyme-triggered demethylation and marked fluorescence enhancement upon esterase activation, allowing the selective confocal imaging of enzyme activity in live cells [222] (Figure 25e), while rhodamine B hybrids exhibit pH-dependent zwitterionic forms for imaging acidic organelles with high-fidelity pH probe example [223] (Figure 25f).

Zinc(II) 1,5-*a* coordination compounds could also be used in fluorescence imaging, in particular to track down H_2S and its anions in HepG2 cells, exploiting a coordination-based reversible mechanism [207].

7.2. Imidazo[1,2-a]pyridines

1,2-*a* derivatives have also found growing application as fluorescent probes for confocal microscopy and live-cell imaging, exploiting their rigid, π-conjugated structure, tunable electronics and biocompatibility. One prominent example is the xanthene-1,2-*a* hybrid, which shows an unusually large Stokes shift (≈75 nm, 2609 cm^{-1}), high selectivity for Hg^{2+}, low citotoxicity and excellent cell permeability, and has been used to image Hg^{2+} in HeLa cells by confocal fluorescence microscopy [209].

Another small-molecule probe, 2-(imidazo[1,2-*a*]pyridin-2-yl)phenyl acrylate, has been reported to selectively detect cysteine in living HepG2 cells and in zebrafish, with very low toxicity and good confocal imaging contrast [224] (Figure 26a), while an earlier work demonstrated that a fused 1,2-*a* sensor is capable of "turn-on" fluorescence in response to Fe^{3+} (and "turn-off" for Hg^{2+}) in aqueous solutions and in HeLa cells, supporting intracellular metal-ion imaging [225] (Figure 26b). The photophysical versatility of this scaffold has been further shown by the design of ESIPT-active derivatives that respond rapidly to nerve-agent simulants with a detection limit of 0.6 μM (although this report does not include confocal imaging), demonstrating the strong fluorescence modulation potential of the core [226] (Figure 26c). Also, fused phenanthro-1,2-*a* heterocycles have yielded probes with strong fluorescence and sufficient photostability to be used in live-cell imaging platforms, including confocal microscopy [227] (Figure 26d).

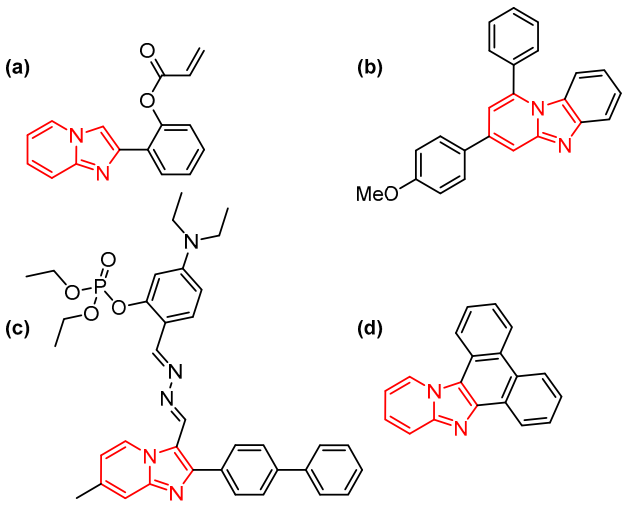

Figure 26. Selected examples of imidazo[1,2-*a*]pyridine derivatives used as luminogens reported in this section. See text for the reported subfigures.

Together, these examples illustrate that 1,2-*a* derivatives combine favorable photophysical characteristics, structural tunability, and cellular compatibility, making them a powerful but still under-explored class of fluorescent probes for confocal microscopy and biological imaging.

7.3. Imidazo[4,5-b]pyridines and Imidazo[4,5-c]pyridines

4,5-*b* and 4,5-*c* derivatives have so far been only sparsely explored as fluorescent probes for cellular imaging and confocal microscopy. While their tunability and environment-sensitive photophysics suggest clear potential for intracellular localization, analyte sensing, enzyme-responsive turn-on behavior and polarity-dependent emission, the number of studies that directly demonstrate these functions in live-cell or confocal imaging contexts remains limited, leaving substantial scope for further development. As a sole example, sulfur-containing ferrocenyl-4,5-*b* were used to visualize Hg^{2+} in living cells via fluorescence microscopy, with test-strip and confocal validation reported alongside the synthetic work, revealing the potential application of such a motif in fluorescent visualization of Hg^{2+} ions in biological and environmental systems [214].

8. Imidazopyridines and Their Coordination Compounds as Catalysts

8.1. Imidazo[1,5-a]pyridines

As already mentioned, the 1,5-*a* scaffold combines a fused imidazole and pyridine ring and can act as a versatile chelating unit (NˆN, or CˆN after cyclometallation) upon appropriate functionalization; this is a substitution that is easily accessible at multiple positions and can be tuned to obtain precise electronics and steric profiles. This tunability allows fine control of ligand donor strength, π-acceptor character, and steric environment at a metal center, all parameters that determine catalytic activity.

A major use of 1,5-*a* derivatives has been as nitrogen ligands in photoactive late-transition metal complexes. Studies on Ir(III) and Rh(III) complexes showed that 1,5-*a*-based cyclometalated compounds displayed interesting photophysical properties (*vide supra*), central for photoredox or energy-transfer catalysis. Photophysical investigations emphasize how small substitutions on the 1,5-*a* core shift emission maxima and excited-state redox properties, enabling rational design for particular photochemical transformations such as [4 + 2] cycloaddition reactions between anilines and maleimides [154,228] (Figure 27a). Oxidative coupling reaction of benzylic amines could also be photocatalyzed by Ir(III) complexes of pincer-type 1,5-*a* [229] (Figure 27b).

N,*N*-coordination motifs for Pd(II)/Pt(II) complexes have also been investigated, revealing that these square-planar geometries are effective in Suzuki–Miyaura cross-couplings (with the active complex being generated in situ) [230] (Figure 27c), Mizoroki-Heck reaction [231–233] and transfer hydrogenations [234,235]. The observed effectiveness is attributable to the 1,5-*a* unit, whose rigid backbone enforces well-defined ligand bite angles and electronic properties, which can improve catalyst longevity and selectivity in cross-coupling reactions.

Copper complexes of 1,5-*a* derivatives are frequently observed and have been used in oxidative transformations and as intermediates that reveal mechanistic insights. One striking observation is the formation of meso-ionic 1,5-*a* species or metal-uncoordinated meso-ionic derivatives that nonetheless participate in catalysis (acting as organocatalytic participants or transient ligand forms) [236] (Figure 27d). On the other hand, isolated Cu(II) and Cu(I) (and also Mn(II)) complexes) of 1,5-*a* have been proven effective as catalysts in the ketalization of ketones, up to quantitative yields [237,238].

Interestingly, Zn(II) coordination compounds of 1,5-*a* also demonstrated effectiveness in the polymerization of L-lactide, even under industrially relevant conditions (i.e.,

technical-grade monomer, no solvent, at 190 °C, and high monomer/catalyst ratios) [239], but also in the depolymerization reaction of the polylactide [240], enabling a circular approach towards polymer recycling.

Besides coordination compounds, 1,5-*a* derivatives could also be used as free organic species in catalysis, as properly functionalized 1,5-*a* have been used as chelating auxiliaries generated in situ [113,241] (Figure 27e). This strategy afforded efficient catalysts in the conversion of CO_2 and ethylene into acrylate, with a turnover number up to 570 and yields up to more than 80%.

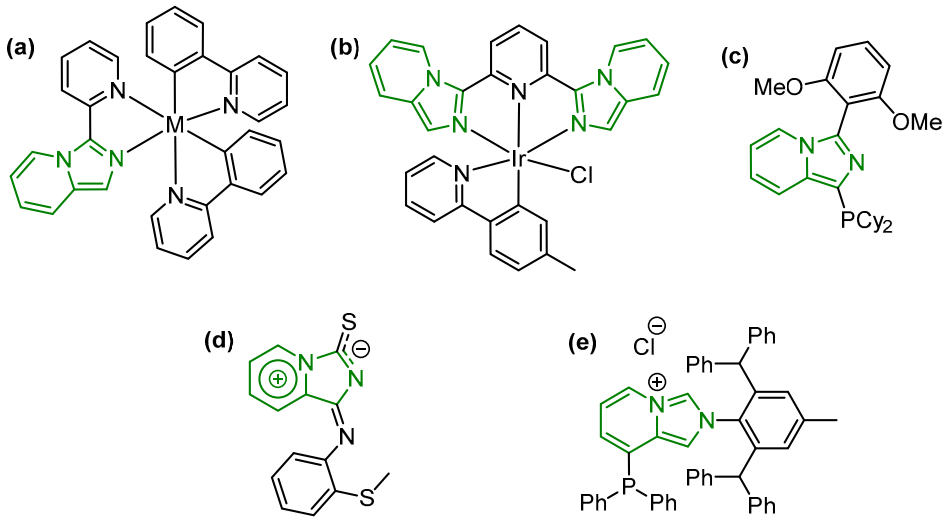

Figure 27. Selected examples of catalysts based on the imidazo[1,5-*a*]pyridine motif reported in this section. See text for the reported subfigures.

8.2. Imidazo[1,2-a]pyridines

The 1,2-*a* nucleus received much less attention with respect to the 1,5-*a* counterparts in its catalytical potential applications. Nonetheless, sparse examples of such systems have been used as catalysts in the Mizoroki-Heck coupling reaction of 4-chloroacetophenone and styrene and in the direct arylation reaction between 1,2-*a* itself and 4-Cyanochlorobenzene, especially in the form of strong σ-donating *N*-heterocyclic carbenes bound to a palladium [131]. Alternatively, 1,2-*a*-based NHC Pd complexes resulted in active catalysts in the Suzuki-Miyaura reaction [133]. Speaking of cross-coupling reactions, phosphine-functionalized 1,2-*a* Pd(II) coordination compounds resulted in efficient catalyst in the Buchwald-Hartwig reaction [230].

8.3. Imidazo[4,5-b]pyridines and Imidazo[4,5-c]pyridines

The 4,5-fused scaffolds 4,5-*b* and 4,5-*c* have been scarcely employed as ligands in the synthesis of coordination compounds (*vide supra*). Consequently, no examples have been reported of homogeneous, heterogeneous, or photocatalysis conducted by complexes containing these two ligands, highlighting a clear gap and an opportunity for future exploration in coordination chemistry and catalysis.

9. Biological and Medical Applications of Imidazopyridines

9.1. Imidazo[1,5-a]pyridines

1,5-*a*, while initially valued mainly for their synthetic versatility, have progressively moved into concrete pharmaceutical applications. The fused imidazole–pyridine core provides a compact and rigid framework with multiple sites for substitution, allowing fine-tuning of interactions with enzymes, receptors, and intracellular targets, similarly

to how luminescence properties can be tuned, while maintaining favorable drug-like properties. For example, 1,5-*a* could be used as enzyme inhibitors, receptor modulators, and cytotoxic compounds. A notable example is the development of insulin-regulated aminopeptidase (IRAP) inhibitors with a potency of 1 μM, followed by structure-activity relationship analysis, highlighting the scaffold's suitability for cognition-focused drug discovery [242] (Figure 28a). Computational and early experimental kinase studies have also used the 1,5-*a* core as a hinge-binding element: molecular dynamics and advanced docking approaches have identified plausible ATP-pocket binding modes for several 1,5-*a* derivatives against epidermal growth factor receptors (EGFR) and related kinases [243] (Figure 28b).

In the anti-infective field, initial medicinal chemistry studies have identified imidazo[1,5-*a*]pyridine/quinoline derivatives with activity against *Mycobacterium tuberculosis*, including metal-complexed analogues showing measurable whole-cell efficacy, with an IC_{90} down to 7.7 μM [244] (Figure 28c).

Several hybrid small molecules incorporating the 1,5-*a* core with additional pharmacophores have demonstrated cytotoxic activity in cell-based anticancer assays. Notably, 1,5-*a*-benzimidazole hybrids showed significant growth inhibition against a panel of human tumor cell lines and effectively inhibited tubulin polymerization, inducing G2/M cell cycle arrest and apoptosis in MCF-7 cells [245] (Figure 28d). Similarly, 1,5-*a*-chalcone derivatives exhibited potent cytotoxicity and microtubule disruption in cancer cells, supporting their potential as tubulin-targeting anticancer agents [246] (Figure 28e). Also, oxazole-appended 1,5-*a* demonstrated interesting anticancer activity, especially towards prostate, lung, breast and ovarian cancer cell lines (PC3, A549, MCF-7 and A2780, respectively) [247] (Figure 28f). In some cases, chelation to a metal center (i.e., Fe(II), Cu(II) or Zn(II)) increases the cytotoxicity of 1,5-*a* derivative by 3–13 fold towards HeLa, HepG2 and Jurkat cells [248].

Alternatively, 1,5-*a*-derived *N*-heterocyclic carbene ligands in palladium allyl complexes also exhibit strong in vitro antitumor effects, including activity against some cisplatin-resistant cell lines [249] (Figure 28g). More recently, thiadiazole conjugates built on this scaffold demonstrated micromolar to sub-micromolar cytotoxicity with IC_{50} lower than that of etoposide used as a standard, especially against breast, lung and ovarian cancer cell lines (MCF-7, A549 and A2780 respectively) [250] (Figure 28h).

Additionally, 1,5-*a* and their derivatives have also emerged as versatile scaffolds for photodynamic therapy (PDT) because the fused heterocycle provides a rigid, conjugated platform that can be readily tuned to control absorption, excited-state energies and cellular targeting. Simple organic 1,5-*a* chromophores and BF_2-chelates derived from 1,5-*a* show strong visible absorption and large Stokes shifts, obtaining mitochondria-localizing photosensitizers that produce reactive oxygen species under light and kill cancer cells in vitro [251] (Figure 28i). In particular, this tridentate 1,5-*a* ligand installed into a boron complex was optimized for two-photon excitation and mitochondrial accumulation, allowing a heavy-atom-free construct to show efficient PDT activity under near-infrared two-photon excitation, achieving deeper-tissue activation without introducing toxic heavy atoms.

The synthetic accessibility of the 1,5-*a* core could also be further exploited to make squaraine-type conjugates [252] (Figure 28j) and ionic 1,5-*a* salts [253] (Figure 28k), showing promising in-cell PDT activity and imaging capability, as well as singlet oxygen sensitization, illustrating the theranostic potential of the class. Taken together with broader reviews of photosensitizer design (which highlight the need for long-wavelength absorption, high triplet yields and tumor selectivity) [254,255], the literature indicates that 1,5-*a* motifs are particularly attractive, even if challenges remain in translating these systems in vivo, especially optimizing tissue penetration, clearance and minimizing off-target phototoxicity.

In summary, 1,5-*a* not only possess interesting luminescent and photophysical properties but also possess relevant biological applications, both in terms of pure applications and as sensitizers for photodynamic therapy.

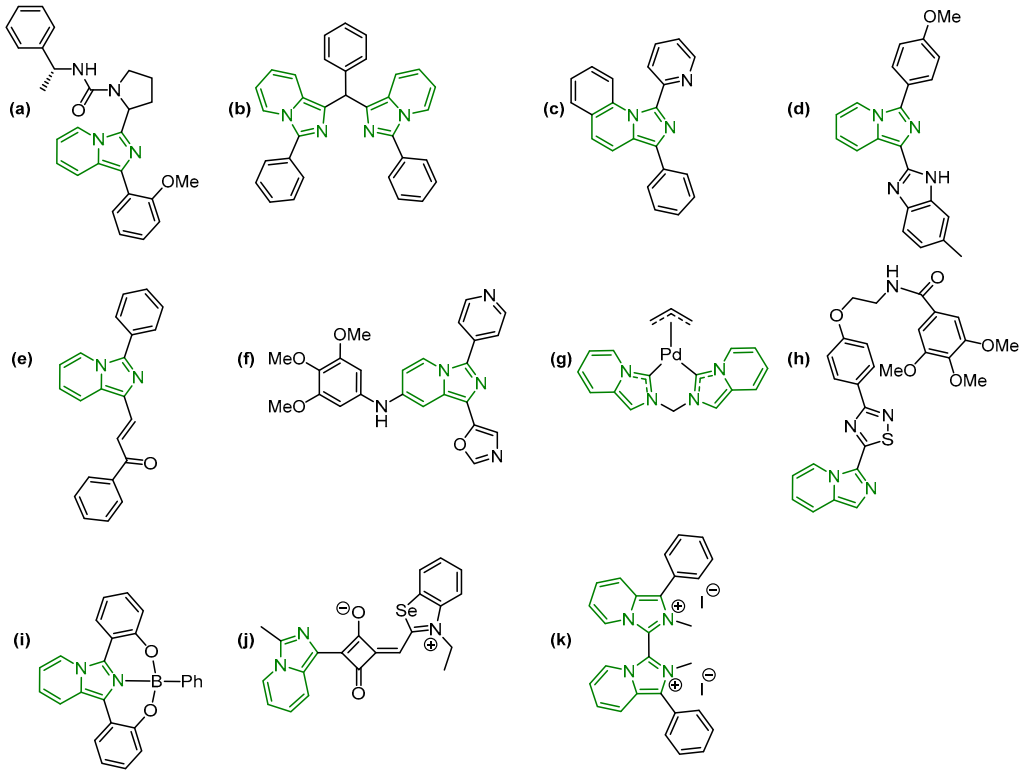

Figure 28. Selected examples of imidazo[1,5-*a*]pyridine-based biologically active molecules reported in this section. See text for the reported subfigures.

9.2. Imidazo[1,2-a]pyridines

1,2-*a* represent one of the most practically productive heterocyclic cores in contemporary medicinal chemistry because their fused imidazole–pyridine bicycle provides a rigid, compact scaffold with multiple substitution possibilities that medicinal chemists can exploit to tune potency, selectivity, permeability and metabolic stability. This pragmatic combination has led to intense, target-directed design that has delivered clinically relevant candidates and numerous diverse primary reports across infectious disease, oncology and antiparasitic discovery.

The tuberculosis program [256,257] is the clearest demonstration of translational success: iterative hit-to-lead optimization of 1,2-*a*-3-carboxamide produced nanomolar antimycobacterial potency, biochemical evidence that these compounds bind and inhibit the QcrB subunit of the mycobacterial cytochrome bc_1 complex (thereby blocking oxidative phosphorylation) and medicinal-chemistry strategies that were explicitly applied to improve in vitro and in vivo metabolic stability, progressing into human safety and pharmacokinetics studies [258] (Figure 29a).

Additionally, the 1,2-*a* nucleus has been incorporated into multiple anticancer discovery efforts, such as selenylated and other redox-modulating derivatives exhibiting potent, often sub-micromolar antiproliferative effects in glioblastoma and other cell models by altering intracellular redox balance [259] (Figure 29b). Alternatively, functionalization of the 1,2-*a* core with kinase-directing scaffolds (for example, 6-(imidazo[1,2-*a*]pyridin-6-yl)quinazoline series) (Figure 29c) [260] has produced PI3K/kinase inhibitory activity, while other conjugates and fused bicyclic constructs functionally interfere with microtubule dynamics to produce mitotic arrest, indicating that the core can serve as either the principal

pharmacophore or as a modular anchoring fragment for multi-target designs. Quaternarization of the imidazolic nitrogen and substitution with coumarin appendages also result in the rising of antiproliferative properties against breast and prostate cancer cell lines [261] (Figure 29d).

Cu(II) and Zn(II) coordination complexes of 1,2-*a* also displayed anticancer activity, in particular against breast cancer leukemia cell lines and colorectal cancer cell lines, in some cases with IC_{50} values smaller than those reported for camptothecin, used as a comparison [129]. Coordination to Au(III) also afforded antibacterial and antitumoral compounds that act by DNA intercalation [262].

Antimicrobial research is also equally extensive, with studies in medicinal chemistry and phenotypic screening consistently reporting 1,2-*a* Schiff bases [263] (Figure 29e) and peptidomimetics [264] (Figure 29f) with quantifiable minimum inhibitory concentration values against both Gram-positive and Gram-negative bacteria, as well as activity against fungal strains. 5,6,7,8-tetrahydro-1,2-*a* instead are reported to be effective antiprotozoal agents as water-soluble photosensitizers [265] (Figure 29g).

The scaffold has also proven productive in antiparasitic drug discovery: libraries of 1,2-*a*-appended chalcones and related conjugates have been screened against kinetoplastid parasites (*Trypanosoma* spp., *Leishmania infantum*), yielding hits with selective antiparasitic activity and acceptable cytotoxicity windows in initial reports. These findings position this core as a valuable starting point for neglected disease campaigns [266] (Figure 29h).

Furthermore, 1,2-*a* derivatives have also demonstrated significant potential as antidiabetic agents [267].

Additionally, 1,2-*a* have emerged as a surprisingly versatile scaffold for photodynamic applications because their fused heteroaromatic core is readily tuned (electronic push–pull substitution, π-extension) to enhance intersystem crossing and triplet-state formation, which is the key prerequisite for efficient singlet-oxygen ($^1O_2$) generation. 1,2-*a* derivatives were shown to produce measurable $^1O_2$ under simulated sunlight or UVA/visible excitation [268] (Figure 29i), and systematic substitution (electron-donating vs. electron-withdrawing groups or aryl-thio substitution) alters both absorption maxima and quantum yields, allowing modest red-shifts and improved phototoxicity in cell assays [269]. In some cases, the photodynamic properties could be directed towards mitochondria with low cytotoxicity towards healthy cells [270].

Collectively, the literature shows a continuum from simple organic imidazopyridine photosensitizers (moderate $^1O_2$ generators) to metal-bound constructs with markedly improved phototoxicity and imaging utility, but challenges remain, such as pushing absorption further into the therapeutic window (650–800 nm), quantifying in vivo selectivity and photostability, and controlling dark toxicity.

Notably, 1,2-*a* are already exploited in commercialized drugs, as they possess favorable physicochemical and pharmacokinetic properties, such as enhanced lipophilicity, metabolic stability, and blood–brain barrier penetration [271,272]. This scaffold underlies several marketed drugs with diverse therapeutic actions, such as zolpidem as a $GABA_A$ receptor-modulating hypnotic, alpidem and necopidem as anxiolytics, and olprinone as a phosphodiesterase-III inhibitor, illustrating central nervous system and cardiovascular targeting in clinical use (Figure 30) [272,273]. The core structure has been extensively derivatized to exploit a broad spectrum of biological activities, including antiulcer, anticonvulsant, antimicrobial, antiviral, anti-inflammatory and anticancer effects, reflecting its adaptability to different molecular targets and structure-activity relationship (SAR) profiles in drug discovery campaigns [274–276]. More recent studies continue to leverage 1,2-*a* in optimization for novel pharmacological activities, reinforcing their status as a versatile scaffold in therapeutic development [277].

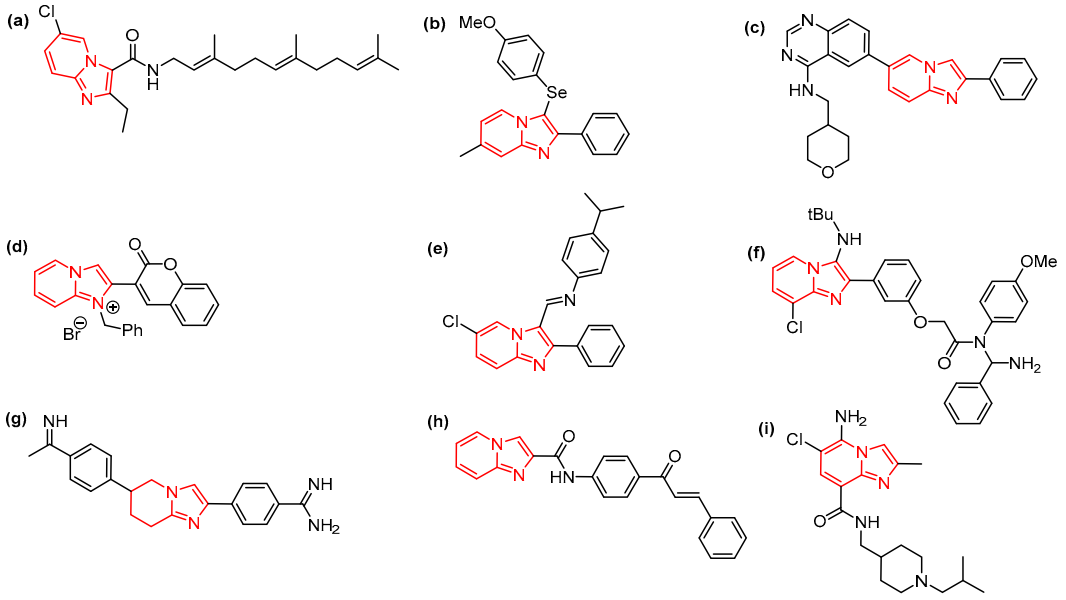

Figure 29. Selected examples of imidazo[1,2-*a*]pyridine-based biologically active molecules reported in this section. See text for the reported subfigures.

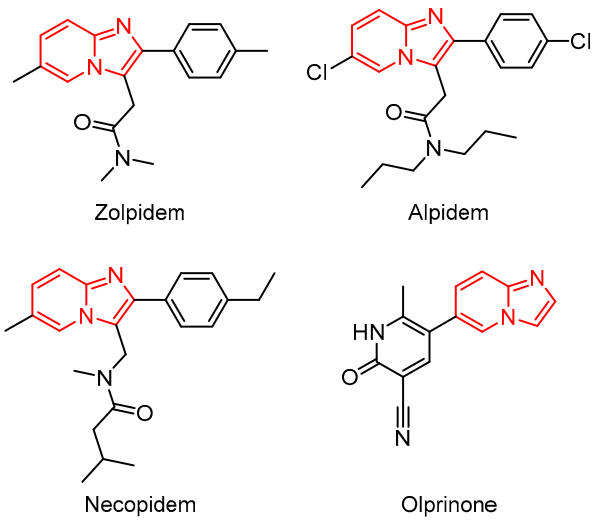

Figure 30. Relevant examples of imidazo[1,2-*a*]pyridine derivatives already commercialized as therapeutic agents.

9.3. Imidazo[4,5-b]pyridines and Imidazo[4,5-c]pyridines

While for other applications 4,5-*b* and 4,5-*c* isomers are often falling behind the 1,5-*a* and 1,2-*a* counterparts, in medicinal chemistry they are far better known, with both isomer classes that can be prepared, compared, and optimized for biological applications. Indeed, such derivatives are known for their antiproliferative effects on a diverse selection of human cancer cell lines, antibacterial activity against chosen Gram-positive and Gram-negative bacterial strains, and antiviral activity on a broad panel of DNA and RNA viruses [278] (Figure 31a).

In the anticancer domain, for instance, tetracyclic 4,5-*b* derivatives with substituted amino side chains show sub-micromolar antiproliferative activity, with emphasis on how isomeric changes in the pyridine ring nitrogen position affect DNA/RNA binding [279] (Figure 31b). 4,5-*b* derivatives also displayed interesting cytotoxicity in multidrug-resistant mouse T-lymphoma cells in vitro [280].

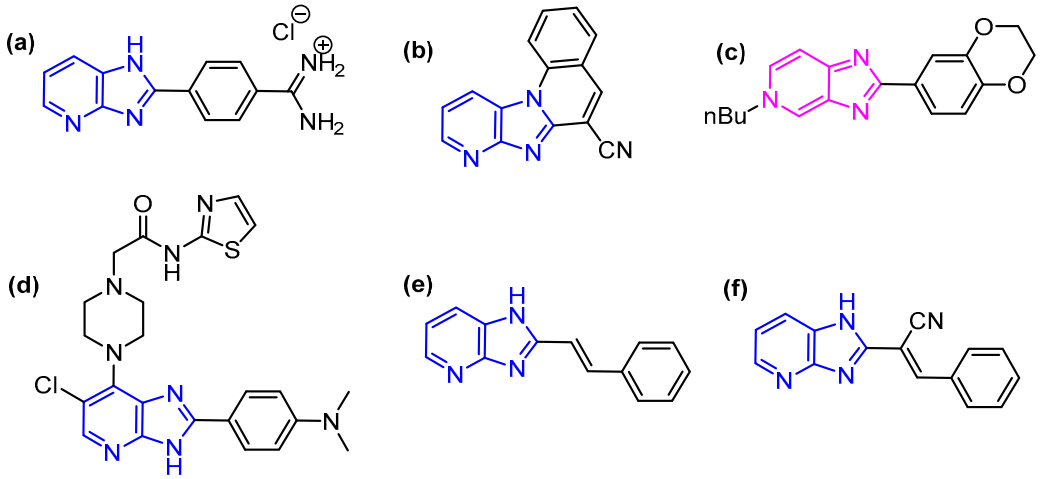

Figure 31. Selected examples of imidazo[4,5-*b*]pyridine- and imidazo[4,5-*c*]pyridine-based biologically active molecules reported in this section. See text for the reported subfigures.

Several antimicrobial investigations have explored 4,5-*b* and 4,5-*c* pyridine frameworks within the same study, enabling comparative evaluation of minimum inhibitory concentrations (MIC) and biological profiles as a function of scaffold topology. For example, parallel libraries of substituted 4,5-*c* and 4,5-*b* pyridines were prepared and screened in vitro against a panel of Gram-positive and Gram-negative bacteria and fungal strains, with some regioisomers of each series exhibiting promising MIC values in the low-to-moderate μg/mL range [281] (Figure 31c).

Mechanistically, these studies show that both 4,5-*b* and 4,5-*c* pyridine isomers can serve as privileged heteroaromatic cores in biologically active small molecules, acting as hinge binders in kinase inhibitors, planar intercalators of nucleic acids, or tubulin-directing agents. In the kinase field, 4,5-*b* are well established as hinge-binding motifs, where the fused topology enables productive hydrogen-bonding interactions with the kinase backbone and translates into pronounced enzyme selectivity (e.g., Aurora kinase inhibitors) [282,283] (Figure 31d). In studies on antiproliferative compounds, planar derivatives related to 4,5-*b* have been shown to interact with DNA in an intercalative mode, indicating that ring planarity and topology can influence nucleic acid binding, reasonably thanks to the simil-purine structure [284,285] (Figure 31e). 4,5-*b*-derived acrylonitriles and related conjugates also inhibit tubulin polymerization and induce cell-cycle arrest in G2/M, underscoring how scaffold topology governs downstream cellular phenotypes [286,287] (Figure 31f).

10. Miscellaneous Applications

Beyond the primary fields reported above, the imidazopyridine scaffold has demonstrated a remarkable versatility, leading to its exploration in a variety of other emerging applications. The intrinsic structural rigidity and the possibility of fine-tuning electronic properties through regioisomerism have paved the way for the development of specialized materials.

While the entire imidazopyridine family shows potential for diverse uses, it is primarily the 1,2-*a* scaffold that has found the broadest range of alternative applications. Due to its high synthetic accessibility and robust framework, this isomer has been extensively employed beyond its classical roles. For example, 1,2-*a* have emerged as highly effective, environmentally friendly corrosion inhibitors for mild steel in 1.0 M hydrochloric acid solutions (Figure 32a) [288–292], reducing both anodic metal dissolution and cathodic hydrogen evolution by blocking the active sites on the steel surface, retrieving inhibition

efficiencies often higher than 90%. Interestingly, the functional groups on the 1,2-*a* core play a significant role, with electron-donating groups increasing efficiency.

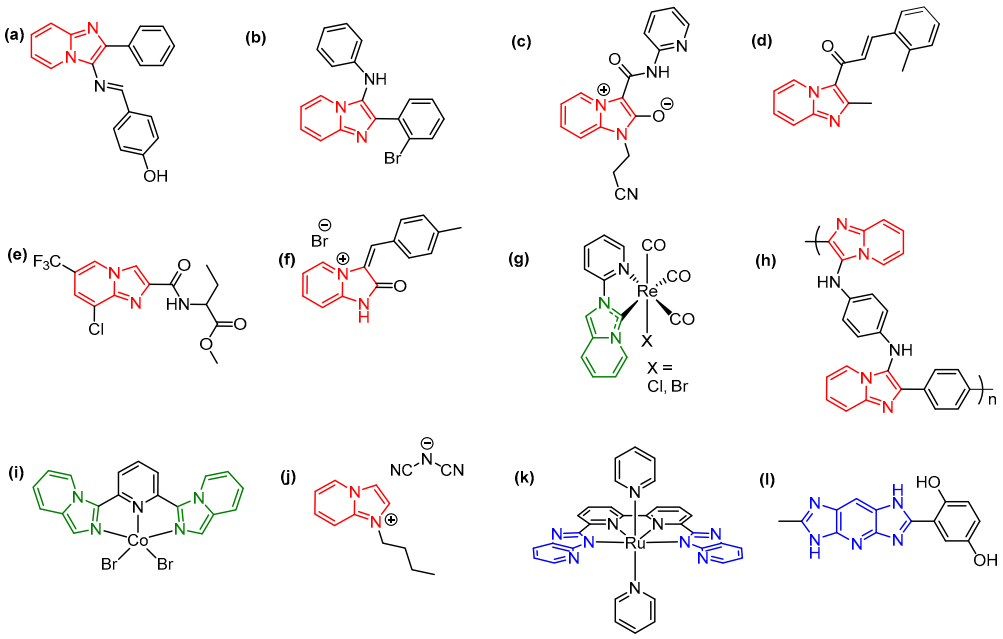

Figure 32. Selected examples of imidazopyridine-based compounds reported in this section. See text for the reported subfigures.

This family of compounds also proved to possess different pesticidal activities, including herbicidal (Figure 32b) [293,294], insecticidal (Figure 32c) [295,296], fungicidal (Figure 32d) [297,298] and nematicidal (Figure 32e) [299,300] effects. It is worth noting that also the 4,5-*b* isomers have exhibited significant biological activities, particularly showing promise as potent insecticides [301].

Imidazopyridine derivatives have demonstrated significant utility in photopolymerization as well, specifically acting as versatile photoinitiators. For instance, 2-oxo-dihydroimidazo[1,2-*a*]pyridines have proven effective in promoting free-radical polymerization reactions (Figure 32f) [302,303]. Additionally, Re(I) complexes based on the 1,5-*a* scaffold (Figure 32g) have shown remarkable activity in photoinitiating the polymerization of polyethylene glycol-acrylate monomers; these systems operate under visible light using iodonium salts and amines as co-initiators, facilitating advanced 3D and 4D printing applications [304]. Beyond their role as initiators, imidazopyridine-based polymers can be directly synthesized through multicomponent reactions involving diisocyanides, dialdehydes, and 2-aminopyridine. This approach paves the way for the development of novel functional materials composed of fused heterocyclic polymer frameworks (Figure 32h) [305].

Additional applications see 1,5-*a* scaffold being successfully employed as a pincer ligand to stabilize pentacoordinate Co(II) complexes (Figure 32i) [306]. These compounds exhibit slow magnetic relaxation under an applied direct current field, a characteristic behavior of single-ion magnets that holds great promise for the development of high-density data storage and quantum computing.

Parallel to these magnetic properties, derivatives of the 1,2-*a* isomer have been utilized to develop a novel class of ionic liquids by introducing alkyl chains at the N_1 position and employing specific counteranions such as bis(fluorosulfonyl)imide or $N(CN)_2$ (Figure 32j) [307]. These materials can achieve a liquid state at room temperature, offering unique physicochemical properties compared to traditional imidazolium-based systems.

Additionally, the use of ruthenium(II) complexes featuring rigid, dianionic, tetradentate ligands based on the 4,5-*b* framework has opened crucial perspectives in artificial photosynthesis. These complexes act as robust catalysts for water oxidation, a key four-electron process required for the sustainable production of hydrogen as a future fuel (Figure 32k) [308].

Finally, the structural utility of this family extends to high-performance energy storage, where bis-imidazo[4,5-*b*]pyridine-based nanofibers have been recently integrated into functional separators for lithium-sulfur batteries (Figure 32l) [309]. These nanofibers facilitate lithium-ion desolvation and mitigate the "shuttle effect" of polysulfides, significantly enhancing the rate capability and cycling stability of next-generation batteries.

11. Conclusions

This review has shown that imidazopyridines are not a single heterocyclic motif but a family of closely related yet functionally distinct scaffolds, in which the position of the nitrogen atoms plays a decisive role in determining chemical reactivity, electronic structure, and functional performance. Across synthetic chemistry, coordination chemistry, photophysics and biological applications, nitrogen positioning emerges as a unifying design principle rather than a marginal structural variation (see Table 1 for a summary of the key properties discussed).

From a synthetic viewpoint, 1,2-*a* remain the most accessible and modular members of the family, while recent advances have significantly expanded the chemical space of 1,5-*a* and 4,5-*b*/*c* frameworks. Importantly, synthetic accessibility is no longer the primary limitation for the latter regioisomers; instead, future efforts can focus on systematic structure–activity and structure–property relationships relevant to both medicinal chemistry and materials science.

In coordination chemistry, imidazopyridine derivatives display versatile donor behavior, acting as *N*-donors, *N*,*N*- or *N*,*O*-chelating ligands, or *N*-heterocyclic carbene precursors. Regioisomerism dictates coordination modes, metal–ligand orbital interactions and supramolecular architectures, which in turn control both reactivity and excited-state properties. While 1,2-*a* and 1,5-*a* derivatives are now established ligands for closed-shell and heavy-metal centers, the coordination chemistry of 4,5-*b* and 4,5-*c* systems remains comparatively underexplored despite their demonstrated potential in photodynamic therapy, bioimaging and phosphorescent materials.

The biological and medical relevance of imidazopyridines is firmly established, particularly for 1,2-*a* derivatives, which have long been recognized as privileged scaffolds in medicinal chemistry. Kinase inhibitors, antiviral agents and other bioactive compounds based on this framework demonstrate how nitrogen positioning influences target recognition, binding modes and pharmacological profiles. More recently, the intrinsic luminescence of selected imidazopyridines and their metal complexes has enabled dual-function systems that combine therapeutic activity with optical readout, bridging medicinal chemistry and bioimaging.

The photophysical behavior of imidazopyridines is also highly sensitive to nitrogen topology. Depending on the regioisomer and substitution pattern, emission can arise from π–π^* fluorescence, intramolecular charge-transfer states, aggregation-induced emission, excited-state intramolecular proton transfer or phosphorescence. These properties underpin applications ranging from fluorescence imaging and molecular sensing to optoelectronic devices. Notably, 4,5-*b* frameworks have emerged as particularly effective building blocks for efficient blue and deep-blue phosphorescent systems, despite having been poorly investigated so far with respect to the other regioisomers, while ESIPT activity is preferentially associated with selected 1,2-*a* and 4,5-*c* architectures.

Finally, imidazopyridine derivatives displayed a plethora of different and various applications, ranging from photoinitiators for polymerization, water oxidation to Li-batteries performance enhancers.

Overall, the key message emerging from this review is that nitrogen positioning in imidazopyridines provides a powerful and rational handle to tailor function across disciplines. By integrating synthetic design, biological activity, coordination chemistry and photophysics, imidazopyridines can evolve from classical heterocycles into multifunctional platforms capable of addressing challenges in medicine, sensing and advanced optoelectronic technologies.

Table 1. Summary of the key properties of the different imidazopyridine regioisomers discussed in this review.

Isomer	1,5-*a*	1,2-*a*	4,5-*b*	4,5-*c*
Synthesis	Acid-catalyzed condensations, oxidative annulations, and decarboxylative pathways.	GBB multicomponent reaction; condensation with α-halo ketones.	Condensation of diaminopyridines with carboxylic acids; reductive pathway.	Condensation of diaminopyridines; solid-state or metal-assisted synthesis.
Coordination	Bidentate *N*,*N*-chelator; NHC precursors; 1D/2D coordination polymers.	Symmetric Zn(II) complexes; NHC ligands; intercalating Au(III) complexes.	Carbene (NHC) precursors for metal complexes.	NHC precursors; lanthanide coordination polymers.
Photophysical behavior	Tunable ICT fluorescence; Aggregation-Induced Emission (AIE).	ESIPT activity (with phenolic donors); blue-shifted fluorescence.	High-performance blue/deep-blue phosphorescence (Ir/Pt complexes).	ESIPT activity; dual fluorescence and solvent-dependent tautomeric emission.
Optoelectronics	Down-conversion layers for LEDs; sky-blue LEC and OLED emitters.	High-efficiency deep-blue OLEDs; n-type semiconductors for OFETs.	Ultra-efficient PhOLEDs (EQE up to 34.7%).	-
Sensing	FRET/ratiometric probes for Hg^{2+} and H_2S; dosimeters for sulfites and hypochlorite.	AIE sensors for Cd^{2+}, Hg^{2+}, and Al^{3+}; ESIPT-based fluoride sensors; cyanide detection.	pH-sensitive iminocoumarins; ferrocene-based probes for Hg^{2+} and Pb^{2+}.	Ln-complexes for Fe^{3+} sensing and dye adsorption.
Bioimaging	Bright probes for plant cells, lipid vesicles, and mitochondria; enzymatic imaging.	Imaging of Hg^{2+}, cysteine, and Fe^{3+} in living cells (HeLa/HepG2) and zebrafish.	Visualization of Hg^{2+} ions in living cells via confocal microscopy.	Sparsely explored for cellular bioimaging.
Catalysis	Photoredox (Ir/Rh); Suzuki/Heck (Pd); polymerization and depolymerization of L-lactide (Zn).	NHC-Pd catalysts for cross-coupling (Heck, Suzuki, and Buchwald-Hartwig).	-	-
Medicine	Enzyme inhibitors (IRAP, EGFR); anti-TB activity; photosensitizers for PDT.	Marketed drugs (Zolpidem); anti-TB (Q203); antiparassitic agents.	Aurora kinase inhibitors; antiviral activity; DNA intercalators.	Antibacterial and antifungal screenings; enzyme inhibitors.
Other	Single-ion magnets (Co); photoinitiators for 3D/4D printing.	Corrosion inhibitors; pesticides (herbicides, insecticides, fungicides); ionic liquids.	Water oxidation (Ru); separators for Li-S batteries; insecticides.	-

Author Contributions: Writing—original draft preparation, A.C., C.V. and G.C.; writing—review and editing, G.A.A., S.B. and G.C.; conceptualization, G.C.; resources, G.A.A. and S.B. All authors have read and agreed to the published version of the manuscript.

Funding: The authors thank the Ministero dell'Università e della Ricerca (MUR) and the University of Insubria for funding. This paper and related research have been partly conducted during and with the support of the Italian national inter-university PhD course in Sustainable Development and Climate change (link: www.phd-sdc.it) at the University School for Advanced Studies IUSS Pavia, Cycle XXXVIII, with the support of a scholarship financed by the Ministerial Decree no. 351 of 9 April 2022, based on the NRRP—funded by the European Union—NextGenerationEU—Mission 4 "Education and Research", Component 1 "Enhancement of the offer of educational services: from nurseries to universities"—Investment 4.1 "Extension of the number of research doctorates and innovative doctorates for public administration and cultural heritage" (AC).

Institutional Review Board Statement: Not applicable.

Informed Consent Statement: Not applicable.

Data Availability Statement: No new data were created or analyzed in this study.

Conflicts of Interest: The authors declare no conflicts of interest.

Abbreviations

The following abbreviations are used in this manuscript:

AIE	Aggregation Induced Emission
ATP	Adenosine TriPhosphate
CRI	Color Rendering Index
CT	Charge Transfer
DMSO	DiMethylSulphOxide
DNA	DeoxyriboNucleic Acid
D-π-A	Donor-π-Acceptor
DSSC	Dye-Sensitized Solar Cell
EGFR	Epidermal Growth Factor Receptor
EQE	External Quantum Efficiency
ESIPT	Excited State Intramolecular Proton Transfer
FMOF	Fluorinated Metal Organic Framework
FRET	Fluorescence Resonance Energy Transfer
GABA	γ-AminoButyric Acid
GBB reaction	Groebke–Blackburn–Bienaymé reaction
HOMO	Highest Occupied Molecular Orbital
ICT	Intramolecular Charge Transfer
IRAP	Insulin-Regulated AminoPeptidase
k_r	Radiative rate constant
LEC	Light-Emitting Electrochemical Cell
LOD	Limit of Detection
LUMO	Lowest Unoccupied Molecular Orbital
MIC	Minimum Inhibitory Concentration
MLCT	Metal to Ligand Charge Transfer
MOF	Metal Organic Framework
NHC	Nitrogen Heterocyclic Carbene
NIR	Near InfraRed
OFET	Organic Field Effect Transistor
OLED	Organic Light Emitting Diodes
OPV	Organic PhotoVoltaic
PDI	Perylene DiImide
PDT	PhotoDynamic Therapy

PhOLED	Phosphorescent Organic Light Emitting Diode
PLQY	PhotoLuminescence Quantum Yield
POP	Bis{2-(diphenylphosphanyl)phenyl}ether
RIR	Restriction of Intramolecular Rotation
RNA	RiboNucleic Acid
SAR	Structure-Activity Relationship
TADF	Thermally Activated Delayed Fluorescence
TD-DFT	Time-Dependent Density Functional Theory
TICT	Twisted Intramolecular Charge Transfer
TMPE	TriMethylolPropane Ethoxylate
TPE	TetraPhenyl Ethylene
T_3P	PropylPhosphonic anhydride
1,2-*a*	Imidazo[1,2-*a*]pyridine
1,5-*a*	Imidazo[1,5-*a*]pyridine
4,5-*b*	Imidazo[4,5-*b*]pyridine
4,5-*c*	Imidazo[4,5-*c*]pyridine
Φ_F	Fluorescence Quantum Yield

References

1. Tschitschibabin, A.E. Zur Tautomerie des α-Amino-pyridins, IV. Mitteilung: Eine Darstellungsmethode des Pyrimidazols und seiner Homologen. *Ber. Dtsch. Chem. Ges.* **1925**, *58*, 1704. [CrossRef]
2. Weidenhagem, R.; Weeden, U. Über neue Imidazoloverbindungen der heterocyclischen Reihe (VII. Mitteil. über Imidazole). *Ber. Dtsch. Chem. Ges.* **1938**, *71*, 2347. [CrossRef]
3. Petrow, V.; Saper, J. 282. Some 5-azaquinoxalines and 4-azabenziminazoles. *J. Chem. Soc.* **1948**, 1389. [CrossRef]
4. Bower, J.D.; Ramage, G.R. Heterocyclic Systems Related to Pyrrocoline. Part I.2: 3a-Diazaindene. *J. Chem. Soc.* **1955**, 2834. [CrossRef]
5. Ashok, P.; Chaudhran, K.; Sharma, A. Progress in the Development of Imidazopyridine-Based Fluorescent Probes for Diverse Applications. *Crit. Rev. Anal. Chem.* **2022**, *54*, 2148. [CrossRef]
6. Volpi, G.; Laurenti, E.; Rabezzana, R. Imidazopyridine Family: Versatile and Promising Heterocyclic Skeletons for Different Applications. *Molecules* **2024**, *29*, 2668. [CrossRef] [PubMed]
7. Volpi, G. Luminescent Imidazo[1,5-*a*]pyridine Scaffold: Synthetic Heterocyclization Strategies-Overview and Promising Applications. *Asian J. Org. Chem.* **2022**, *11*, e202200171. [CrossRef]
8. Bukhryakov, K.V.; Kurkin, A.V.; Yurovskaya, M.A. Synthetic approaches to imidazo[4,5-*b*]pyridine derivatives (review). *Chem. Heterocycl. Compd.* **2011**, *47*, 646. [CrossRef]
9. Ramana Reddy, M.; Darapaneni, C.M.; Patil, R.D.; Kumari, H. Recent synthetic methodologies for imidazo[1,5-*a*]pyridines and related heterocycles. *Org. Biomol. Chem.* **2022**, *20*, 3440. [CrossRef]
10. Panda, J.; Raigurum, B.P.; Mishra, M.; Mohapatra, S.; Nayak, S. Recent Advances in the Synthesis of Imidazo[1,2-*a*]pyridines: A Brief Review. *ChemistrySelect* **2022**, *7*, e202103987. [CrossRef]
11. Kishbaugh, T.L.S. Pyridines and Imidazopyridines with Medicinal Significance. *Curr. Top. Med. Chem.* **2016**, *16*, 3274. [CrossRef]
12. Mali, S.N.; Pandey, A. Recent Developments in Medicinal and In Silico Applications of Imidazopyridine Derivatives: Special Emphasis on Malaria, Trypanosomiasis, and Tuberculosis. *Chem. Afr.* **2022**, *5*, 1215. [CrossRef]
13. Reddy Sanapalli, B.K.; Ashames, A.; Sigalapalli, D.K.; Shaik, A.B.; Bhandare, R.R.; Yele, V. Synthetic Imidazopyridine-Based Derivatives as Potential Inhibitors against Multi-Drug Resistant Bacterial Infections: A Review. *Antibiotics* **2022**, *11*, 1680. [CrossRef]
14. Khatun, S.; Singh, A.; Bader, G.N.; Ahmad Sofi, F. Imidazopyridine, a promising scaffold with potential medicinal applications and structural activity relationship (SAR): Recent advances. *J. Biomol. Struct. Dyn.* **2022**, *40*, 14279. [CrossRef] [PubMed]
15. Delgado, O.; Delgado, F.; Vega, J.A.; Trabanco, A.A. *N*-bridged 5,6-bicyclic pyridines: Recent applications in central nervous system disorders. *Eur. J. Med. Chem.* **2015**, *97*, 719. [CrossRef] [PubMed]
16. Lefin, R.; van der Walt, M.M.; Milne, P.J.; Terre'Blanche, G. Imidazo[1,2-*a*]pyridines possess adenosine A_1 receptor affinity for the potential treatment of cognition in neurological disorders. *Bioorg. Med. Chem. Lett.* **2017**, *27*, 3963. [CrossRef] [PubMed]
17. Priyadarsini Mishra, N.; Mohapatra, S.; Das, T.; Nayak, S. Imidazo[1,2-*a*]pyridine as a promising scaffold for the development of antibacterial agents. *J. Heterocycl. Chem.* **2022**, *59*, 2051. [CrossRef]
18. Altaher, A.M.H.; Adris, M.A.; Aliwaini, S.H. Imidazo[1,2-*a*]pyridine Based Compounds, The Hopeful Anti-Cancer Therapy. *Sys. Rev. Pharm.* **2021**, *12*, 79.

19. Sucu, B.O. Biological evaluation of imidazopyridine derivatives as potential anticancer agents against breast cancer cells. *Med. Chem. Res.* **2022**, *31*, 2231. [CrossRef]
20. Lee, Y.-Y.; Zseng, H.-W.; Tsai, Z.-H.; Su, Y.-S.; Hu, C.-H.; Lee, H.M. Isomeric Palladium Complexes Bearing Imidazopyridine-Based Abnormal Carbene Ligands: Synthesis, Characterization, and Catalytic Activity in Direct C–H Arylation Reaction. *Organometallics* **2019**, *38*, 805. [CrossRef]
21. Mihorianu, M.; Franz, M.H.; Jones, P.G.; Freytag, M.; Kelter, G.; Fiebig, H.-H.; Tamm, M.; Neda, I. N-Heterocyclic carbenes derived from imidazo-[1,5-*a*]pyridines related to natural products: Synthesis, structure and potential biological activity of some corresponding gold(I) and silver(I) complexes. *Appl. Organomet. Chem.* **2016**, *30*, 581. [CrossRef]
22. Volpi, G.; Rabezzana, R. Imidazo[1,5-*a*]pyridine derivatives: Useful, luminescent and versatile scaffolds for different applications. *New J. Chem.* **2021**, *45*, 5737. [CrossRef]
23. Yashwantrao, G.; Naik, V.; Badani, P.; Saha, S. Designing Multifunctional AIEgens by Molecular Engineering of Imidazo[1,2-*a*]pyridine For Color Tunable Molecular Salts, Anti-Counterfeit Applications and Sensing of Mn^{2+}, Ag^{+}, and Fe^{3+}. *Chem. Eur. J.* **2025**, *31*, e202500047. [CrossRef]
24. Hong, Y.; Zhao, Y.; Guo, Y.; Wang, Y.; Ma, L. AIE activity, mechanochromism, acidchromism, and high-level anti-counterfeiting based on multifunctional tetraphenylvinyl imidazolopyridine. *J. Lumin.* **2024**, *273*, 120678. [CrossRef]
25. Ahmad Tali, J.; Kumar, G.; Kumar Sharma, B.; Rasool, Y.; Sharma, Y.; Shankar, R. Synthesis and site selective C–H functionalization of imidazo-[1,2-*a*]pyridines. *Org. Biomol. Chem.* **2023**, *21*, 7267. [CrossRef] [PubMed]
26. Krishnamoorthy, I.G. The suppression of intramolecular charge transfer emission by tautomerism in 2-(4′-amino-2′-hydroxyphenyl)-1H-imidazo-[4,5-*c*]pyridine: Intramolecular proton transfer versus intermolecular proton transfer. *J. Photochem. Photobiol. A Chem.* **2021**, *413*, 113199.
27. Kothavale, S.; Lee, K.H.; Lee, J.Y. 3-Cyano Imidazopyridine Acceptor-based Bipolar and *n*-type Host Materials for Phosphorescent Organic Light-Emitting Diodes. *Asian J. Org. Chem.* **2018**, *7*, 2218. [CrossRef]
28. Wang, J.; Mason, R.; Van Derveer, D.; Feng, K.; Bu, X.R. Convenient Preparation of a Novel Class of Imidazo[1,5-*a*]pyridines: Decisive Role by Ammonium Acetate in Chemoselectivity. *J. Org. Chem.* **2003**, *68*, 5415. [CrossRef] [PubMed]
29. Magra, K.; Darari, M.; Domenichini, E.; Francés-Monerris, A.; Cebrián, C.; Beley, M.; Pastore, M.; Monari, A.; Assfeld, X.; Haacke, S.; et al. Photophysical Investigation of Iron(II) Complexes Bearing Bidentate Annulated Isomeric Pyridine-NHC Ligands. *J. Phys. Chem. C* **2020**, *124*, 18379. [CrossRef]
30. Wang, L.B.; Pan, J.; Tang, C.L.; Bu, X.R.; Wang, J. Microwave-prompted rapid and efficient synthesis of 3-alkyl substituted imidazo[1,5-*a*]pyridines. *Chin. Chem. Lett.* **2007**, *18*, 390. [CrossRef]
31. Rahmati, A.; Khalesi, Z. One-Pot Three-Component Synthesis of Imidazo[1,5-*a*]pyridines. *Int. J. Org. Chem.* **2011**, *1*, 15. [CrossRef]
32. Patil, S.G.; Jadhav, J.S.; Sankpal, S.T. Mg_3N_2-assisted one-pot synthesis of 1,3-disubstituted imidazo[1,5-*a*]pyridine. *RSC Adv.* **2020**, *10*, 11808. [CrossRef]
33. Mandal, A.; Patel, B.K. Rationalization of weak interactions in two fluorescence active imidazo-[1,5-*a*]-pyridine derivatives: A combined experimental and computational study. *J. Mol. Struct.* **2017**, *1147*, 735. [CrossRef]
34. Li, M.Y.; Xie, Y.; Ye, Y.; Zou, Y.; Jiang, H.F.; Zeng, W. Cu(I)-Catalyzed Transannulation of N-Heteroaryl Aldehydes or Ketones with Alkylamines via C(sp^3)–H Amination. *Org. Lett.* **2014**, *16*, 6232. [CrossRef]
35. Wang, H.; Xu, W.; Wang, Z.; Yu, L.; Xu, K. Copper-Catalyzed Oxidative Amination of sp^3 C–H Bonds under Air: Synthesis of 1,3-Diarylated Imidazo[1,5-*a*]pyridines. *J. Org. Chem.* **2015**, *80*, 2431. [CrossRef] [PubMed]
36. Nguyen, H.T.H.; Nguyen, O.T.K.; Truong, T.; Phan, N.T.S. Synthesis of imidazo[1,5-*a*]pyridines via oxidative amination of the C(sp^3)-H bond under air using metal-organic framework Cu-MOF-74 as an efficient heterogeneous catalyst. *RSC Adv.* **2016**, *6*, 36039. [CrossRef]
37. Gupta, A.K.; De, D.; Tomar, K.; Bharadwaj, P.K. A Cu(II) metal–organic framework with significant H_2 and CO_2 storage capacity and heterogeneous catalysis for the aerobic oxidative amination of C(sp^3)–H bonds and Biginelli reactions. *Dalton Trans.* **2018**, *47*, 1624. [CrossRef]
38. Monika, S.; Ramesh, R. One-pot synthesis of 1,3-disubstituted imidazo[1,5-*a*]pyridines via acceptorless dehydrogenative coupling of primary alcohols promoted by binuclear ruthenium(II) NˆO-chelating complexes. *Appl. Oragnomet. Chem.* **2022**, *37*, e6986. [CrossRef]
39. Tanomsiri, G.; Boonmee, S.; Chaisan, N.; Tummatorn, J.; Thongsornkleeb, C.; Ruchirawat, S. Strategic Methodologies for Efficient Synthesis of Imidazo[1,5-*a*]pyridine and Benzazepine Analogs via the Unique Ritter-Type Reaction. *ACS Org. Inorg. Au* **2025**, *5*, 117. [CrossRef] [PubMed]
40. Hu, Z.; Hou, J.; Liu, J.; Yu, W.; Chang, J. Synthesis of imidazo[1,5-*a*]pyridines via I_2-mediated sp^3 C–H amination. *Org. Biomol. Chem.* **2018**, *16*, 5653. [CrossRef]
41. Fukuda, T.; Miyake, H.; Abe, S.; Yagishita, F.; Iida, H. Flavin–Iodine-Catalyzed Aerobic Oxidative Tandem C(sp^3)−H Imination and Amination: Synthesis of Fluorescent Imidazo[1,5-*a*]pyridines from Pyridylmethanes and Aminomethanes. *Adv. Synth. Catal.* **2024**, *367*, e202400854. [CrossRef]

42. Shibahara, F.; Sugiura, R.; Yamaguchi, E.; Kitagawa, A.; Murai, T. Synthesis of Fluorescent 1,3-Diarylated Imidazo[1,5-*a*]pyridines: Oxidative Condensation−Cyclization of Aryl-2-Pyridylmethylamines and Aldehydes with Elemental Sulfur as an Oxidant. *J. Org. Chem.* **2009**, *74*, 3566. [CrossRef]
43. Crawforth, J.M.; Paoletti, M. A one-pot synthesis of imidazo[1,5-*a*]pyridines. *Tetrahedron Lett.* **2009**, *50*, 4916. [CrossRef]
44. Ramesha, A.B.; Sandhya, N.C.; Pavan Kumar, C.S.; Hiremath, M.; Mantelingu, K.; Rangappa, K.S. A novel approach for the synthesis of imidazo and triazolopyridines from dithioesters. *New J. Chem.* **2016**, *40*, 7637. [CrossRef]
45. Ramesha, A.B.; Pavan Kumar, C.S.; Sandhya, N.C.; Kumara, M.N.; Mantelingu, K.; Rangappa, K.S. Tandem approach for the synthesis of 3-sulfenylimidazo[1,5-*a*]pyridines from dithioesters. *RSC Adv.* **2016**, *6*, 48375–48378. [CrossRef]
46. Shibahara, F.; Kitagawa, A.; Yamaguchi, E.; Murai, T. Synthesis of 2-Azaindolizines by Using an Iodine-Mediated Oxidative Desulfurization Promoted Cyclization of N-2-Pyridylmethyl Thioamides and an Investigation of Their Photophysical Properties. *Org. Lett.* **2006**, *8*, 5621. [CrossRef]
47. Tahara, S.; Shibahara, F.; Maruyama, T.; Murai, T. Iodine-mediated cyclization of N-thioacyl-1-(2-pyridyl)-1,2-aminoalcohols and their subsequent condensation leading to the formation of novel bis(1-imidazo[1,5-*a*]pyridyl)arylmethanes. *Chem. Commun.* **2009**, 7009. [CrossRef]
48. Singh, D.; Sharma, S.; Kumar, M.; Kaur, I.; Shankar, R.; Pandey, S.K.; Singh, V. An AcOH-mediated metal free approach towards the synthesis of bis-carbolines and imidazopyridoindole derivatives and assessment of their photophysical properties. *Org. Biomol. Chem.* **2019**, *17*, 835. [CrossRef] [PubMed]
49. Wang, Q.; Zhang, S.; Guo, F.; Zhang, B.; Hu, P.; Wang, Z. Natural α-Amino Acids Applied in the Synthesis of Imidazo[1,5-*a*]N-heterocycles under Mild Conditions. *J. Org. Chem.* **2012**, *77*, 11161. [CrossRef] [PubMed]
50. Wang, H.; Xu, W.; Xin, L.; Liu, W.; Wang, Z.; Xu, K. Synthesis of 1,3-Disubstituted Imidazo[1,5-*a*]pyridines from Amino Acids via Catalytic Decarboxylative Intramolecular Cyclization. *J. Org. Chem.* **2016**, *81*, 3681. [CrossRef]
51. Arvapalli, V.S.; Chen, G.; Kosarev, S.; Tan, M.E.; Xie, D.; Yet, L. Microwave-assisted organic synthesis of 3-substituted-imidazo[1,5-*a*]pyridines. *Tetrahedron Lett.* **2010**, *51*, 284. [CrossRef]
52. Wu, Y.-D.; Geng, X.; Gao, Q.; Zhang, J.; Wu, X.; Wu, A.-X. Iodine-promoted sequential dual oxidative Csp^3–H amination/Csp^3–H iodination reactions: Efficient synthesis of 1-iodoimidazo[1,5-*a*]pyridines. *Org. Chem. Front.* **2016**, *3*, 1430. [CrossRef]
53. Herr, J.M.; Rössiger, C.; Albrecht, G.; Yanagi, H.; Göttlich, R. Solvent-free microwave-assisted synthesis of imidazo[1,5-*a*]pyridine and –quinoline derivatives. *Synth. Commun.* **2019**, *49*, 2931. [CrossRef]
54. Groebke, K.; Weber, L.; Mehlin, F. Synthesis of Imidazo[1,2-*a*] annulated Pyridines, Pyrazines and Pyrimidines by a Novel Three-Component Condensation. *Synlett* **1998**, *6*, 661. [CrossRef]
55. Blackburn, C.; Guan, B.; Fleming, P.; Shiosaki, K.; Tsai, S. Parallel synthesis of 3-aminoimidazo[1,2-*a*]pyridines and pyrazines derived from isonitriles. *Tetrahedron Lett.* **1998**, *39*, 3635. [CrossRef]
56. Bienaymé, H.; Bouzid, K. A new heterocyclic multicomponent reaction for the combinatorial synthesis of fused 3-aminoimidazoles. *Angew. Chem. Int. Ed.* **1998**, *37*, 2234. [CrossRef]
57. Calderón-Rangel, D.; Corona-Díaz, A.; González-Gámez, I.A.; Gámez-Montaño, R. One-Pot Synthesis of Imidazo[1,2-*a*]pyridines via Groebke–Blackburn–Bienaymé Reaction. *Chem. Proc.* **2025**, *18*, 10.
58. Varma, R.S.; Kumar, D. Microwave-accelerated three-component condensation reaction on clay: Solvent-free synthesis of imidazo[1,2-*a*] annulated pyridines, pyrazines and pyrimidines. *Tetrahedron Lett.* **1999**, *40*, 7665. [CrossRef]
59. Zhu, D.-J.; Chen, J.-X.; Liu, M.-C.; Ding, J.-C.; Wu, H.-Y. Catalyst- and Solvent-free Synthesis of Imidazo[1,2-*a*]pyridines. *J. Braz. Chem. Soc.* **2009**, *20*, 482. [CrossRef]
60. Stasyuk, A.J.; Banasiewicz, M.; Cyrański, M.K.; Gryko, D.T. Imidazo[1,2-*a*]pyridines Susceptible to Excited State Intramolecular Proton Transfer: One-Pot Synthesis via an Ortoleva–King Reaction. *J. Org. Chem.* **2012**, *77*, 5552. [CrossRef]
61. Monreal-Corona, R.; Stasyuk, A.J.; Solà, M.; Pla-Quintana, A.; Poater, A. Unveiling the Reaction Mechanisms of the Synthesis and the Excited State Intramolecular Proton Transfer of 2-(2′-hydroxyphenyl)imidazo[1,2-*a*]pyridine. *ChemPhysChem* **2024**, *25*, e202400069. [CrossRef]
62. Veer, B.; Singh, R. Facile synthesis of 2-arylimidazo[1,2-*a*]pyridines catalysed by DBU in aqueous ethanol. *Proc. R. Soc. A* **2019**, *475*, 20190238. [CrossRef]
63. Doraghi, F.; Serajian, A.; Karimian, S.; Larijani, B.; Mahdavi, M. The cyclization and functionalization reactions involving N-phenacylpyridinium salts. *Chem. Pap.* **2024**, *78*, 6821. [CrossRef]
64. Li, X. Cu(I)-Catalysed Oxidative Coupling of 2-Aminopyridines with β-Keto Esters: Synthesis of Imidazo[1,2-*a*]Pyridine-3-Carboxylates. *J. Chem Res.* **2012**, *35*, 525. [CrossRef]
65. Wang, X.; Ma, L.; Yu, W. Synthesis of Imidazo[1,2-*a*]pyridines by the Bis(acetyloxy)(phenyl)-λ^3-iodane-Mediated Oxidative Coupling of 2-Aminopyridines with β-Keto Esters and 1,3-Diones. *Synthesis* **2011**, *15*, 2445. [CrossRef]
66. Reen, G.K.; Kumar, A.; Sharma, P. Recent advances on the transition-metal-catalyzed synthesis of imidazo[1,2-*a*]pyridines. *Beilstein J. Org. Chem.* **2019**, *15*, 165. [CrossRef]

67. Wang, Y.; Li, S.; Wang, X.; Yao, Y.; Feng, L.; Ma, C. A multi pathway coupled domino strategy: I2/TBHP-promoted synthesis of imidazopyridines and thiazoles via sp^3, sp^2 and sp C–H functionalization. *RSC Adv.* **2022**, *12*, 5919. [CrossRef] [PubMed]
68. Yu, Y.; Su, Z.; Cao, H. Strategies for Synthesis of Imidazo[1,2-*a*]pyridine Derivatives: Carbene Transformations or C−H Functionalizations. *Chem. Rec.* **2019**, *19*, 2105. [CrossRef]
69. Santra, S.; Mitra, S.; Bagdi, A.K.; Hajra, A. Iron(III)-catalyzed three-component domino strategy for the synthesis of imidazo[1,2-*a*]pyridines. *Tetrahedron Lett.* **2014**, *55*, 5151. [CrossRef]
70. Chen, X.; Sun, P.; Mo, B.; Chen, C.; Peng, J. Palladium-Catalyzed Synthesis of Fluorescent Benzo[4,5]imidazo[1,2-*a*]pyridines through Annulation Reaction of Benzimidazoles and Alkynyl Bromides with Internal Alkynes. *J. Org. Chem.* **2021**, *86*, 352. [CrossRef] [PubMed]
71. Jiang, S. Copper (II) complex supported on magnetic nanoparticles as a novel nanocatalyst for the synthesis of imidazo[1,2-*a*]pyridines. *Mol. Divers.* **2024**, *28*, 3859. [CrossRef]
72. Zhou, Z.; Luo, D.; Li, G.; Yang, Z.; Cui, L.; Yang, W. Copper-catalyzed three-component reaction to synthesize polysubstituted imidazo[1,2-*a*]pyridines. *RSC Adv.* **2022**, *12*, 20199. [CrossRef]
73. Yan, R.-L.; Yan, H.; Ma, C.; Ren, Z.-Y.; Gao, X.-A.; Huang, G.-S.; Liang, Y.-M. Cu(I)-Catalyzed Synthesis of Imidazo[1,2-*a*]pyridines from Aminopyridines and Nitroolefins Using Air as the Oxidant. *J. Org. Chem.* **2012**, *77*, 2024. [CrossRef] [PubMed]
74. Reddy, K.R.; Reddy, A.S.; Shankar, R.; Kant, R.; Das, P. Copper-Catalyzed Oxidative C−H Amination: Synthesis of Imidazo[1,2-*a*]-N-Heterocycles from N-Heteroaryl Enaminones. *Asian J. Org. Chem.* **2015**, *4*, 573. [CrossRef]
75. Cacchi, S.; Ciogli, A.; Demitri, N.; Fabrizi, G.; Ghirha, F.; Goggiamani, A.; Iazzetti, A.; Lamba, D. Copper-Catalyzed C-N Bond Formation via C-H Functionalization: Facile Synthesis of Multisubstituted Imidazo[1,2-*a*]pyridines from N-(2-Pyridinyl)enaminones. *Synthesis* **2018**, *50*, 3513.
76. Cao, H.; Liu, X.; Zhao, L.; Cen, J.; Lin, J.; Zhu, Q.; Fu, M. One-pot regiospecific synthesis of imidazo[1,2-*a*]pyridines: A novel, metal-free, three-component reaction for the Formation of C–N, C–O, and C–S Bonds. *Org. Lett.* **2014**, *16*, 146. [CrossRef] [PubMed]
77. Changunda, C.R.K.; Venkatesh, B.C.; Mokone, W.K.; Rousseaus, A.L.; Brady, D.; Fernandes, M.A.; Bode, M.L. Efficient one-pot synthesis of functionalised imidazo[1,2-*a*]pyridines and unexpected synthesis of novel tetracyclic derivatives by nucleophilic aromatic substitution. *RSC Adv.* **2020**, *10*, 8104. [CrossRef]
78. Sanaeishoar, H.; Bashirpour, M.; Mohave, F. An Expeditious One-pot Synthesis of Imidazo[1,2-*a*]pyridines using $ZnCl_2.SiO_2$ as a Recyclable HeterogeneousCatalyst under Solvent-free Condition. *J. Appl. Chem. Res.* **2016**, *10*, 75.
79. Subba Reddy, B.V.; Sivaramakrishna Reddy, P.; Jayasudhan Reddy, Y.; Yadav, J.S. $InBr_3$-catalyzed three-component, one-pot synthesis of imidazo[1,2-*a*]pyridines. *Tetrahedron Lett.* **2011**, *52*, 5789. [CrossRef]
80. Kundu, S.; Basu, B. Graphene-oxide catalysed multi-component reactions: Green synthesis of a library of 3-sulfenylimidazo[1,2-*a*]pyridines. *RSC Adv.* **2015**, *5*, 50178. [CrossRef]
81. Mahaur, P.; Pandey, H.; Srivastava, V.; Singh, S. Photocatalytic synthesis of imidazo[1,2-*a*]pyridines via $C(sp)^3$–H functionalization using ethylarene as a sustainable surrogate of acetophenone and luminescence studies. *Org. Biomol Chem.* **2025**, *23*, 10867. [CrossRef]
82. Yang, B.; Tao, C.; Shao, T.; Gong, J.; Che, C. One-pot synthesis of tetracyclic fused imidazo[1,2-*a*] systems via cascade/retro-aza-ene sequences. *Beilstein J. Org. Chem.* **2016**, *12*, 145. [CrossRef]
83. Bhutia, Z.T.; Das, D.; Chatterjee, A.; Banerjee, M. Efficient and "Green" Synthetic Route to Imidazo[1,2-*a*]pyridine by Cu(II)–Ascorbate-Catalyzed A^3-Coupling in Aqueous Micellar Media. *ACS Omega* **2019**, *4*, 4481. [CrossRef]
84. Corona-Díaz, A.; Calderón-Rangel, D.; García-García, D.; Rentería-Gómez, M.A.; Gámez-Montaño, R. Sonochemical Synthesis of Imidazo[1,2-*a*]pyridines via Groebke–Blackburn–Bienaymé Reaction Catalyzed by TSOH. *Chem. Proc.* **2025**, *18*, 25.
85. Yu, X.; Wei, F. Synthesis of a novel imidazo[1,2-*a*]pyridines derivative as high selective fluorescent sensor for cyanide detection. *J. Mol. Struct.* **2025**, *1330*, 141528. [CrossRef]
86. Karale, U.B.; Kalari, S.; Shivakumar, J.; Makane, V.B.; Babar, D.A.; Thakare, R.P.; Nagendra Babu, B.; Chopra, S.; Rode, H.B. Ligand-free Pd-catalysed decarboxylative arylation of imidazo[1,2-*a*]pyridine-3-carboxylic acids with aryl bromides. *RSC Adv.* **2016**, *6*, 65095. [CrossRef]
87. Mondal, B.; Ghosh, P.; Kundu, M.K.; Kumar Das, T.; Das, S. Palladium catalyzed 8-aminoimidazo[1,2-*a*]pyridine (AIP) directed selective β-$C(sp^2)$–H arylation. *Org. Biomol. Chem.* **2021**, *19*, 360. [CrossRef] [PubMed]
88. Wu, D.; Liu, M.; Li, Z.; Dang, M.; Liu, X.; Li, J.; Huang, L.; Ren, Y.; Zhang, Z.; Liu, W.; et al. Synthesis and fungicidal activity of novel imidazo[4,5-*b*]pyridine derivatives. *Heterocycl. Commun.* **2019**, *25*, 8. [CrossRef]
89. Padmaja, R.D.; Devi, V.C.; Mukku, N.; Chanda, K.; Maiti, B. Rapid Construction of an Imidazo[4,5-*b*]pyridine Skeleton from 2-Chloro-3-nitropyridine via Tandem Reaction in H_2O-IPA Medium. *ACS Omega* **2018**, *3*, 4583. [CrossRef]
90. Krause, M.; Foks, H.; Gobis, K. Pharmacological Potential and Synthetic Approaches of Imidazo[4,5-*b*]pyridine and Imidazo[4,5-*c*]pyridine Derivatives. *Molecules* **2017**, *22*, 399. [CrossRef]

91. Dymińska, L.; Gagor, A.; Maczka, M.; Węgliński, Z.; Hanuza, J. XRD studies, vibrational spectra, and molecular structure of 1*H*-imidazo[4,5-*b*]pyridine based on DFT quantum chemical calculations. *J. Raman Spectrosc.* **2010**, *41*, 1021. [CrossRef]
92. Casimiro-Garcia, A.; Heemstra, R.J.; Bigge, C.F.; Chen, J.; Ciske, F.A.; Davis, J.A.; Ellis, T.; Esmaeil, N.; Flynn, D.; Han, S.; et al. Design, synthesis, and evaluation of imidazo[4,5-*c*]pyridin-4-one derivatives with dual activity at angiotensin II type 1 receptor and peroxisome proliferator-activated receptor-γ. *Bioorg. Med. Chem. Lett.* **2013**, *23*, 767. [CrossRef] [PubMed]
93. Martínez-Palou, R.; Gerardo Zepeda, L.; Höpfl, H.; Montoya, A.; Guzmán-Lucero, D.J.; Guzmán, J. Parallel and automated library synthesis of 2-long alkyl chain benzoazoles and azole[4,5-*b*]pyridines under microwave irradiation. *Mol. Divers.* **2005**, *9*, 361. [CrossRef]
94. Myllymäki, M.J.; Koskinen, A.M.P. A rapid method for the preparation of 2-substituted oxazolo[4,5-*b*]pyridines using microwave-assisted direct condensation reactions. *Tetrahedron Lett.* **2007**, *48*, 2295–2298. [CrossRef]
95. Dekhane, D.V.; Pawar, S.S.; Gupta, S.V.; Shingare, M.S.; Thore, S.N. Lithium bromide catalyzed solvent free method for synthesis of 2-substituted benzimidazoles and imidazopyridines. *Chin. Chem. Lett.* **2010**, *21*, 519. [CrossRef]
96. René, O.; Souverneva, A.; Magnuson, S.R.; Fauber, B.P. Efficient syntheses of 2-fluoroalkylbenzimidazoles and -benzothiazoles. *Tetrahedron Lett.* **2013**, *54*, 201. [CrossRef]
97. Gobis, K.; Foks, H.; Serocki, M.; Augustynowicz-Kopeć, E.; Napiórkowska, A. Synthesis and evaluation of in vitro antimycobacterial activity of novel 1*H*-benzo[*d*]imidazole derivatives and analogues. *Eur. J. Med. Chem.* **2015**, *89*, 13. [CrossRef] [PubMed]
98. Kale, R.P.; Shaikh, M.U.; Jadhav, R.G.; Gill, C.H. Eco-friendly and facile synthesis of 2-substituted-1*H*-Imidazo[4,5-*b*]pyridine in aqueous medium by air oxidation. *Tetrahedron Lett.* **2009**, *50*, 1780. [CrossRef]
99. Wang, F.; Tran-Dubé, M.; Scales, S.; Johnson, S.; McAlpine, I.; Ninkovic, S. A simple and convenient two-step, one-pot synthesis of hetero-imidazoles from nitroaminoaryls catalyzed by Ytterbium triflate. *Tetrahedron Lett.* **2013**, *54*, 4054. [CrossRef]
100. Harer, S.L.; Bhatia, M.S. In-silico docking based design and synthesis of [1*H*,3*H*] imidazo[4,5-*b*] pyridines as lumazine synthase inhibitors for their effective antimicrobial activity. *J. Pharm. Bioallied Sci.* **2014**, *6*, 285. [CrossRef]
101. Lemrová, B.; Smyslová, P.; Popa, I.; Oždian, T.; Zajdel, P.; Soural, M. Directed solid-phase synthesis of trisubstituted imidazo[4,5-*c*]pyridines and imidazo[4,5-*b*]pyridines. *ACS Comb. Sci.* **2014**, *16*, 558. [CrossRef]
102. Álvarez, C.M.; Álvarez-Miguel, L.; García-Rodríguez, R.; Martín-Álvarez, J.M.; Miguel, D. 3-(pyridin-2-yl)imidazo[1,5-*a*]pyridine (pyridylindolizine) as ligands in complexes of transition and main-group metals. *Eur. J. Inorg. Chem.* **2015**, *29*, 4921. [CrossRef]
103. Durini, S.; Ardizzoia, G.A.; Therrien, B.; Brenna, S. Tuning the fluorescence emission in mononuclear heteroleptic trigonal silver(I) complexes. *New J. Chem.* **2017**, *41*, 3006. [CrossRef]
104. Ardizzoia, G.A.; Brenna, S.; Durini, S.; Therrien, B.; Veronelli, M. Synthesis, Structure, and Photophysical Properties of Blue-Emitting Zinc(II) Complexes with 3-Aryl-Substituted 1-Pyridylimidazo[1,5-*a*]pyridine Ligands. *Eur. J. Inorg. Chem.* **2014**, *26*, 4310. [CrossRef]
105. Cerrato, V.; Volpi, G.; Priola, E.; Giordana, A.; Garino, C.; Rabezzana, R.; Diana, E. Mono-, Bis-, and Tris-Chelate Zn(II) Complexes with Imidazo[1,5-*a*]pyridine: Luminescence and Structural Dependence. *Molecules* **2023**, *28*, 3703. [CrossRef] [PubMed]
106. Imada, Y.; Mukai, S.; Tahara, K.; Kozai, N.; Itaya, M.; Yoshida, Y.; Ueta, S.; Arakawa, Y.; Minagawa, K.; Yagishita, F. Divalent metal complexes of *N*,*O*- and *N*,*N*-bidentate imidazo[1,5-*a*]pyridine ligands: Synthesis, crystal structures, and photophysical properties. *Inorg. Chim. Acta* **2023**, *555*, 121584. [CrossRef]
107. Tronnier, A.; Schleicher, D.; Strassner, T. (C^C*)-cyclometalated platinum(II) imidazo[1,5-*a*]pyridine NHC complexes—Synthesis and characterization. *J. Organomet. Chem.* **2015**, *775*, 155. [CrossRef]
108. Zhang, X.; He, C.; Yang, X.; Zhang, Q.; Li, Y.; Yao, J. Fe^{II}, Co^{II} and Ni^{II} complexes based on 1-chloro-3-(pyridin-2-yl)imidazo[1,5-*a*]pyridine: Synthesis, structures, single-molecule magnetic and electrocatalytic properties. *New J. Chem.* **2022**, *46*, 21780. [CrossRef]
109. Kundu, N.; Abtab, S.M.T.; Kundu, S.; Endo, A.; Teat, S.J.; Chaudhury, M. Triple-Stranded Helicates of Zinc(II) and Cadmium(II) Involving a New Redox-Active Multiring Nitrogenous Heterocyclic Ligand: Synthesis, Structure, and Electrochemical and Photophysical Properties. *Inorg. Chem.* **2012**, *51*, 2652. [CrossRef]
110. Zhang, Y.-W.; Das, R.; Li, Y.; Wang, Y.-Y.; Ha, Y.-F. Synthesis, Characterization, and Properties of Organometallic Molecular Cylinders Bearing Bulky Imidazo[1,5-*a*]pyridine-Based N-Heterocyclic Carbene Ligands. *Chem. Eur. J.* **2019**, *25*, 5472. [CrossRef]
111. Pischedda, S.; Stoccoro, S.; Zucca, A.; Sciortino, G.; Ortu, F.; Clarkson, G.J. Synthesis and characterization of new Pd(II) and Pt(II) complexes with 3-substituted 1-(2-pyridyl)imidazo[1,5-*a*]pyridine ligands. *Dalton Trans.* **2021**, *50*, 4859. [CrossRef]
112. Zhou, T.; Gao, P.; Bisz, E.; Dziuk, B.; Lalancette, R.; Szostak, R.; Szostak, M. Well-defined, air- and moisture-stable palladium–imidazo[1,5-*a*]pyridin-3-ylidene complexes: A versatile catalyst platform for cross-coupling reactions by L-shaped NHC ligands. *Catal. Sci. Technol.* **2022**, *12*, 6581. [CrossRef] [PubMed]
113. Kim, J.; Hahm, H.; Ryu, J.Y.; Byun, S.; Park, D.-A.; Lee, S.H.; Lim, H.; Lee, J.; Hong, S. Pyridine-Chelated Imidazo[1,5-*a*]Pyridine N-Heterocyclic Carbene Nickel(II) Complexes for Acrylate Synthesis from Ethylene and CO_2. *Catalysts* **2020**, *10*, 758. [CrossRef]

114. Burstein, C.; Lehmann, C.W.; Glorious, F. Imidazo[1,5-*a*]pyridine-3-ylidenes—Pyridine derived N-heterocyclic carbene ligands. *Tetrahedron* **2005**, *61*, 6207. [CrossRef]
115. Roseblade, S.J.; Ros, A.; Monge, D.; Alcarazo, M.; Alvarez, E.; Lassaletta, J.M.; Fernandez, R. Imidazo[1,5-*a*]pyridin-3-ylidene/Thioether Mixed C/S Ligands and Complexes Thereof. *Organometallics* **2007**, *26*, 2570. [CrossRef]
116. Cinco, A.; Ardizzoia, G.A.; Brenna, S.; Therrien, B.; Colombo, G. Boron-Centered Compounds: Exploring the Optical Properties of Spiro Derivatives with Imidazo[1,5-*a*]Pyridines. *Molecules* **2025**, *30*, 2552. [CrossRef]
117. Colombo, G.; Cinco, A.; Brenna, S.; Furrer, J.; Therrien, B.; Ardizzoia, G.A. Luminescent blue emissive bis(alkynyl) borane compounds with a *N*,*O*-coordinated ligand. *Dyes Pig.* **2023**, *220*, 111722. [CrossRef]
118. Colombo, G.; Ardizzoia, G.A.; Furrer, J.; Therrien, B.; Brenna, S. Driving the Emission Towards Blue by Controlling the HOMO-LUMO Energy Gap in BF_2-Functionalized 2-(Imidazo[1,5-*a*]pyridin-3-yl)phenols. *Chem. Eur. J.* **2021**, *27*, 12380. [CrossRef]
119. Colombo, G.; Romeo, A.; Ardizzoia, G.A.; Furrer, J.; Therrien, B.; Brenna, S. Boron difluoride functionalized (tetrahydroimidazo[1,5-*a*]pyridin-3-yl)phenols: Highly fluorescent blue emissive materials. *Dyes Pigment.* **2020**, *182*, 108636. [CrossRef]
120. Mahajan, S.; Sawant, S.D. C–H Functionalization of Imidazo[1,5-*a*]pyridines: A Metal-Free Approach for Methylene Insertion to Access $C(sp^2)$–$C(sp^3)$–H–$C(sp^2)$ Bond Formation. *ACS Omega* **2024**, *9*, 49071. [CrossRef]
121. Colombo, G.; Cinco, A.; Vola, C.; Therrien, B.; Ardizzoia, G.A.; Brenna, S. Blue-Emissive Fluorescent Zinc(II) Complexes with Bis(imidazo[1,5-*a*]pyridine)methane Ligands. *Eur. J. Inorg. Chem.* **2024**, *27*, e202400251. [CrossRef]
122. Cavinato, L.M.; Volpi, G.; Fresta, E.; Garino, C.; Fin, A.; Barolo, C. Microwave-Assisted Synthesis, Optical and Theoretical Characterization of Novel 2-(imidazo[1,5-*a*]pyridine-1-yl)pyridinium Salts. *Chemistry* **2021**, *3*, 714. [CrossRef]
123. Guckian, A.L.; Doering, M.; Ciesielski, M.; Walter, O.; Hjelm, J.; O'Boyle, N.M.; Henry, W.; Browne, W.R.; McGarvey, J.J.; Vos, J.G. Assessment of intercomponent interaction in phenylene bridged dinuclear ruthenium(ii) and osmium(ii) polypyridyl complexes. *Dalton Trans.* **2004**, 3934. [CrossRef] [PubMed]
124. Panda, S.; Baliyan, R.; Dhara, S.; Huang, K.-H.; Lahiri, G.K. Redox induced oxidative C–C coupling of non-innocent bis(heterocyclo)methanides. *Dalton Trans.* **2021**, *50*, 16647. [CrossRef]
125. Sozzi, M.; Chierotti, M.R.; Gobetto, R.; Gomila, R.M.; Marzaroli, V.; Priola, E.; Volpi, G.; Zago, S.; Frontera, A.; Garino, C. One-Dimensional and Two-Dimensional Zn(II) Coordination Polymers with Ditopic Imidazo[1,5-*a*]pyridine: A Structural and Computational Study. *Molecules* **2024**, *29*, 653. [CrossRef]
126. Kulmaczewski, R.; Halcrow, M.A. Iron(II) complexes of 2,6-bis(imidazo[1,2-*a*]pyridin-2-yl)pyridine and related ligands with annelated distal heterocyclic donors. *Dalton Trans.* **2023**, *52*, 14928. [CrossRef]
127. Giuso, V.; Jouaiti, E.; Cebrián, C.; Parant-Aury, S.; Kyritsakas, N.; Gourlaouen, C.; Mauro, M. Symmetry-Broken Charge-Transfer Excited State in Homoleptic Zinc(II) Imidazo[1,2-*a*]pyridine Complexes. *ChemPhotoChem* **2023**, *7*, e202300092. [CrossRef]
128. Divya, D.; Mala, R.; Nandhagopal, M.; Narayanasamy, M.; Thennarasu, S. Coordination of Distal Carboxylate Anion Alters Metal Ion Specific Binding in Imidazo[1,2-*a*]pyridine Congeners. *J. Fluoresc.* **2023**, *33*, 1397. [CrossRef]
129. Dam, J.; Ismail, Z.; Kurebwa, T.; Gangat, N.; Harmse, L.; Marques, H.M.; Lemmerer, A.; Bode, M.L.; de Koning, C.B. Synthesis of copper and zinc 2-(pyridin-2-yl)imidazo[1,2-*a*]pyridine complexes and their potential anticancer activity. *Eur. J. Med. Chem.* **2017**, *126*, 353. [CrossRef]
130. Yong, G.; Qiao, S.; Xie, Y.; Wang, Z. Cadmium(II) and Zinc(II) Coordination Polymers with 1D Ladder and 2D Basket Weave Layer Structures Constructed from a New T-Shaped Ligand. *Eur. J. Inorg. Chem.* **2006**, *22*, 4483. [CrossRef]
131. Chang, Y.-C.; Lee, J.-Y.; Chiang, C.-F.; Chung, T.-Y.; Lee, H.M. Isomeric Imidazopyridine-Based NHC Ligands: Enhanced Catalytic Activity of an Electron-Donating Remote NHC in a PEPPSI-Type Palladium Complex. *ACS Omega* **2025**, *10*, 52076. [CrossRef]
132. Song, G.; Zhang, Y.; Li, X. Rhodium and Iridium Complexes of Abnormal N-Heterocyclic Carbenes Derived from Imidazo[1,2-*a*]pyridine. *Organometallics* **2008**, *27*, 1936. [CrossRef]
133. Modak, S.; Borah, S.; Prakasham, A.P.; Shaikh, M.M.; Butcher, R.J.; Gangwar, M.; Ghosh, P. A comparison between (*a*/*n*-NHC)PdX_2(pyridine) and (*a*/*n*-NHC)$_2PdX_2$ (X = I, Cl) type complexes of abnormal fused-bicyclic imidazo[1,2-*a*]pyridine based N-heterocyclic carbene (*a*-NHC) and of normal imidazole based N-heterocyclic carbene (*n*-NHC) ligands in the Suzuki-Miyaura coupling reactions. *Inorg. Chim. Acta* **2019**, *498*, 119090.
134. Vrban, L.; Martinac, I.A.; Hranjec, M.; Pocrnić, M.; Galić, N.; Kobetić, R.; Vianello, R. Proton and Metal Dication Affinities of Tetracyclic Imidazo[4,5-*b*]Pyridine-Based Molecules: Insights from Mass Spectrometry and DFT Analysis. *Molecules* **2025**, *30*, 2684. [CrossRef] [PubMed]
135. Wu, Y.; Xin, Y.; Pan, Y.; Yiu, S.-M.; Yan, J.; Lau, K.C.; Duan, L.; Chi, Y. Ir(III) Metal Emitters with Cyano-Modified Imidazo[4,5-*b*]pyridin-2-ylidene Chelates for Deep-Blue Organic Light-Emitting Diodes. *Adv. Sci.* **2024**, *11*, 2309389. [CrossRef]
136. Colombo, G.; Ardizzoia, G.A.; Brenna, S. Imidazo[1,5-*a*]pyridine-based derivatives as highly fluorescent dyes. *Inorg. Chim. Acta* **2022**, *535*, 120849. [CrossRef]
137. Mohbiya, D.R.; Sekar, N. Tuning 'Stokes Shift' and ICT Character by Varying the Donor Group in Imidazo[1,5-*a*]pyridines: A Combined Optical, DFT, TD-DFT and NLO Approach. *ChemistrySelect* **2018**, *3*, 1635. [CrossRef]

138. Debata, B.P.; Patel, S.; Vaidyanathan, S. Imidazo[1,5-*a*]pyridine–benzilimidazole conjugated (donor–π–acceptor) greenish-yellow fluorophores and their applications in white light-emitting diodes, acidochromism and anticounterfeiting. *J. Mater. Chem. C* **2025**, *13*, 10413. [CrossRef]
139. Giordano, M.; Volpi, G.; Garino, C.; Cardano, F.; Barolo, C.; Viscardi, G.; Fin, A. New fluorescent derivatives from papaverine: Two mechanisms to increase the quantum yield. *Dyes Pigment.* **2023**, *218*, 111482. [CrossRef]
140. Volpi, G.; Garino, C.; Fresta, E.; Casamassa, E.; Giordano, M.; Barolo, C.; Viscardi, G. Strategies to increase the quantum yield: Luminescent methoxylated imidazo[1,5-*a*]pyridines. *Dyes Pigment.* **2021**, *192*, 109455. [CrossRef]
141. Volpi, G.; Galliano, S.; Buscaino, R.; Viscardi, G.; Barolo, C. Fluorescent trifluoromethylated imidazo[1,5-*a*]pyridines and their application in luminescent down-shifting conversion. *J. Lumin.* **2022**, *242*, 118529. [CrossRef]
142. Marchesi, A.; Brenna, S.; Ardizzoia, G.A. Synthesis and emissive properties of a series of tetrahydro (imidazo[1,5-*a*]pyrid-3-yl)phenols: A new class of large Stokes shift organic dyes. *Dyes Pigment.* **2019**, *161*, 457. [CrossRef]
143. Renno, G.; Cardano, F.; Volpi, G.; Barolo, C.; Viscardi, G.; Fin, A. Imidazo[1,5-*a*]pyridine-Based Fluorescent Probes: A Photophysical Investigation in Liposome Models. *Molecules* **2022**, *27*, 3856. [CrossRef] [PubMed]
144. Yagishita, F.; Kozai, N.; Nii, C.; Tezuka, Y.; Uemura, N.; Yoshida, Y.; Mino, T.; Sakamoto, M.; Kawamura, Y. Synthesis of Dimeric Imidazo[1,5-*a*]pyridines and Their Photophysical Properties. *ChemistrySelect* **2017**, *2*, 10694. [CrossRef]
145. Vasylets, O.; Kulhanek, N.; Kirchner, M.; Göttlich, R. Symmetrical Imidazo[1,5-*a*]pyridine Dimers as Novel Organic Light Emitters: Bidirectional Synthesis and Photoluminescence Characterization. *Eur. J. Org. Chem.* **2026**, *29*, e202500888. [CrossRef]
146. Yagishita, F.; Hoshi, K.; Mukai, S.; Kinouchi, T.; Katayama, T.; Yoshida, Y.; Minagawa, K.; Furube, A.; Imada, Y. Effect of Phenolic Substituent Position in Boron Complexes of Imidazo[1,5-*a*]pyridine. *Asian J. Org. Chem.* **2022**, *11*, e202200040. [CrossRef]
147. Hazarika, S.; Ilango, B.; Parthasarathy, V.; Velusamy, M.; Kathiravan, A. Tetraphenylethylene tethered 1-(pyridine-2-yl)imidazo[1,5-*a*]pyridine: Synthesis, aggregation induced emission, copper(II) ion detection and imaging of latent fingerprint. *Dyes Pigment.* **2024**, *231*, 112387. [CrossRef]
148. Yagishita, F.; Kinouchi, T.; Hoshi, K.; Tezuka, Y.; Jibu, Y.; Karatsu, T.; Uemura, N.; Yoshida, Y.; Mino, T.; Sakamoto, M.; et al. Highly efficient blue emission from boron complexes of 1-(*o*-hydroxyphenyl)imidazo[1,5-*a*]pyridine. *Tetrahedron* **2018**, *74*, 3728. [CrossRef]
149. Ardizzoia, G.A.; Brenna, S.; Durini, S.; Therrien, B. Synthesis and characterization of luminescent zinc(II) complexes with a *N*,*N*-bidentate 1-pyridylimidazo[1,5-*a*]pyridine ligand. *Polyhedron* **2015**, *90*, 214. [CrossRef]
150. Ardizzoia, G.A.; Colombo, G.; Therrien, B.; Brenna, S. Tuning the Fluorescence Emission and HOMO-LUMO Band Gap in Homoleptic Zinc(II) Complexes with N,O-Bidentate (Imidazo[1,5-*a*]pyrid-3-yl)phenols. *Eur. J. Inorg. Chem.* **2019**, *13*, 1825. [CrossRef]
151. Volpi, G.; Priola, E.; Garino, C.; Daolio, A.; Rabezzana, R.; Benzi, P.; Giordana, A.; Diana, E.; Gobetto, R. Blue fluorescent zinc(II) complexes based on tunable imidazo[1,5-*a*]pyridines. *Inorg. Chim. Acta* **2020**, *509*, 119662. [CrossRef]
152. Volpi, G.; Giordana, A.; Priola, E.; Rabezzana, R.; Diana, E. Luminescent Imidazo[1,5-*a*]pyridine Cores and Corresponding Zn(II) Complexes: Structural and Optical Tunability. *Inorganics* **2025**, *13*, 283. [CrossRef]
153. Herr, J.M.; Rössiger, C.; Locke, H.; Wilhelm, M.; Becker, J.; Heimbrodt, W.; Schlettwein, D.; Göttlich, R. Synthesis, optical and theoretical characterization of heteroleptic Iridium(III) Imidazo[1,5-*a*]pyridine and -quinoline complexes. *Dyes Pigment.* **2020**, *180*, 108512. [CrossRef]
154. Yang, X.; Dou, C.; Wang, B.; Zhang, Q.; Li, Y. Iridium(III) complexes containing imidazo[1,5-*a*]pyridine-based ligands as photocatalysts for the [4 + 2] cycloaddition reactions of maleimides and *N*,*N*-dimethylanilines. *J. Mol. Struct.* **2025**, *1325*, 141015. [CrossRef]
155. Stipurin, S.; Strassner, T. Phosphorescent Cyclometalated Platinum(II) Hexahydroimidazo[1,5-*a*]pyridinylidene Complexes. *Eur. J. Inorg. Chem.* **2022**, *25*, e202200295. [CrossRef]
156. Asbai, Z.; Bonfiglio, A.; Mercandelli, P.; Polo, F.; Mauro, M. Cationic rhenium(I) complexes bearing a π-accepting pyridoannulated N-heterocyclic carbene ligand: Synthesis, photophysical, electrochemical and theoretical investigation. *Polyhedron* **2021**, *197*, 115025. [CrossRef]
157. Salassa, L.; Garino, C.; Albertino, A.; Volpi, G.; Nervi, C.; Gobetto, R.; Hardcastle, K.I. Computational and Spectroscopic Studies of New Rhenium(I) Complexes Containing Pyridylimidazo[1,5-*a*]pyridine Ligands: Charge Transfer and Dual Emission by Fine-Tuning of Excited States. *Organometallics* **2008**, *27*, 1427. [CrossRef]
158. Blanco-Rodríguez, A.M.; Kvapilová, H.; Sýkora, J.; Towrie, M.; Nervi, C.; Volpi, G.; Záliš, S.; Vlček, A., Jr. Photophysics of Singlet and Triplet Intraligand Excited States in [$ReCl(CO)_3$(1-(2-pyridyl)-imidazo[1,5-*a*]pyridine)] Complexes. *J. Am. Chem. Soc.* **2014**, *136*, 5963. [CrossRef] [PubMed]
159. Giuso, V.; Gourlaouen, C.; Delporte-Pébay, M.; Groizard, T.; Vanthuyne, N.; Crassous, J.; Daniel, C.; Mauro, M. Chiroptical activity of benzannulated N-heterocyclic carbene rhenium(I) tricarbonyl halide complexes: Towards efficient circularly polarized luminescence emitters. *Phys. Chem. Chem. Phys.* **2024**, *26*, 4855. [CrossRef]

160. Uoyama, H.; Goushi, K.; Shizu, K.; Nomura, H.; Adachi, C. Highly efficient organic light-emitting diodes from delayed fluorescence. *Nature* **2012**, *492*, 234. [CrossRef] [PubMed]
161. Douhal, A.; Amat-Guerri, F.; Acuña, A.U. Photoinduced Intramolecular Proton Transfer and Charge Redistribution in Imidazopyridines. *J. Phys. Chem.* **1995**, *99*, 76. [CrossRef]
162. Jouaiti, E.; Giuso, V.; Cianfrani, D.; Kyritsakas, N.; Gourlaouen, C.; Mauro, M. Bright V-Shaped *bis*-Imidazo[1,2-*a*]pyridine Fluorophores with Near-UV to Deep-Blue Emission. *Chem. Asian J.* **2022**, *17*, e202200903. [CrossRef]
163. Zucolotto Cocca, L.H.; Pelosi, A.G.; Valverde, J.V.P.; le Bescont, J.; Breton-Patient, C.; Piguel, S.; Mendonça, C.R.; De Boni, L. 3-arylthioimidazo[1,2-*a*]pyridine derivatives: A theoretical and experimental study of its photophysical properties. *J. Photochem. Photobiol. A Chem.* **2023**, *440*, 114675. [CrossRef]
164. Velázquez-Olvera, S.; Salgado-Zamora, H.; Velázquez-Ponce, M.; Campos-Aldrete, E.; Reyes-Arellano, A.; Pérez-González, C. Fluorescent property of 3-hydroxymethyl imidazo[1,2-*a*]pyridine and pyrimidine derivatives. *Chem. Cent. J.* **2012**, *6*, 83. [CrossRef]
165. Tomoda, H.; Hirano, T.; Saito, S.; Mutai, T.; Araki, K. Substituent Effects on Fluorescent Properties of Imidazo[1,2-*a*]pyridine-Based Compounds. *Bull. Chem. Soc. Jpn.* **1999**, *72*, 1327. [CrossRef]
166. Zheng, Q.; Li, X.; Kurpiewska, K.; Dömling, A. Synthesis of Tunable Fluorescent Imidazole-Fused Heterocycle Dimers. *Org. Lett.* **2022**, *24*, 5014. [CrossRef] [PubMed]
167. Abe, S.; Katayama, T.; Furube, A.; Tabata, A.; Yoshida, Y.; Ueta, S.; Arakawa, Y.; Minagawa, K.; Imada, Y.; Yagishita, F. Synthesis of naphthalene-fused imidazo[1,2-*a*]pyridinium salts showing green luminescence with high quantum yields and large Stokes shift. *Org. Biomol. Chem.* **2025**, *23*, 4355. [CrossRef] [PubMed]
168. Zhu, Y.; Sun, X.; Yuan, Y.; Zhao, X.; Zhai, Z.; Song, B.; Zhang, W.; Zhu, X.; Hao, X.-Q. Imidazo[1,2-*a*]pyridine-based polarity and viscosity-dependent fluorescent probes and application in selective detection of 2,6-dichloro-4-nitroaniline. *Dyes Pigment.* **2024**, *231*, 112425. [CrossRef]
169. Valverde, J.V.P.; Pelosi, A.G.; Zucolotto Cocca, L.H.; Marbello, O.D.; le Bescont, J.; Breton-Patient, C.; Piguel, S.; Silva, D.L.; De Boni, L.; Mendonça, C.R. Two-photon absorption in imidazo[1,2-*a*]pyridine derivatives: Study of nonlinear optical response and dipolar properties. *J. Mol. Liq.* **2023**, *373*, 121250. [CrossRef]
170. Mala, R.; Divya, D.; Vijayan, P.; Narayanasamy, M.; Thennarasu, S. Two Imidazo[1,2-*a*]pyridine Congeners Show Aggregation-Induced Emission (AIE): Exploring AIE Potential for Sensor and Imaging Applications. *ChemistrySelect* **2022**, *7*, e202103408. [CrossRef]
171. Tong, L.; Yang, Y.; Zhang, L.; Tao, J.; Sun, B.; Song, C.; Qi, M.; Yang, F.; Zhao, M.; Jiang, J. Design, Synthesis of Hydrogen Peroxide Response AIE Fluorescence Probes Based on Imidazo[1,2-*a*] Pyridine. *Molecules* **2024**, *29*, 882. [CrossRef]
172. Xiao, S.; Liu, Z.; Zhao, J.; Pei, M.; Zhang, G.; He, W. A novel fluorescent sensor based on imidazo[1,2-*a*]pyridine for Zn^{2+}. *RSC Adv.* **2016**, *6*, 27119. [CrossRef]
173. Mala, R.; Suman, K.; Nandhagopak, M.; Narayanasamy, M.; Thennarasu, S. Chelation of specific metal ions imparts coplanarity and fluorescence in two imidazo[1,2-*a*]pyridine derivatives: Potential chemosensors for detection of metal ions in aqueous and biosamples. *Biomol. Spectr.* **2019**, *222*, 117236. [CrossRef]
174. Sun, J.; Xi, M.; Su, Z.-S.; He, H.-X.; Tian, M.; Li, H.-Y.; Zhang, H.-K.; Mao, T.; Zhang, Y.-X. Highly Efficient Greenish-Yellow Phosphorescent Organic Light-Emitting Diodes Based on a Novel 2,3-Diphenylimidazo[1,2-*a*]Pyridine Iridium(III) Complex. *Chin. Phys. Lett.* **2016**, *33*, 038501. [CrossRef]
175. Yao, C.; Xue, Z.; Lian, M.; Xu, X.; Zhao, J.; Zhou, G.; Wu, Y.; Yu, D.; Wong, W.-Y. Phosphorescent iridium(III) complexes based on 2-phenylimidazo[1,2-*a*]pyridine-type ligands: Synthesis, photophysical, electrochemical, and electrophosphorescent properties. *J. Organomet. Chem.* **2015**, *784*, 31. [CrossRef]
176. Takizawa, S.; Nishida, J.; Tsuzuki, T.; Tokito, S.; Yamashita, Y. Phosphorescent Iridium Complexes Based on 2-Phenylimidazo[1,2-*a*]pyridine Ligands: Tuning of Emission Color toward the Blue Region and Application to Polymer Light-Emitting Devices. *Inorg. Chem.* **2007**, *46*, 4308. [CrossRef]
177. Zargariyan, M.; Roohi, H. Fine-tuning the photophysical properties of Imidazo[1,2-*a*]pyridine-based dyes by the change in substituent and solvent media: DFT and TD-DFT studies. *Mol. Phys.* **2025**, *123*, e2376212. [CrossRef]
178. Bhosle, A.A.; Banerjee, M.; Thakuri, A.; Vishwakarma, O.D.; Chatterjee, A. An ESIPT-active orange-emissive 2-(2′-hydroxyphenyl)imidazo[1,2-*a*]pyridine-derived chemodosimeter for turn-on detection of fluoride ions via desilylation. *RSC Adv.* **2024**, *14*, 33312. [CrossRef] [PubMed]
179. Mutai, T.; Ohkawa, T.; Shono, H.; Araki, K. The development of aryl-substituted 2-phenylimidazo[1,2-*a*]pyridines (PIP) with various colors of excited-state intramolecular proton transfer (ESIPT) luminescence in the solid state. *J. Mater. Chem. C* **2016**, *4*, 3599. [CrossRef]
180. Mutai, T.; Sawatani, H.; Shinda, T.; Shono, H.; Araki, K. Tuning of excited-state intramolecular proton transfer (ESIPT) fluorescence of imidazo[1,2-*a*]pyridine in rigid matrices by substitution effect. *J. Org. Chem.* **2013**, *78*, 2482. [CrossRef]

181. Shigemitsu, Y.; Mutai, T.; Houjou, H.; Araki, K. Excited-State Intramolecular Proton Transfer (ESIPT) Emission of Hydroxyphenylimidazopyridine: Computational Study on Enhanced and Polymorph-Dependent Luminescence in the Solid State. *J. Phys. Chem. A* **2012**, *116*, 12041. [CrossRef]
182. Paras; Vivek; Sharma, S.; Ramachandran, C.N. Effect of Electron-Donating Substituents and an Electric Field on the ΔE_{ST} of Selected Imidazopyridine Derivatives: A DFT Study. *J. Phys. Chem. A* **2024**, *128*, 8428. [CrossRef]
183. Lai, D.; Hajra, A.; Sinha, S. Synthesis, Characterization, and Photophysical Investigation of a Dyad Comprising 8-Methyl-2-phenylimidazo[1,2-*a*]pyridine and N-methyl Maleimide for Photoinduced Electron Transfer. *ChemistrySelect* **2025**, *10*, e01958. [CrossRef]
184. Boček, I.; Hranjec, M.; Vianello, R. Imidazo[4,5-*b*]pyridine derived iminocoumarins as potential pH probes: Synthesis, spectroscopic and computational studies of their protonation equilibria. *J. Mol. Liq.* **2022**, *355*, 118982. [CrossRef]
185. Hranjec, M.; Perin, N.; Boček Pavlinac, I.; Vianello, R. When position matters—Diverse optical properties of two tetracyclic imidazo[4,5-*b*]pyridine regioisomers differing in one nitrogen atom position. *J. Mol. Struct.* **2026**, *1350*, 144109. [CrossRef]
186. Yang, X.; Zhou, X.; Zhang, Y.-X.; Li, D.; Li, C.; You, C.; Chou, T.-C.; Su, S.-J.; Chou, P.-T.; Chi, Y. Blue Phosphorescence and Hyperluminescence Generated from Imidazo[4,5-*b*]pyridin-2-ylidene-Based Iridium(III) Phosphors. *Adv. Sci.* **2022**, *9*, 2201150. [CrossRef] [PubMed]
187. Pinter, P.; Pittkowski, R.; Soellner, J.; Strassner, T. The Chameleonic Nature of Platinum(II) Imidazopyridine Complexes. *Chem. Eur. J.* **2017**, *23*, 14173. [CrossRef] [PubMed]
188. Behera, S.K.; Karak, A.; Krishnamoorthy, G. Photophysics of 2-(4′-Amino-2′-hydroxyphenyl-1*H*-imidazo[4,5-*c*]pyridine and Its Analogues: Intramolecular Proton Transfer versus Intramolecular Charge Transfer. *J. Phys. Chem. B* **2015**, *119*, 2330. [CrossRef]
189. Brenlla, A.; Veiga, M.; Pérez Lustres, J.L.; Ríos Rodríguez, M.C.; Rodríguez-Prieto, F.; Mosquera, M. Photoinduced Proton and Charge Transfer in 2-(2′-Hydroxyphenyl)imidazo[4,5-*b*]pyridine. *J. Phys. Chem. B* **2013**, *117*, 884. [CrossRef] [PubMed]
190. Colombo, G.; Cinco, A.; Ardizzoia, G.A.; Brenna, S. Long-Alkyl Chain Functionalized Imidazo[1,5-*a*]pyridine Derivatives as Blue Emissive Dyes. *Colorants* **2023**, *2*, 179. [CrossRef]
191. Albrecht, G.; Rössiger, C.; Herr, J.M.; Locke, H.; Yanagi, H.; Göttlich, R.; Schlettwein, D. Optimization of the Substitution Pattern of 1,3-Disubstituted Imidazo[1,5-*a*]Pyridines and -Quinolines for Electro-Optical Applications. *Phys. Status Solidi B* **2019**, *257*, 1900677. [CrossRef]
192. Girase, J.D.; Kajjam, A.B.; Dubey, D.K.; Kesavan, K.K.; Jou, J.-H.; Vaidyanathan, S. Unipolar 1-phenylimidazo[1,5-*a*]pyridine: A new class of ultra-bright sky-blue emitters for solution-processed organic light emitting diodes. *New J. Chem.* **2022**, *46*, 16717. [CrossRef]
193. Fresta, E.; Volpi, G.; Garino, C.; Barol, C.; Costa, R.D. Contextualizing yellow light-emitting electrochemical cells based on a blue-emitting imidazo-pyridine emitter. *Polyhedron* **2018**, *140*, 129. [CrossRef]
194. Weber, M.D.; Garino, C.; Volpi, G.; Casamassa, E.; Milanesio, M.; Barolo, C.; Costa, R.D. Origin of a counterintuitive yellow light-emitting electrochemical cell based on a blue-emitting heteroleptic copper(I) complex. *Dalton Trans.* **2016**, *45*, 8984. [CrossRef] [PubMed]
195. Irfan, A.; Chaudhry, A.R.; Al-Sehemi, A.G.; Assiri, M.A.; Hussain, A. Charge carrier and optoelectronic properties of phenylimidazo[1,5-*a*]pyridine-containing small molecules at molecular and solid-state bulk scales. *Comput. Mater. Sci.* **2019**, *170*, 109179. [CrossRef]
196. Nagarajan, N.; Velmurugan, G.; Prakas, A.; Shakti, N.; Katiyar, M.; Venuvanalingam, P.; Renganathan, R. Highly emissive luminogens based on imidazo[1,2-*a*]pyridine for electroluminescent applications. *Chem. Asian J.* **2014**, *9*, 294. [CrossRef]
197. Zheng, X.-H.; Zhao, J.-W.; Chen, X.; Cai, R.; Yang, G.-X.; Zhu, J.-J.; Tang, S.-S.; Lin, Z.-H.; Tao, S.-L.; Tong, Q.-X. Imidazo[1,2-*a*]pyridine as an Electron Acceptor to Construct High-Performance Deep-Blue Organic Light-Emitting Diodes with Negligible Efficiency Roll-Off. *Chemistry* **2020**, *26*, 8588. [CrossRef]
198. Yahwantrao, G.; Poojary, M.; Verma, A.; Thakkar, C.; Tripathi, A.; Badani, P.; Bose, S.; Saha, S. Rationally designed imidazo[1,2-*a*]pyridine based AIEgens for non-doped OLEDs with high efficiency and low-efficiency roll-offs. *J. Mater. Chem. C* **2025**, *13*, 23120. [CrossRef]
199. Liao, Y.; Wang, C.; Dai, L.; Shao, G.; Chen, X.; Wu, D.; Xia, J. *ortho*-π-Extension of perylene diimides via one-pot annulation of imidazo[1,2-*a*]pyridine or imidazo[1,2-*a*]pyrazine for n-type organic field-effect transistors. *J. Mater. Chem. C* **2025**, *13*, 6888. [CrossRef]
200. Lee, J.; Chen, H.-F.; Batagoda, T.; Coburn, C.; Djurovich, P.I.; Thompson, M.E.; Forrest, S.R. Deep blue phosphorescent organic light-emitting diodes with very high brightness and efficiency. *Nat. Mater.* **2016**, *15*, 92. [CrossRef]
201. Wu, C.; Wu, Y.; Tong, K.-N.; Kuhn, M.; Yiu, S.-M.; Kung, Y.-C.; Hung, W.-Y.; Yan, J.; Zhou, X.; Wei, G.; et al. Blue-emitting iridium(III) phosphors with functional imidazo[4,5-*b*]pyridin-2-ylidene cyclometalates: Designs aimed at greater steric hindrance. *J. Mater. Chem. C* **2025**, *13*, 12663. [CrossRef]

202. Yan, J.; Feng, Z.-Q.; Wu, Y.; Zhou, D.-Y.; Yiu, S.-M.; Chan, C.-Y.; Pan, Y.; Lau, K.C.; Liao, L.-S.; Chi, Y. Blue Electrophosphorescence from Iridium(III) Phosphors Bearing Asymmetric Di-N-aryl 6-(trifluoromethyl)-2*H*-imidazo[4,5-*b*]pyridin-2-ylidene Chelates. *Adv. Mater.* **2023**, *36*, 2305273. [CrossRef]
203. Liu, T.-Z.; Yuan, Y.-C.; Zhao, B.-X. An imidazo[1,5-*a*]pyridines-based ratiometric fluorescent probe for sensing sulfur dioxide derivatives in real samples based on a FRET mechanism. *Spectrochim. Acta Part A Mol. Biomol. Spectrosc.* **2022**, *282*, 121694. [CrossRef]
204. Ge, Y.; Xing, X.; Liu, A.; Ji, R.; Shen, S.; Cao, X. A novel imidazo[1,5-*a*]pyridine-rhodamine FRET system as an efficient ratiometric fluorescent probe for Hg^{2+} in living cells. *Dyes Pigment.* **2017**, *146*, 136. [CrossRef]
205. Yuan, Q.; Chen, L.-L.; Zhu, X.-H.; Yuan, Z.-H.; Duan, Y.-T.; Yang, Y.-S.; Wang, B.-Z.; Wang, X.-M.; Zhu, H.-L. An imidazo[1,5-*a*]pyridine-derivated fluorescence sensor for rapid and selective detection of sulfite. *Talanta* **2020**, *217*, 121087. [CrossRef]
206. Hwang, S.M.; Yun, D.; Kim, C. An Imidazo[1,5-α]Pyridine-Based Fluorometric Chemodosimeter for the Highly Selective Detection of Hypochlorite in Aqueous Media. *J. Fluoresc.* **2019**, *29*, 451. [CrossRef] [PubMed]
207. Chen, S.; Li, H.; Hou, P. A large stokes shift fluorescent probe for sensing of thiophenols based on imidazo[1,5-*a*]pyridine in both aqueous medium and living cells. *Anal. Chim. Acta* **2017**, *993*, 63. [CrossRef]
208. Strianese, M.; Brenna, S.; Ardizzoia, G.A.; Guarnieri, D.; Lamberti, M.; D'Auria, I.; Pellecchia, C. Imidazo-pyridine-based zinc(II) complexes as fluorescent hydrogen sulfide probes. *Dalton Trans.* **2021**, *50*, 17075. [CrossRef]
209. Han, X.-H.; Zhao, P.; Tank, M.-K.; Yang, L.; Wang, Q.; Zhang, S.-S. An imidazo[1,2-*a*]pyridine-functionalized xanthene fluorescent probe for naked-eye detection of Hg^{2+} and its application in cell imaging and test strips. *Sens. Diagn.* **2024**, *3*, 1062. [CrossRef]
210. Li, D.; Wang, Q.; Rao, N.; Zhang, Y.; Le, Y.; Liu, L.; Li, L.; Huang, L.; Yan, L. Development of Imidazo[1,2-*a*]pyridine-based probe for detection of hydrazine and its applications in imaging of HepG2 cell. *J. Mol. Struct.* **2021**, *1239*, 130521. [CrossRef]
211. Dhamapurkar, Y.A.; Chaudhran, P.A.; Chandrakar, L.; Bahiram, Y.M.; Sharma, A. Imidazo[1,2-*a*]pyridine Based D-π-A Fluorescent Sensor for Detection of Diethylcyanophosphonate. *ChemistrySelect* **2024**, *9*, e202303240. [CrossRef]
212. Zhu, Y.; Liao, K.; Li, Y.; Zhang, W.; Song, B.; Hao, X.-Q.; Zhu, X. Dual-state emissive imidazo[1,2-*a*]pyridines with full color emission, acidochromism, viscosity-dependent fluorescence, and bioimaging applications. *Dyes Pigment.* **2024**, *224*, 112004. [CrossRef]
213. Zhang, B.; Suo, Q.; Li, Q.; Hu, J.; Zhu, Y.; Gao, Y.; Wang, Y. Multiresponsive chemosensors based on ferrocenylimidazo[4,5-*b*]pyridines: Solvent-dependent selective dual sensing of Hg^{2+} and Pb^{2+}. *Tetrahedron* **2022**, *120*, 132878. [CrossRef]
214. Kitagawa, T.; Hanai, N.; Kawano, T.; Tono, A.; Tabata, H.; Kobayashi, T.; Hirai, K.; Okazaki, T. Metal-ion sensor composed of self-assembled monolayer of amine ligand formed by the use of molecular tripod. *J. Phys. Org. Chem.* **2023**, *36*, e4493. [CrossRef]
215. Zhang, B.; Suo, Q.; Li, Q.; Zhu, Y.; Gao, X.; Lv, L.; Gao, Y.; Jia, H.; Wang, Y. New Sulfur-Containing Ferrocenylimidazo[4,5-*b*]pyridines: Multiresponsive Hg^{2+} Ion Sensing and Structure-Sensing Correlation. *ChemistrySelect* **2022**, *7*, e202103565. [CrossRef]
216. Xie, Z.-B.; Yue, T.-C.; Dong, Q.-W.; Ma, Q.-C.; Cao, Q.-W.; Wang, L.-L.; Wang, D.-Z. Selective detection of Fe^{3+} and Congo red adsorption properties studies of Ln-complexes based on imidazopyridine carboxylic acid ligand. *Polyhedron* **2024**, *249*, 116777. [CrossRef]
217. Volpi, G.; Lace, B.; Garino, C.; Priola, E.; Artuso, E.; Cerreia Vioglio, P.; Barolo, C.; Fin, A.; Genre, A.; Prandi, C. New substituted imidazo[1,5-*a*]pyridine and imidazo[5,1-a]isoquinoline derivatives and their application in fluorescence cell imaging. *Dyes Pigment.* **2018**, *157*, 298. [CrossRef]
218. Chen, S.; Li, H.; Hou, P. A novel imidazo[1,5-*a*]pyridine-based fluorescent probe with a large Stokes shift for imaging hydrogen sulfide. *Sens. Actuators B Chem.* **2018**, *256*, 1086. [CrossRef]
219. Xia, H.; Wang, X.; Huang, W.; Jiang, X.; Han, X.; Wang, C. A fluorescent probe with a vanillin–pyridine–imidazole core structure for carboxylesterase detection in macrophage polarization during bone homeostasis. *Front. Chem.* **2025**, *13*, 1666238. [CrossRef] [PubMed]
220. Cui, R.; Liu, C.; Zhang, P.; Qin, K.; Ge, Y. An Imidazo[1,5-*a*]pyridine Benzopyrylium-Based NIR Fluorescent Probe with Ultra-Large Stokes Shifts for Monitoring SO_2. *Molecules* **2023**, *28*, 515. [CrossRef]
221. Yagishita, F.; Katayama, T.; Kawamura, Y.; Watanabe, G.; Abe, S.; Ogawa, I.; Tabata, A.; Yoshida, Y.; Masu, H.; Ueta, S.; et al. Blue Luminescent Boron Complexes Based on N,N-Type Imidazo[1,5-*a*]pyridine Ligand for Mitochondrial Imaging. *Asian J. Org. Chem.* **2024**, *13*, e202400189. [CrossRef]
222. Reviglio, C.; Volpi, G.; Wyart, E.; Ciubini, B.; Prandi, C.; Barolo, C.; Porporato, P.E.; Garino, C. Imidazopyridines as fluorogenic substrates for esterase detection. *J. Photochem. Photobiol. A Chem.* **2025**, *462*, 116256. [CrossRef]
223. Song, G.-J.; Bai, S.-Y.; Dai, X.; Cao, X.-Q.; Zhao, B.-X. A ratiometric lysosomal pH probe based on the imidazo[1,5-*a*]pyridine–rhodamine FRET and ICT system. *RSC Adv.* **2016**, *6*, 41317. [CrossRef]
224. Zhu, M.; Wang, L.; Wu, X.; Na, R.; Wang, Y.; Li, Q.X.; Hammock, B.D. A novel and simple imidazo[1,2-*a*]pyridin fluorescent probe for the sensitive and selective imaging of cysteine in living cells and zebrafish. *Anal. Chim. Acta* **2019**, *1058*, 155. [CrossRef] [PubMed]

225. Srivastava, S.; Thakur, N.; Singh, A.; Shukla, P.; Maikhuri, V.K.; Garg, N.; Prasad, A.; Pandey, R. Development of a fused imidazo[1,2-*a*]pyridine based fluorescent probe for Fe^{3+} and Hg^{2+} in aqueous media and HeLa cells. *RSC Adv.* **2019**, *9*, 29856. [CrossRef]
226. Thakur, A.; Sharma, A. Imidazo[1,2-*a*]pyridine based small organic fluorescent molecules for selective detection of nerve agents simulants. *Spectrochim. Acta Part A Mol. Biomol. Spectrosc.* **2022**, *282*, 121633. [CrossRef]
227. Banerji, B.; Chatterjee, S.; Chandrasekar, K.; Bera, S.; Majumder, L.; Prodha, C.; Chaudhuri, K. Expedient synthesis of a phenanthro-imidazo-pyridine fused heteropolynuclear framework via CDC coupling: A new class of luminophores. *Org. Biomol. Chem.* **2017**, *15*, 4130. [CrossRef]
228. Yang, X.; Wang, B.; Li, Y. Iridium(III) and Rhodium(III) Complexes with Imidazo[1,5-*a*]pyridine-Based Cyclometalating Ligands: Synthesis, Photophysical and Electrochemical Properties, and Catalytic Activities Toward the [4 + 2] Cycloaddition Reactions of Tertiary Anilines and Maleimides. *Appl. Organomet. Chem.* **2024**, *39*, e7934.
229. Yaghishita, F.; Nagamori, T.; Shimokawa, S.; Hoshi, K.; Yoshida, Y.; Imada, Y.; Kawamura, Y. Visible-light-induced oxidative coupling reaction of benzylic amines using iridium(III) complex of pincer type imidazo[1,5-*a*]pyridine ligand. *Tetrahedron Lett.* **2020**, *61*, 151782. [CrossRef]
230. Jacoby, S.A.; Harris, N.W.; Wiemann, A.; Glenn, C.D.; Kantzler, A.R.; Dinh, L.P.; Yet, L. Suzuki-Miyaura and Buchwald-Hartwig Cross-Coupling Reactions Utilizing a Set of Complementary Imidazopyridine Monophosphine Ligands. *ChemistrySelect* **2024**, *9*, e202305085. [CrossRef]
231. Yagishita, F.; Shimokawa, S.; Uemura, N.; Yoshida, Y.; Mino, T.; Sakamoto, M.; Kawamura, Y. Palladium-Catalyzed Mizoroki–Heck Reaction of Aryl Iodides with Allyl Aryl Ethers Using Imidazo[1,5-*a*]pyridines. *ChemistrySelect* **2017**, *2*, 10143. [CrossRef]
232. Yagishita, F.; Nomura, K.; Shiono, S.; Nii, C.; Mino, T.; Sakamoto, M.; Kawamura, Y. Palladium–catalyzed Mizoroki–Heck Reaction Using Imidazo[1,5-*a*]pyridines. *ChemistrySelect* **2016**, *1*, 4560. [CrossRef]
233. Ardizzoia, G.A.; Ghiotti, D.; Therrien, B.; Brenna, S. Homoleptic complexes of divalent metals bearing *N*,*O*-bidentate imidazo[1,5-*a*]pyridine ligands: Synthesis, X-ray characterization and catalytic activity in the Heck reaction. *Inorg. Chim. Acta* **2018**, *471*, 384. [CrossRef]
234. Rayasingh, A.R.; Manivannan, V. Palladium(II) and platinum(II) complexes of disubstituted imidazo[1,5-*a*]pyridine and imidazolylpyridine: Coordination chemistry, versatile catalysis, and biophysical study. *Dalton Trans.* **2025**, *54*, 7741. [CrossRef]
235. Shibahara, F.; Shibata, Y.; Murai, T. Imidazo[1,5-*a*]pyridinylidenes as π-Accepting NHC Ligands in Catalysis. *Chem. Lett.* **2021**, *50*, 1892. [CrossRef]
236. Roy, S.; Javed, S.; Olmstead, M.M.; Patra, A.K. First structural example of a metal uncoordinated mesoionic imidazo[1,5-*a*]pyridine and its precursor intermediate copper complex: An insight to the catalytic cycle. *Dalton Trans.* **2011**, *40*, 12866. [CrossRef] [PubMed]
237. Jia, B.; Liu, Z.; Gao, Z.; Zhou, S.; Wu, M.; Zhang, Q.; Zhang, X.; Chen, S.; Yang, X.; Li, Y. Cu(II) and Cu(I) complexes based on derivatives of imidazo[1,5-*a*]pyridine: Synthesis, structures, in situ metal-ligand reactions, and catalytic activity. *Chin. J. Inorg. Chem.* **2025**, *41*, 1020.
238. Zhang, Q.; Cui, Y.-F.; Zhang, X.-M.; Li, Y.-H.; Yao, J.-L. Manganese(II) and Copper(I) Compounds Based on Two Derivatives of Imidazo[1,5-*a*]pyridine: Synthesis, Structures, Magnetic Properties, and Catalytic Activity. *Chin. J. Struct. Chem.* **2022**, *41*, 2203148.
239. D'Alterio, M.C.; D'Auria, I.; Gaeta, L.; Tedesco, C.; Brenna, S.; Pellecchia, C. Are Well Performing Catalysts for the Ring Opening Polymerization of L-Lactide under Mild Laboratory Conditions Suitable for the Industrial Process? The Case of New Highly Active Zn(II) Catalysts. *Macromolecules* **2022**, *55*, 5115. [CrossRef]
240. Gentile, M.; Gaeta, L.; Brenna, S.; Pellecchia, C. Efficient chemical recycling of poly(L-lactic acid) via either alcoholysis to alkyl lactate or thermal depolymerization to L-lactide promoted by Zn(II) catalysts. *Polym. Test.* **2025**, *143*, 108727. [CrossRef]
241. Kang, C.; Kim, S.; Han, W.; Tyu, H.; Seong, W.; Kim, J.; Park, D.-E.; Park, S.; Park, K.; Park, H.M.; et al. In situ generated diphenylphosphine-chelated imidazo[1,5-*a*]pyridin-3-ylidene nickel(0) catalysts for highly efficient acrylate synthesis from ethylene and CO_2. *J. CO2 Util.* **2025**, *91*, 103004. [CrossRef]
242. Engen, K.; Lundbäck, T.; Yadav, A.; Puthiyaparambath, S.; Rosenström, U.; Gising, J.; Jenmalm-Jensen, A.; Hallberg, M.; Larhed, M. Inhibition of Insulin-Regulated Aminopeptidase by Imidazo[1,5-*a*]pyridines-Synthesis and Evaluation. *Int. J. Mol. Sci.* **2024**, *25*, 2516. [CrossRef] [PubMed]
243. Truong, D.T.; Ho, K.; Nhi, H.T.Y.; Nguyen, V.H.; Dang, T.T.; Nguyen, M.T. Imidazole[1,5-*a*]pyridine derivatives as EGFR tyrosine kinase inhibitors unraveled by umbrella sampling and steered molecular dynamics simulations. *Sci. Rep.* **2024**, *14*, 12218. [CrossRef] [PubMed]
244. Marner, M.; Kulhanek, N.; Eichberg, J.; Hardes, K.; Dal Molin, M.; Rybniker, J.; Kirchner, M.; Schäberle, T.F.; Göttlich, R. Design, synthesis and antimycobacterial activity of imidazo[1,5-*a*]quinolines and their zinc-complexes. *RSC Med. Chem.* **2024**, *15*, 1746. [CrossRef]

245. Kamal, A.; Subba Rao, A.V.; Lakshma Nayak, V.; Subba Reddy, N.V.; Swapna, K.; Ramakrishna, G.; Alvala, M. Synthesis and biological evaluation of imidazo[1,5-*a*]pyridine-benzimidazole hybrids as inhibitors of both tubulin polymerization and PI3K/Akt pathway. *Org. Biomol. Chem.* **2014**, *12*, 9864. [CrossRef]
246. Gopathi, R.; Pradeep Kumar, M.; Jagadeeesh Kumar, G.; Syamprasad, N.P.; Geetanjali Kodiripala, B.; Naidu, V.G.M.; Nagendra Babu, B. Exploration of the cytotoxic and microtubule disruption potential of novel imidazo[1,5-*a*]pyridine-based chalcones. *RSC Med. Chem.* **2025**, *16*, 1188. [CrossRef]
247. Alapati, K.B.; Sravani, D.; Gouthamsri, S.; Sailaja, B.B.V.; Sarith, B.; Nalla, S. Design, synthesis and biological various aryl derivatives of (pyridin-4-yl) imidazo[1,5-*a*]pyridin-1-yl)oxazoles as anticancer agents. *Chem. Data Collect.* **2024**, *54*, 101162. [CrossRef]
248. Roy, M.; Chakravarthi, B.V.S.K.; Jayabaskaran, C.; Karande, A.A.; Chakravarty, A.R. Impact of metal binding on the antitumor activity and cellular imaging of a metal chelator cationic imidazopyridine derivative. *Dalton Trans.* **2011**, *40*, 4855–4864. [CrossRef] [PubMed]
249. Scattolin, T.; Andreetta, G.; Mauceri, M.; Rizzolio, F.; Demitri, N.; Canzonieri, V.; Visentin, F. Imidazo[1,5-*a*]pyridine-3-ylidenes and dipyridoimidazolinylidenes as ancillary ligands in Palladium allyl complexes with potent in vitro anticancer activity. *J. Organomet. Chem.* **2021**, *952*, 122014. [CrossRef]
250. Ghanta, S.; Chandrasekhar, C.; Sravani, D.; Bhuvan Tej, M.; Syed, T.; Kumar Kapavarapu, R.; Ramesh Raju, R. Design and Synthesis of Various Aryl Amide Derivatives of Imidazo[1,5-*a*] Pyridine-1,2,4-Thiadiazoles: In Vitro Cytotoxicity Evaluation and In Silico Molecular Docking Studies. *Chem. Biodiver.* **2024**, *22*, e202401380. [CrossRef]
251. Hoshi, K.; Itaya, M.; Tahara, K.; Matsumoto, A.; Tabata, A.; Nagamune, H.; Yoshida, Y.; Hase, E.; Minamikawa, T.; Yasui, T.; et al. Two-photon excitable boron complex based on tridentate imidazo[1,5-*a*]pyridine ligand for heavy-atom-free mitochondria-targeted photodynamic therapy. *RSC Adv.* **2021**, *11*, 26403. [CrossRef]
252. Prostota, Y.; Kachkovsky, O.D.; Reis, L.V.; Santos, P.F. New unsymmetrical squaraine dyes derived from imidazo[1,5-*a*]pyridine. *Dyes Pigment.* **2013**, *96*, 554. [CrossRef]
253. Yagishita, F.; Tanigawa, J.; Nii, C.; Tabata, A.; Nagamune, H.; Takanari, H.; Imada, Y.; Kawamura, Y. Fluorescent Imidazo[1,5-*a*]pyridinium Salt for a Potential Cancer Therapy Agent. *ACS Med. Chem. Lett.* **2019**, *10*, 1110. [CrossRef]
254. Correia, J.H.; Rodrigues, J.A.; Pimenta, S.; Dong, T.; Yang, Z. Photodynamic Therapy Review: Principles, Photosensitizers, Applications, and Future Directions. *Pharmaceutics* **2021**, *13*, 1332. [CrossRef] [PubMed]
255. Zhao, X.; Liu, J.; Fan, J.; Chao, H.; Peng, X. Recent progress in photosensitizers for overcoming the challenges of photodynamic therapy: From molecular design to application. *Chem. Soc. Rev.* **2021**, *50*, 4185. [CrossRef]
256. Liu, R.; Marshall, K.; Ma, R.; Thi Pham, K.L.; Shetye, G.; Liu, Z.; Cho, S.; Jeong, H.; Franzblau, S.G.; Moraski, G.C.; et al. Syntheses and studies of deuterated Imdiazo[1,2-*a*] pyridine-3-carboxamides with potent anti-tuberculosis activity and improved metabolic properties. *Bioorg. Chem.* **2022**, *128*, 106074. [CrossRef] [PubMed]
257. Kang, S.; Kim, R.Y.; Seo, M.J.; Lee, S.; Kim, Y.M.; Seo, M.; Seo, J.J.; Ko, Y.; Choi, I.; Jang, J.; et al. Lead Optimization of a Novel Series of Imidazo[1,2-*a*]pyridine Amides Leading to a Clinical Candidate (Q203) as a Multi- and Extensively-Drug-Resistant Anti-tuberculosis Agent. *J. Med. Chem.* **2014**, *57*, 5293. [CrossRef]
258. Abdelaziz, R.; Di Trani, J.M.; Sahile, H.; Mann, L.; Richter, A.; Liu, Z.; Bueler, S.A.; Cowen, L.E.; Rubinstein, J.L.; Imming, P. Imidazopyridine Amides: Synthesis, Mycobacterium smegmatis $CIII_2CIV_2$ Supercomplex Binding, and In Vitro Antimycobacterial Activity. *ACS Omega* **2023**, *8*, 19081. [CrossRef]
259. Dos Santos, D.C.; Rafique, J.; Saba, S.; Grinevicius, V.M.A.S.; Filho, D.W.; Zamoner, A.; Braga, A.L.; Pedrosa, R.C.; Ourique, F. IP-Se-06, a Selenylated Imidazo[1,2-*a*]pyridine, Modulates Intracellular Redox State and Causes Akt/mTOR/HIF-1 α and MAPK Signaling Inhibition, Promoting Antiproliferative Effect and Apoptosis in Glioblastoma Cells. *Oxid. Med. Cell. Longev.* **2022**, *1*, 3710449. [CrossRef]
260. Li, M.; Wang, D.; Li, Q.; Luo, F.; Zhong, T.; Wu, H.; Xiong, L.; Yuan, M.; Su, M.; Fan, Y. Design, Synthesis and Biological Evaluation of 6-(Imidazo[1,2-*a*]pyridin-6-yl)quinazoline Derivatives as Anticancer Agents via PI3Kα Inhibition. *Int. J. Mol. Sci.* **2023**, *24*, 6851. [CrossRef]
261. Armendariz-Barrientos, K.; Pérez, L.A.; Lagunas-Rivera, S.; Alcaraz-Contreras, Y.; García-Revilla, M.A.; Prado-Garcia, H.; García-Becerra, R.; Vazquez, M. Novel N-quaternary coumarin-3-yl-imidazo[1,2-*a*]pyridines as fluorescent hybrids: Their synthesis and biological evaluation in cancer cells. *Results Chem.* **2025**, *13*, 101959. [CrossRef]
262. Kanthecha, D.A.; Bhatt, B.S.; Patel, M.N. Synthesis, characterization and biological activities of imidazo[1,2-*a*]pyridine based gold(III) metal complexes. *Helyon* **2019**, *5*, e01968. [CrossRef]
263. Roby, O.; Kadiri, F.Z.; Loukhmi, Z.; Moutaouakil, M.; Tighadouini, S.; Saddik, R.; Aboulmouhajir, A. Synthesis of new set of imidazo[1,2-*a*]pyridine-schiff bases derivatives as potential antimicrobial agents: Experimental and theoretical approaches. *J. Mol. Struct.* **2023**, *1292*, 136186. [CrossRef]

264. Kolomiiets, O.; Tsygankov, A.V.; Kornet, M.N.; Brazhko, A.A.; Musatov, V.I.; Chebanov, V.A. Synthesis of imidazo[1,2-*a*]pyridine-containing peptidomimetics by tandem of Groebke-Blackburn-Bienaymé and Ugi reaction. *Beilstein J. Org. Chem.* **2023**, *26*, 727. [CrossRef]
265. Abdel-Shafi, A.A.; Fathi, A.M.; Ismail, M.A.; Boykin, D.W. Antiprotozoal agents as water soluble singlet oxygen photosensitizers: Imidazo[1,2-*a*]pyridine and 5,6,7,8-tetrahydro-imidazo[1,2-*a*]pyridine derivatives. *J. Luminesc.* **2017**, *181*, 164. [CrossRef]
266. Agarwal, D.S.; Beteck, R.M.; Ilbeigi, K.; Caljon, G.; Legoabe, L.J. Design and synthesis of imidazo[1,2-*a*]pyridine-chalcone conjugates as antikinetoplastid agents. *Chem. Biol. Drug Des.* **2023**, *103*, e14400. [CrossRef] [PubMed]
267. Hussain, R.; Rehman, W.; Khan, S.; Maalik, A.; Hefnawy, M.; Alanazi, A.S.; Khan, Y.; Rasheed, L. Imidazopyridine-Based Thiazole Derivatives as Potential Antidiabetic Agents: Synthesis, In Vitro Bioactivity, and In Silico Molecular Modeling Approach. *Pharmaceuticals* **2023**, *16*, 1288. [CrossRef]
268. Onoue, S.; Igarashi, N.; Yamauchi, Y.; Kojima, T.; Murase, N.; Zhou, Y.; Yamada, S.; Tsuda, Y. In vitro phototoxic potential and photochemical properties of imidazopyridine derivative: A novel 5-HT4 partial agonist. *J. Pharm. Sci.* **2008**, *97*, 4307. [CrossRef]
269. Zucolotto Cocca, L.H.; Valverde, J.V.P.; le Bescont, J.; Breton-Patient, C.; Piguel, S.; Silva, D.L.; Mendonca, C.R.; De Boni, L. Photophysical properties of 3-arylthioimidazo[1,2-*a*]pyridine derivatives: The role of peripheral electron-donating and electron-withdrawing groups in the advance of organic materials engineering. *J. Mol. Struct.* **2024**, *1300*, 137221. [CrossRef]
270. Hase, E.; Takanari, H.; Hoshi, K.; Okamoto, M.; Tabata, A.; Nagamune, H.; Minamikawa, T.; Yasui, T.; Yoshida, Y.; Minagawa, K.; et al. Two- and three-photon excitable quaternized imidazo[1,2-*a*]pyridines as mitochondrial imaging and potent cancer therapy agents. *Org. Biomol. Chem.* **2020**, *18*, 7571. [CrossRef]
271. Devi, N.; Singh, D.; Rawal, R.K.; Bariwal, J.; Singh, V. Medicinal Attributes of Imidazo[1,2-*a*]pyridine Derivatives: An Update. *Curr. Top. Med. Chem.* **2016**, *16*, 2963. [CrossRef]
272. Goel, R.; Luxami, V.; Paul, K. Imidazo[1,2-*a*]pyridines: Promising Drug Candidate for Antitumor Therapy. *Curr. Top. Med. Chem.* **2016**, *16*, 3590. [CrossRef] [PubMed]
273. Deep, A.; Bhatia, R.K.; Kaur, R.; Kumar, S.; Jain, U.K.; Singh, H.; Batra, S.; Kaushik, D.; Deb, P.K. Imidazo[1,2-*a*]pyridine Scaffold as Prospective Therapeutic Agents. *Curr. Top. Med. Chem.* **2017**, *17*, 238. [CrossRef]
274. Narayan, A.; Patel, S.; Baile, S.B.; Jain, S.; Sharma, S. Imidazo[1,2-*a*]Pyridine: Potent Biological Activity, SAR and Docking Investigations (2017–2022). *Infect. Disord. Drug Targets* **2024**, *24*, e200324228067. [CrossRef] [PubMed]
275. Reddyrajula, R.; Dalimba, U.K. Structural modification of zolpidem led to potent antimicrobial activity in imidazo[1,2-*a*]pyridine/pyrimidine-1,2,3-triazoles. *New J. Chem.* **2019**, *43*, 16281. [CrossRef]
276. Tahiroğlu, V.; Gören, K.; Bağlan, M. In Silico drug evaluation by molecular docking, ADME studies and DFT calculations of 2-(6-chloro-2-(4-chlorophenyl)imidazo[1,2-*a*]pyridin-3-yl)-*N*,*N*-dipropylacetamide. *BMC Pharmacol. Toxicol.* **2025**, *26*, 116. [CrossRef]
277. Samanta, S.; Kumar, S.; Aratikatla, E.K.; Ghorpade, S.R.; Singh, V. Recent developments of imidazo[1,2-*a*]pyridine analogues as antituberculosis agents. *RSC Med. Chem.* **2023**, *14*, 644. [CrossRef]
278. Boček Pavlinac, I.; Zlatić, K.; Persoons, L.; Daelemans, D.; Banjanac, M.; Radonanović, V.; Butković, K.; Kralk, M.; Hranjec, M. Biological Activity of Amidino-Substituted Imidazo[4,5-*b*]pyridines. *Molecules* **2022**, *28*, 34. [CrossRef]
279. Lončar, B.; Perin, N.; Mioč, M.; Boček, I.; Grgić, L.; Kralij, M.; Tomić, S.; Radić Stojković, M.; Hranjec, M. Novel amino substituted tetracyclic imidazo[4,5-*b*]pyridine derivatives: Design, synthesis, antiproliferative activity and DNA/RNA binding study. *Eur. J. Med. Chem.* **2021**, *217*, 113342. [CrossRef]
280. Bourichi, S.; Misbahi, H.; Rodi, Y.K.; Chahdi, F.O.; Essassi, E.M.; Szabó, S.; Szalontai, B.; Gajdács, M.; Molnár, J.; Spengler, G. In Vitro Evaluation of the Multidrug Resistance Reversing Activity of Novel Imidazo[4,5-*b*]pyridine Derivatives. *Anticancer Res.* **2018**, *38*, 3999. [CrossRef]
281. Altaib, M.; Doganc, F.; Kaşkatepe, B.; Göker, H. Synthesis of some new 2-(substituted-phenyl)imidazo[4,5-*c*] and[4,5-*b*]pyridine derivatives and their antimicrobial activities. *Mol. Diver.* **2024**, *28*, 2817. [CrossRef]
282. Bavetsias, V.; Sun, C.; Bouloc, N.; Reynisson, J.; Workman, O.; Linardopoulos, S.; McDonald, E. Hit generation and exploration: Imidazo[4,5-*b*]pyridine derivatives as inhibitors of Aurora kinases. *Bioorg. Med. Chem. Lett.* **2007**, *17*, 6567. [CrossRef]
283. Bavetsias, V.; Large, J.M.; Sun, C.; Bouloc, N.; Kosmopoulou, V.; Matteucci, M.; Wilsher, N.E.; Martins, V.; Reynisson, J.; Atrash, B.; et al. Imidazo[4,5-*b*]pyridine derivatives as inhibitors of Aurora kinases: Lead optimization studies toward the identification of an orally bioavailable preclinical development candidate. *J. Med. Chem.* **2010**, *53*, 5213. [CrossRef]
284. Hranjec, M.; Lučić, B.; Ratkaj, I.; Kraljević Pavelić, S.; Piantanida, I.; Pavelić, K.; Karminski-Zamola, G. Novel imidazo[4,5-*b*]pyridine and triaza-benzo[c]fluorene derivatives: Synthesis, antiproliferative activity and DNA binding studies. *Eur. J. Med. Chem.* **2011**, *46*, 2748. [CrossRef] [PubMed]
285. Boček Pavlinac, I.; Šljubura, C.; Zlatić, K.; Kralj, M.; Fabijanić, I.; Banjanac, M.; Radić Stojković, M.; Hranjec, M. Synthesis, Biological Evaluation, and Interaction with Calf Thymus-DNA of Mono- and Diamidino-Substituted Imidazo[4,5-*b*]pyridines. *ChemMedChem* **2025**, *20*, e202500640.

286. Mullagiri, K.; Nayak, V.L.; Sunkari, S.; Sai Mani, G.; Devi Guggilapu, S.; Nagaraju, B.; Alariffi, A.; Kamal, A. New (3-(1*H*-benzo[*d*]imidazol-2-yl))/(3-(3*H*-imidazo[4,5-*b*]pyridin-2-yl))-(1*H*-indol-5-yl)(3,4,5-trimethoxyphenyl)methanone conjugates as tubulin polymerization inhibitors. *MedChemComm* **2018**, *9*, 275. [CrossRef]
287. Boček, I.; Hok, L.; Persoons, L.; Daelemans, D.; Vianello, R.; Hranjec, M. Imidazo[4,5-*b*]pyridine derived tubulin polymerization inhibitors: Design, synthesis, biological activity in vitro and computational analysis. *Bioorg. Chem.* **2022**, *127*, 106032. [CrossRef]
288. Elyoussfi, A.; Azghay, I.; Dadou, S.; Daoudi, W.; Ahari, M.H.; Amhamdi, H.; Benchat, N.; El Aatiaoui, A.; Salhi, A.; Dafali, A. The effect of functional groups on the inhibitory efficacy of newly synthesized Imidazopyridines compounds against the corrosion of mild steel in acidic environments: Electrochemical, thermodynamic, surface and computational investigations (Part B). *J. Mol. Struct.* **2023**, *1291*, 136025. [CrossRef]
289. Ech-chihbi, E.; Nahlé, A.; Salim, R.; Oudda, H.; El Hajjaji, F.; El Kalai, F.; El Aatiaoiu, A.; Taleb, M. An Investigation into Quantum Chemistry and Experimental Evaluation of Imidazopyridine Derivatives as Corrosion Inhibitors for C-Steel in Acidic Media. *J. Bio Tribo-Corros.* **2019**, *5*, 24. [CrossRef]
290. Salim, R.; Nahlé, A.; El Hajjaji, F.; Ech-chihbi, E.; Benhiba, F.; El Kalai, F.; Benchat, N.; Oudda, H.; Guenbour, A.; Taleb, M.; et al. Experimental, Density Functional Theory, and Dynamic Molecular Studies of Imidazopyridine Derivatives as Corrosion Inhibitors for Mild Steel in Hydrochloric Acid. *Surf. Eng. Appl. Electrochem.* **2021**, *57*, 233. [CrossRef]
291. Idlahoussaine, N.; El Ibrahimi, B.; Ait Addi, A.; Daoudi, W.; Idouhli, R.; Lasri, M.; Yilmaz, M.; El Ouardi, M.; El Aatiaoui, A.; Abouelfida, A. Investigating the effectiveness of an imidazopyridine-based compound as an anti-corrosive additive for mild steel in molar hydrochloric acid solutions: A mutual multi-facet experimental and computational approach. *Phys. Chem. Chem. Phys.* **2025**, *27*, 11144. [CrossRef]
292. Yadav, M.; Behera, D.; Kumar, S. Experimental and theoretical investigation on adsorption and corrosion inhibition properties of imidazopyridine derivatives on mild steel in hydrochloric acid solution. *Surf. Interface Anal.* **2014**, *46*, 640. [CrossRef]
293. Martinho, L.A.; de Lima, D.M.; Praciano, V.H.J.G.; Oliveira, S.C.C.; Andrade, C.K.Z. Phytotoxicity Study of (Amino)imidazo[1,2-*a*]pyridine Derivatives Toward the Control of Bidens pilosa, Urochloa decumbens, and Panicum maximum Weeds. *J. Agric. Food Chem.* **2025**, *73*, 298. [CrossRef] [PubMed]
294. Ishida, Y.; Ota, K.; Ito, S.; Nakahama, T.; Miki, H.; Yoshikawa, H. Synthesis of novel herbicidal sulfonylureas containing an imidazo[1,2-*a*]pyridine moiety. *J. Pestic. Sci.* **1993**, *18*, 175. [CrossRef]
295. Liu, Z.; Song, R.; Zhang, D.; Wu, R.; Liu, T.; Wu, Z.; Zhang, J.; Hu, D. Synthesis, insecticidal activity, and mode of action of novel imidazopyridine mesoionic derivatives containing an amido group. *Pest Manag. Sci.* **2022**, *78*, 4983. [CrossRef]
296. Liu, Z.; Song, R.; Zhang, D.; Wu, R.; Liu, T.; Wu, Z.; Song, B. New Synthetic Method and Insecticidal Activities of Novel Imidazopyridine Mesoionic Derivatives Containing an Ester Group. *J. Agric. Food Chem.* **2022**, *70*, 1019. [CrossRef]
297. N'guessan, J.-P.D.U.; Coulibaly, S.; Kouaho, A.T.; Angora, K.E.; Drissa, S.; Ouattara, M. Anti-fungal Activities of imidazo[1,2-*a*]pyridine-based Chalcone Hybrids Against *Aspergillus fumigatus*. *J. Chem. Res.* **2025**, *10*, 210.
298. Nandhagopal, M.; Mala, R.; Somarathinam, K.; Dhakshinamurthy, D.; Narayanasamy, M.; Vijayan, P.; Shankar, M.M. Anti-fungal effects of novel *N*-(*tert*-butyl)-2-(pyridin-2-yl)imidazo[1,2-*a*]pyridin-3-amine derivative and it's in-vitro, in-silico, and mode of action against *Candida* spp. *Arch. Microbiol.* **2024**, *206*, 186. [CrossRef] [PubMed]
299. Lu, Y.; Wu, K.; Yan, Y.; Xu, Z. Design, synthesis, nematicidal and fungicidal activities of imidazo[1,2-*a*] pyridine derivatives containing amino acids. *Results Chem.* **2025**, *18*, 102780. [CrossRef]
300. Lu, Y.; Guo, Q.; Zhao, W.; Zhao, W.; Xu, Z. Design, synthesis, and nematicidal and fungicidal activity of 8-chloro-6-(trifluoromethyl) imidazo[1,2-*a*]pyridine thiadiazole/triazole derivatives. *Chin. J. Pestic. Sci.* **2025**, *27*, 842.
301. Yao, Y.; Li, X.; Zhou, L.; Liu, J.; Zhong, W.; Liu, M. Design, Synthesis, and Insecticidal Activities of Imidazo[4,5-*b*]Pyridine Compounds Containing Amino Fragment. *Chem. Biodivers.* **2025**, *22*, e00514. [CrossRef]
302. Plutecka, A.; Hoffmann, M.; Rychlewska, U.; Kucybała, Z.; Pączkowski, J.; Pyszka, I. Relationship between structure and photoinitiating abilities of selected bromide salts of 2-oxo-2,3-dihydro-1*H*-imidazo[1,2-*a*]pyridine (IMP): Influence of the solvent and the substitution in benzaldehyde on the course of its reaction with IMP. *Acta Crystallogr. B Struct. Sci.* **2006**, *B62*, 135. [CrossRef] [PubMed]
303. Pyszka, I.; Kucybała, Z.; Pączkowski, J. Development of new dyeing photoinitiators based on benzylideneimidazopyridine dyes. *J. Polym. Sci. Part A Polym. Chem.* **2003**, *41*, 3048. [CrossRef]
304. Chen, H.; Zhang, Y.; Bonfiglio, A.; Morlet-Savary, F.; Mauro, M.; Lalevée, J. Rhenium(I) N-Heterocyclic Carbene Complexes in Photoinitiating Systems for Polymerization upon Visible Light: Development of Photosensitive Resins for 3D and 4D Applications. *ACS Appl. Polym. Mater.* **2021**, *3*, 464. [CrossRef]
305. Chen, T.; Ye, F.; Hu, R.; Tang, B.Z. Multicomponent Polymerizations of Isocyanides, Aldehydes, and 2-Aminopyridine toward Imidazo[1,2-*a*]pyridine-Containing Fused Heterocyclic Polymers. *Macromolecules* **2022**, *55*, 8590. [CrossRef]
306. Cui, Y.; Ge, Y.; Li, Y.; Tao, J.; Yao, J.; Dong, Y. Single-ion magnet behavior of two pentacoordinate CoII complexes with a pincer ligand 2,6-bis(imidazo[1,5-*a*]pyridin-3-yl)pyridine. *Struct. Chem.* **2020**, *31*, 547. [CrossRef]

307. Kitaoka, S.; Kitagawa, Y.; Nozoe, R.; Nobuoka, K. Syntheses and properties of imidazopyridine-based ionic liquids. *J. Ion. Liq.* **2024**, *4*, 100100. [CrossRef]
308. Rajabi, S.; Rüttger, F.; Lücken, J.; Dechert, S.; John, M.; Meyer, F. Ruthenium Complexes of Rigid, Dianionic, Tetradentate N-Donor Ligands and their Potential as Catalysts for Water Oxidation. *Eur. J. Inorg. Chem.* **2022**, *26*, e202200597. [CrossRef]
309. Yang, H.; Liu, H.; Zhang, J.; Zhang, T.; Zhu, X.; Liu, Z.; Zhu, L.; Cao, C.C.; Xu, G.; Zhu, M. Enhancing lithium-ion desolvation with robust polyhydroquinone-diimidazopyridine nanofibers for high-rate Li–S batteries. *EES Batter.* **2025**, *1*, 1301. [CrossRef]